1

2   How Well Do We Understand the Land-Ocean-Atmosphere Carbon Cycle?

3   **David Crisp[1], Han Dolman[2], Toste Tanhua[3], Galen A. McKinley[4], Judith Hauck[5], Simon**
4   **Eggleston[6], Valentin Aich[6]**

5   [1]Jet Propulsion Laboratory, California Institute of Technology, Pasadena, CA, USA.

6   [2]Department of Earth Sciences, Vrije Universiteit Amsterdam, Amsterdam, The Netherlands.

7   [3]GEOMAR Helmholtz Centre for Ocean Research Kiel, Marine Biogeochemistry, Kiel,
8   Germany.

9   [4]Columbia University and Lamont Doherty Earth Observatory, Palisades, NY, USA.

10   [5]Alfred-Wegener-Institut, Helmholtz-Zentrum für Polar und Meeresforschung, Bremerhaven,
11   Germany.

12   [6]Global Climate Observing System, World Meteorological Organization, Geneva, Switzerland.

13   Corresponding author: first and last name (David Crisp david.crisp@jpl.nasa.gov)

14   **Key Points:**

15   • Carbon dioxide (CO_2) emissions from fossil fuel use and other human activities have
16   increased its atmospheric abundance by almost 50% during the industrial age.

17   • These increases would have been much larger if natural sinks in the ocean and on land
18   had not removed over half of this CO_2, maintaining an airborne fraction $< 45\%$.

19   • New measurements and models are providing insights into the carbon cycles as the land
20   and ocean sinks continue to respond to human activities and climate change.
21

22 **Abstract**

23 Fossil fuel combustion, land use change and other human activities have increased the
24 atmospheric carbon dioxide (CO_2) abundance by almost 50% since the beginning of the
25 industrial age. These changes would have been much larger if natural sinks in the land biosphere
26 and ocean had not removed over half of this anthropogenic CO_2. Here, we review the current
27 state of knowledge of the ocean, land and atmospheric carbon cycles, identify emerging
28 measurement and modeling capabilities, and gaps that must be addressed to diagnose the
29 processes driving the carbon cycle and predict their response to human activities and a changing
30 climate. The anthropogenic CO_2 uptake by the ocean has increased over this period, as the
31 atmospheric CO_2 partial pressure (pCO_2) has increased. For the land carbon cycle, the emerging
32 picture is more complicated. Over the past three decades, the uptake of CO_2 by intact tropical
33 humid forests appears to be declining, but these effects are offset by a net greening across mid-
34 and high-latitudes associated with afforestation, agricultural, and longer growing seasons. These
35 studies have also revealed measurement gaps and other limitations in our understanding of the
36 evolving carbon cycle. They show that continued ship-based observations combined with
37 expanded deployments of autonomous platforms are needed to quantify ocean-atmosphere fluxes
38 on policy relevant spatial and temporal scales. They also reinforce the urgent need for more
39 comprehensive measurements of stocks, fluxes and atmospheric CO_2 in humid tropical forests
40 and across the Arctic and boreal regions, which appear to be experiencing rapid change.

41

42 **Plain Language Summary**

43 Since the beginning of the industrial age in the mid-1700s, fossil fuel combustion, land use
44 change and other human activities have increased the atmospheric carbon dioxide (CO_2)
45 concentration to levels never before seen in human history such that CO_2 is now the primary
46 driver of climate change. The atmospheric CO_2 abundance and its effect on the climate would
47 have been much larger if natural processes in the ocean and on land carbon cycle had not
48 absorbed over half of the CO_2 emitted by these human activities. Here, we review our
49 understanding of anthropogenic CO_2 emissions and the processes controlling the emissions and
50 uptake of CO_2 by the natural carbon cycle as it responds to continuing human activities a
51 changing climate.

52

53 **1   Introduction**

54   Since the beginning of the industrial age, human activities have increased the
55 atmospheric concentrations of carbon dioxide (CO_2) and other greenhouse gases (GHGs) to
56 levels never before seen in human history. These large increases are driving climate change,
57 because CO_2 is an efficient greenhouse gas with an atmospheric lifetime measured in centuries.
58 Bottom-up statistical inventories indicate that fossil fuel combustion, industry, agriculture,
59 forestry, and other human activities are now adding more than 11.5 petagrams of carbon (Pg C)
60 to the atmosphere each year (Friedlingstein et al., 2019; 2020). Direct measurements of CO_2 in
61 the atmosphere and in air bubbles in ice cores indicate that these and other human activities have
62 increased the globally averaged atmospheric CO_2 dry air mole fraction from less than 277 parts
63 per million (ppm) in 1750 to more than 410 ppm today. Measurements from Mauna Loa

64 Observatory show that over half of this increase has occurred since 1985 and over a quarter has
65 happened within the past 15 years (Dlugokencky et al., 2018).

66   These increases would be much larger if processes operating in the natural carbon cycle
67 had not removed over half of these anthropogenic CO_2 emissions. Carbon cycle measurements
68 and modeling studies show that these anthropogenic CO_2 emissions are superimposed on an
69 active natural carbon cycle that regulates CO_2 through photosynthesis and respiration on land
70 and in the ocean (Beer et al., 2010), as well as temperature-driven solubility coupled with the
71 ocean circulation (Takahashi et al., 2002; 2009). The land biosphere and ocean emit almost 20
72 times as much CO_2 into the atmosphere as human activities each year, but then reabsorb a
73 comparable amount along with about half of the anthropogenic CO_2 emissions (Jones and Cox,
74 2005; Canadell et al., 2007; Raupach et al., 2008; Knorr 2009; Bennedsen et al., 2019,
75 Friedlingstein et al., 2020). While the fraction of the anthropogenic CO_2 that stays in the
76 atmosphere (the "airborne fraction") is remarkably constant, at about 0.45 for the multi-year
77 average (e.g. Ballantyne et al., 2012; Raupach et al., 2008; 2014), it can change substantially
78 from year to year. In some years, the airborne fraction can be as high as 80%, while in others, it
79 can be as low as 30% (Raupach et al., 2008; 2014). Some of the largest changes in this airborne
80 fraction appear to be associated with changes in uptake of CO_2 by the land biosphere (the land
81 sink) in response to large-scale temperature and precipitation anomalies, like those associated
82 with major El Niño events or large volcanic aerosol injections into the stratosphere (Frölicher et
83 al., 2013). The ocean uptake also responds to El Niño events and large volcanic eruptions
84 (Eddebbar et al., 2019; McKinley et al., 2004; 2020), but has a smaller impact on the amplitude
85 of variability in the airborne fraction (Chatterjee et al., 2017). The relative roles of these and
86 other processes that link the land, ocean and atmospheric carbon cycles with the climate are less
87 well understood, compromising our ability to predict how the atmospheric CO_2 growth rate
88 might change as the carbon cycle responds to climate change (Ballantyne et al., 2012, McKinley
89 et al., 2017).

90   Over the past two decades, our understanding of the natural and anthropogenic
91 contributions to the carbon cycle has grown steadily with the deployment of progressively more
92 sophisticated ground-based, oceanic, airborne, and space-based carbon cycle measurement
93 systems. These advances have been accompanied by the development of far more comprehensive
94 diagnostic and prognostic carbon cycle modeling tools. On time scales of a decade or longer,
95 "bottom-up" measurements of changes in carbon stocks on land and in the ocean provide a
96 reliable indicator of the stability of these reservoirs and a useful integral constraint on their
97 fluxes of carbon to the atmosphere. On shorter time scales, stock measurements are less reliable
98 for estimating atmospheric emissions because land and ocean stock changes that are too small to
99 be accurately quantified can produce large changes in the atmospheric CO_2 concentration. On
100 these scales, direct measurements of CO_2 fluxes at the surface, fluxes derived from vertical
101 gradients in pCO_2 across the air-sea interface or "top-down" fluxes estimated from spatial and
102 temporal gradients in atmospheric CO_2 concentrations can provide more reliable results.

103   Both bottom-up stock and flux estimates and "top-down" atmospheric estimates are
104 providing key insights into the carbon cycle. Bottom-up methods use empirical or process-based
105 models of the land biosphere and ocean to estimate fluxes, or to upscale in situ measurements of
106 the time change of stocks or of direct flux observations (e.g. Sabine et al., 2004; Doney et al.,
107 2004; Gruber et al., 2019a; Pan et al., 2011; Sitch et al., 2015; Hubau et al., 2020; Piao et al.,
108 2020; Jung et al., 2020; Long et al., 2013; Landschützer, et al., 2013; Rödenbeck et al., 2014;

109 2015; Gregor et al., 2019; Watson et al., 2020; Hauck et al., 2020; Carroll et al., 2020). "Top-
110 down" models use inverse methods to estimate the surface CO_2 fluxes from the land or ocean
111 needed to maintain the observed atmospheric or ocean CO_2 concentrations in the presence of the
112 prevailing winds and ocean circulation (e.g. Enting et al., 1995; Mikaloff-Fletcher et al., 2006;
113 Jacobson et al., 2007; Khatiwala et al., 2009; Chevallier et al., 2010; 2019; DeVries 2014;
114 Crowell et al., 2019).

115 Both bottom-up and top-down methods benefit from remote sensing as well as in situ
116 data. For example, a bottom-up forest stock inventory might use in situ measurements to estimate
117 the above ground biomass from an ensemble of specific plots and then use remote sensing
118 measurements to upscale those measurements to larger areas. Similarly, a top-down approach
119 might combine in situ and remote sensing observations of atmospheric CO_2 along with models of
120 atmospheric transport constrained by both in situ and satellite meteorological measurements to
121 estimate regional-scale fluxes. In practice, top-down and bottom-up methods can be combined.
122 For example, top-down methods for estimating net biospheric exchange (NBE) may use fossil
123 fuel emissions derived from bottom-up inventories as a static (i.e. not optimized) input (i.e.
124 Crowell et al., 2019).

125 As the world embarks on efforts to monitor and control CO_2 emissions, there is growing
126 evidence that the natural carbon cycle is evolving in response to human activities, severe
127 weather, disturbances and climate change. In this context, an improved understanding of both the
128 anthropogenic and natural processes in the land biosphere and ocean that control the emissions
129 and uptake of CO_2 is critical to our ability to predict its rate of increase in the CO_2 in the
130 atmosphere and its impact on the climate. To address this need, advanced measurement
131 capabilities are being deployed and their results are being analyzed with more comprehensive
132 diagnostic and prognostic modeling tools. While these advances do not yet provide the full
133 capabilities of the policy-relevant carbon observing system advocated by Ciais et al. (2014) or
134 envisioned by the WMO Integrated Global Greenhouse Gas Information System (IG3IS), they
135 are providing substantial new insights with respect to the anthropogenic and natural processes
136 operating in the carbon cycle.

137 Here, we review the current state of knowledge of the anthropogenic and natural
138 processes driving the land, ocean and atmospheric carbon cycles. We summarize advances in
139 each domain and identify ongoing efforts to exploit this new information to create a more
140 accurate and complete baseline and to identify trends. We also identify critical measurement and
141 modeling gaps that must be addressed to produce an effective carbon monitoring system.

142 **2   A Note on Units**

143   Because the bottom-up and top-down land, ocean and atmospheric carbon communities
144   focus on different aspects of the carbon cycle, they have developed a sometimes confusing array
145   of units to quantify stocks and fluxes of carbon and CO_2. For example, the land carbon
146   community typically quantifies the mass of stocks and fluxes carbon, the atmospheric
147   community typically measures and reports the CO_2 dry air mole fraction, X_{CO2} and the ocean

Table 1: Quantities and Units Describing the Carbon Cycle

Quantity	Acronym	Typical units	Comment
carbon dioxide dry air mole fraction	CO_2, xCO_2 or X_{CO2}	parts per million by volume (ppm)	Number of CO_2 molecules relative to each million (10^6) molecules of dry air. If CO_2 is assumed to be an ideal gas and its dry air mole fraction is increased by 1 ppm at constant temperature, the CO_2 partial pressure will increase by one micro atmosphere (μatm).
partial pressure of carbon dioxide	pCO_2	μatm	At sea level, $pCO_2 = (P - pH_2O) \times X_{CO2}$, where P is the total atmospheric pressure and pH_2O is the water vapor saturation vapor pressure (see Woolf et al., 2016). 1 μatm = 10^{-6} atmospheres = 0.10325 Pascals.
carbon dioxide fugacity	fCO_2	μatm	Effective ideal gas partial pressure of CO_2 that has the same temperature and Gibbs free energy as the real gas. At the surface, $fCO_2 = X_{CO2} \times \varphi_{CO2}$, where $\varphi_{CO2} \approx 0.0002$/K is the fugacity coefficient for CO_2 and K is the temperature in Kelvin.
column averaged carbon dioxide dry air mole fraction	XCO_2	ppm	This vertically-averaged quantity used by the atmospheric remote sensing community is derived from the ratio of the CO_2 column abundance and the dry air column abundance. The dry air column abundance is estimated from the measured molecular oxygen (O_2) column abundance, assuming an O_2 dry air mole fraction of 0.20955.
carbon stock or stock change		petagrams of carbon per year (Pg C yr^{-1})	1 Pg C = 10^{15} g C. 1 PgC = 10^{12} kg C = 10^9 tons of carbon = 1 Gt C. When oxidized to form CO_2, 1 Pg C generates 3.664 Pg CO_2.
Gross Primary Production	GPP	Pg C yr^{-1}	Total flux of carbon fixed through photosynthetic reduction of CO_2 by plants in an ecosystem.
Net Primary Production	NPP	Pg C yr^{-1}	Net flux of organic carbon produced by plants in an ecosystem. NPP equals GPP minus autotrophic respiration by plants, R_a.
Net Ecosystem Exchange or Net Ecosystem Production	NEE or NEP	Pg C yr^{-1}	Net primary production, NPP, minus carbon losses by heterotrophic (non plant) respiration, R_h. NEE and NEP are generally interchangeable, with NEE used more often to refer to fluxes measured in the atmosphere, while NEP is more often used for fluxes inferred from measurements of carbon stock changes.
Net Biospheric Exchange or Net Biome Exchange	NBE	Pg C yr^{-1}	Change in mass of carbon stocks after episodic carbon losses due to natural or anthropogenic disturbance.

148   community uses the partial pressure, pCO_2, fugacity, fCO_2, and the air-sea carbon flux. To relate
149   these units, it is useful to note that one petagram of carbon (1 Pg C) in the atmospheric CO_2 is
150   equivalent to a concentration of ~ 2.124 ppm (c.f. Ballantyne et al., 2012; Friedlingstein et al.,
151   2020). Table 1 summarizes these and other commonly used quantities and units used by the
152   carbon cycle community and describes their relationships.

3   Anthropogenic Contributions to the Carbon Cycle

Atmospheric CO_2 emissions from fossil fuel combustion, cement production, land use change and other human activities are currently being tracked by the regulatory, commercial and scientific communities (e.g. Andrew, 2020). International organizations such as the International Energy Agency (IEA) originally compiled fossil fuel statistics to avoid disruptions in the world's oil supplies, but now provide annual reports on a range of technologies to support sustainable energy development (IEA 2020). Those from national organizations, such as the U.S. Energy Information Administration (EIA) serve a similar purpose, tracking short-term and long-term trends in supply and demand around the world to support the energy industry, while those from national regulatory organizations such as the U.S. Environmental Protection Agency (EPA) compile statistics for regulating and reporting national emissions to other government agencies or organizations such as the United Nations Framework Convention on Climate Change (UNFCCC). Commercial organizations, such as British Petroleum, produce inventories to track trends in energy markets (BP 2020).

Similarly, to track emissions from land use change, international organizations such as the United Nations Food and Agriculture Organization (FAO) collect and disseminate global information on agriculture, forestry and other land use (AFOLU). Two methods are typically used to track emissions from land use change. In the first, data collected by FAO are used in so-called bookkeeping models that prescribe carbon loss per pool over time (Hansis et al., 2015, Houghton and Nassikas, 2017). In the second, satellite remote sensing data are used to determine the amount of land cover change and associate emission losses with the change by emission factors or more detailed biogeochemical models (van der Werf et al., 2017). For tracking historical land use changes, a map of historical land use is required such as LUH2-GCB2020 (Hurrt et al., 2020; see also Friedlingstein et al., 2020). Using this information, it is possible to project land use change impact on the carbon cycle using the new generation of dynamic global vegetation models (DGVMs). At the national level, land use change emissions are compiled and delivered to the UNFCCC by country level organizations such as the U.S. EPA, Japan's Ministry of the Environment and the European Union's European Environment Agency.

Scientific inventories, such as those compiled by the Carbon Dioxide Information Analysis Center (CDIAC; Boden et al., 2017) and the annual reports compiled by the Global Carbon Project (GCP), combine information from all of these sources to support scientific investigations of the energy and carbon cycles as well as other applications. The science community has also produced high resolution gridded inventories such as EDGAR (Janssen-Maehout et al., 2019), ODIAC (Oda et al., 2018), and Hestia (Gurney et al., 2019). These inventories use other data (population, night lights, etc.) to disaggregate national scale emissions to support carbon cycle investigations on spatial scales spanning individual forest plots or urban areas to full biomes. These gridded inventories also provide more actionable information on anthropogenic CO_2 emissions for policy makers working on urban to sub-national scales.

3.1   Regulating Greenhouse Gas Emissions - the Paris Agreement

The primary international regulatory framework for tracking anthropogenic CO_2 emissions is the UNFCCC. This treaty was established in 1994 to stabilize "greenhouse gas concentrations in the atmosphere at a level that would prevent dangerous anthropogenic interference in the climate system." To implement this treaty, parties to the 2015 UNFCCC Paris Agreement resolved to define Nationally Determined Contributions (NDCs) to a global GHG

197   reduction effort and to report progress toward these NDCs, at 5-year intervals through Global
198   Stocktakes, the first of which is scheduled for 2023. The NDC reports are to be compiled based
199   on the Intergovernmental Panel on Climate Change (IPCC) Guidelines for National Greenhouse
200   Gas Inventories (IPCC 2006; 2019) and consist of bottom-up emission inventories, compiled
201   from a statistical analysis of emissions reported from sources in specific sectors, including
202   Energy, Industrial Processes Product use, Agriculture, Forestry, and Other Land Use (AFOLU),
203   and Waste. Each sector is subdivided into a series of categories. For example, AFOLU is divided
204   into six categories, including Forest Land, Cropland, Grassland, Wetlands, Settlements, and
205   Other Land categories.

206   While CO_2 emissions from fossil fuel combustion in the energy sector constitute the
207   largest direct anthropogenic contribution to the global carbon cycle, emissions of CO_2 and other
208   greenhouse gases from managed lands tracked under the AFOLU sector are responsible for
209   almost one quarter of all anthropogenic GHG emissions (Smith et al., 2014). These emissions
210   originate primarily from deforestation and forest degradation, but also include contributions from
211   agricultural land and livestock management. The IPCC Guidelines only require reporting of
212   emissions on managed lands, but they acknowledge that natural disturbances (wildfires, insects,
213   severe weather) contribute a significant source of interannual variability and uncertainty in this
214   sector. The concept of natural and anthropogenic changes are becoming more diffuse as climate
215   change itself affects "natural disturbances". A comprehensive understanding of the processes
216   operating in the natural carbon cycle is therefore essential for tracking and attributing observed
217   interannual changes in atmospheric CO_2 concentrations, and for linking bottom-up inventories
218   with top-down monitoring, recording, and verification (MRV) strategies (Janssens-Maenhout et
219   al., 2020).

220   *3.2   Carbon Cycle Insights from Scientific Inventories*

221   The Global Carbon Budget (GCB) compiled annually by the Global Carbon Project
222   document the globally-averaged budget of anthropogenic carbon fluxes for five key components:
223   atmosphere, fossil fuel emissions, land use change, uptake by the terrestrial biosphere ("land
224   sink") and uptake by the ocean ("ocean sink"). From 2000-2006 to 2019, emissions from fossil
225   fuel use and cement production increased from 7.6 to 9.7 Pg C yr^{-1}, with a peak of 10 Pg C yr^{-1} in
226   2018. The ocean and land sinks increased during the same time from 2.2 to 2.6 and 2.8 to 3.6 Pg
227   C yr^{-1} respectively (Friedlingstein et al., 2020). The anthropogenic sinks are defined as their
228   perturbation caused by direct effects of increasing atmospheric CO_2 and indirect effects by
229   climate change.

230   In addition to these flux estimates, the GCBs document uncertainties, expressed as one
231   standard deviation around the mean. Figure 1 shows the relative error of these estimates
232   (uncertainty/mean) as they progress along the years for the 2006-2019 budgets. The estimates
233   refer to each individual year for which the budget was prepared. As such, they indicate the
234   progression in understanding of the uncertainties in the budget at that time (as opposed to an *a*
235   *posteriori* analysis of the uncertainties of all years in a similar manner). The relatively low,
236   stable uncertainties associated with both the fossil fuel emissions and atmospheric CO_2
237   concentrations result from two factors (Ballantyne et al., 2012). The first is the precision of the
238   atmospheric in situ CO_2 measurements and efficient mixing of CO_2 throughout the atmosphere,
239   although analytical errors and sampling bias do play a role. Second, while fossil fuel combustion
240   is the primary source of anthropogenic CO_2 emissions, the relative error on this contribution is

241 relatively small because the fossil fuel industry provides reliable numbers on their sales, which
242 are well correlated with the amount of fossil fuel burned. The highest relative errors are
243 associated with land use change emissions. These estimates are based on either bookkeeping
244 methods (Houghton, 2003; Houghton and Nassikas, 2017), and since 2018, also on DGVMs
245 (Friedlingstein et al., 2019, 2020). Compared to the early period, 2000-2006, the relative error
246 has not substantially decreased, nor has the mean value of the land use change emissions of 1.5
247 to 1.8 Pg C yr^{-1}, respectively.

248 In the GCB published in 2016 and before, the land sink was calculated as a residual: land
249 sink = emissions - atmosphere - ocean sink. Since 2017, the land sink in the Global Carbon
250 Budget has been calculated directly from DGVMs with a corresponding increase in relative error
251 due to the divergence of the individual DGVM estimates. Since then, the ocean sink estimate
252 from models is no longer normalized to a data-based estimate from the 1990s (Denman et al.,
253 2007), which was previously applied to ensure the land sink estimate from the budget residual
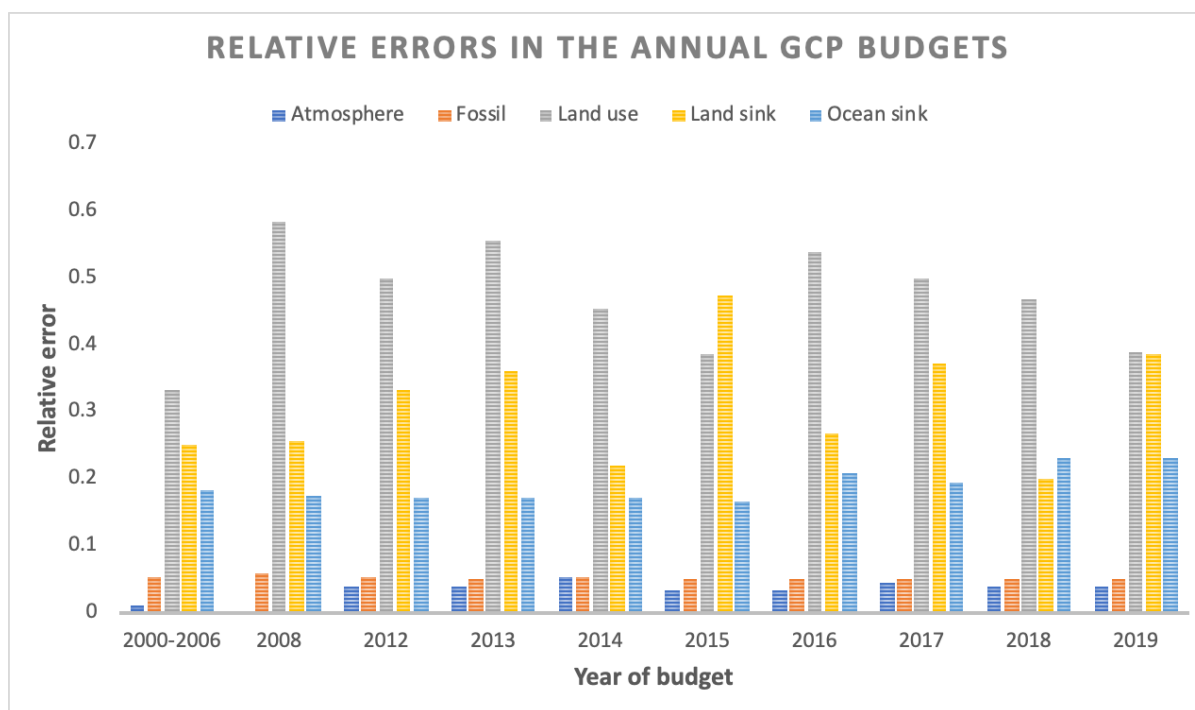

Figure 1. Relative error (1 standard deviation uncertainty / mean) for the Global Carbon
Budget estimates since 2000. Numbers are taken for the individual year(s) reported each year
from Canadell et al. (2007), LeQuéré et al. (2009) and LeQuéré et al. (2013-2018) and
Friedlingstein et al. (2019-2020) and refer to the annual estimates.

254 had a realistic mean value. This change in methodology also affected the ocean sink uncertainty,
255 which slightly increased from 17% in 2015 to 19% in 2016. The fact that the ocean sink was no
256 longer scaled to the mean 1990s value led to a smaller ocean sink estimate that, together with the
257 same absolute uncertainty, resulted in the slightly higher relative uncertainty. The ocean sink
258 uncertainty had also varied between 17 and 19% for the years 2006 to 2015.

259 With the advent of a direct estimate of the land sink from DGVMs, it is now possible to
260 assess the degree to which the overall global carbon budget can be closed, i.e., the difference

261 between the sum of the fluxes and the atmospheric accumulation. This budget imbalance was
262 estimated at 0.3 Pg C for 2018 and 2019, or approximately 10% of the magnitude of the land and
263 ocean sinks (Friedlingstein et al., 2019, 2020). The budget imbalance indicates that there remains
264 substantial uncertainty in global annual mean fluxes.

265 **4   The Ocean Carbon Cycle**

266 The ocean holds a large natural reservoir of carbon that exchanges with the atmosphere
267 on short (non-geological) time-scales. Superimposed upon the cycling of this natural reservoir,
268 the increasing atmospheric CO_2 concentration is causing the ocean to absorb a significant
269 fraction of anthropogenic carbon emissions. Due to the natural carbon cycle of the ocean, 39,000
270 Pg C is stored in the ocean, which amounts to ~90% of the carbon contained in the combined
271 land, ocean and atmosphere domains (Bolin 1983; Sundquist 1993; Sabine and Tanhua, 2010).
272 The natural carbon cycle is driven by ocean circulation, seasonal heating and cooling, and
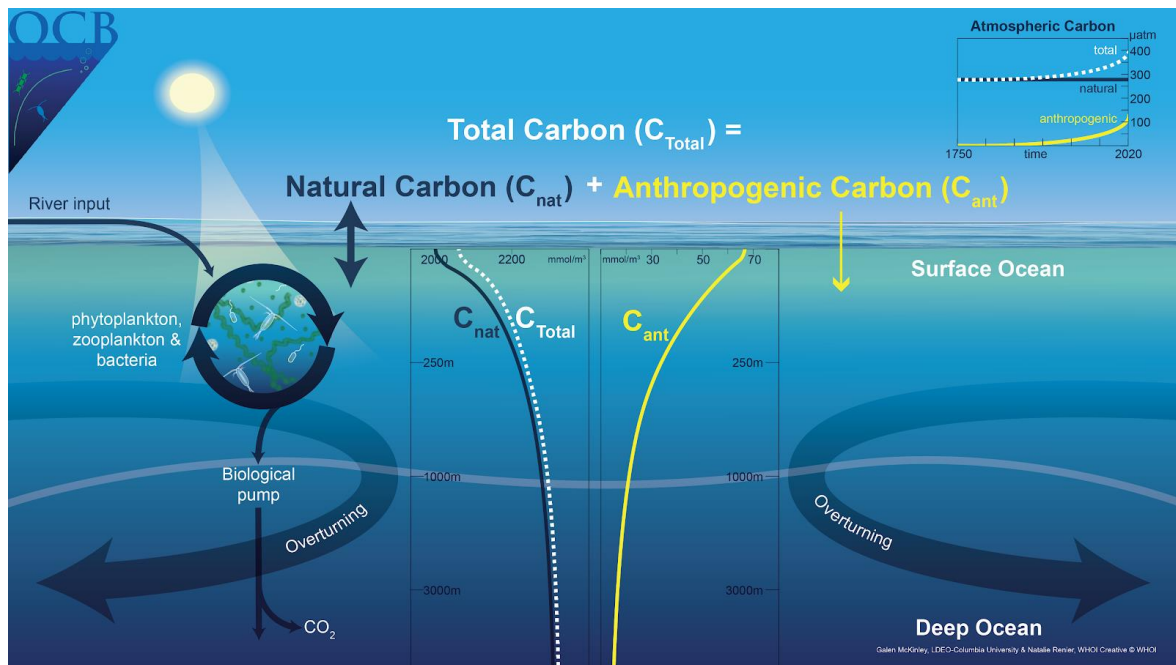273 biological processes (Figure 2, left).

Figure 2: The total carbon cycle in the ocean (C_{Total}) is the sum of the natural carbon cycle
(C_{nat}) and the anthropogenic carbon cycle (C_{ant}). The natural carbon cycle is quantitatively
dominant, as shown in the observed data (GLODAPv2, Olsen et al., 2016) plotted in the
center, and includes contributions from biological activity and the large-scale circulation of
the ocean. Overlain is the uptake of additional carbon due to anthropogenic emissions to the
atmosphere that occurs in the present ocean as atmospheric pCO_2 continues to rise.

274 The ocean carbon budget can be quantified as the storage of inorganic and organic carbon
275 in the ocean, the fluxes of carbon across the air-sea interface, river input, and a small term for
276 sedimentation. The natural carbon inventory is very large compared to the anthropogenic
277 component and is believed to have been in an approximate long-term steady state in preindustrial
278 times, such that there was zero global mean air-sea flux of natural carbon (F_{nat}). The

279 anthropogenic uptake flux (F_{ant}) is the additional ocean uptake due to the direct effect of
280 increasing atmospheric CO_2 concentration and occurs as a perturbation to the vigorous natural
281 cycle (Figure 2, right), with the column inventory of anthropogenic carbon (C_{ant}) from the latest
282 data-based estimates mapped in Figure 3 (bottom).

283   The downward increase in natural carbon (C_{nat}) from surface to depth (Figure 2) is
284 largely due to the biological carbon pump (BCP) (Sarmiento & Gruber, 2006). If the BCP did not
285 operate, the atmospheric CO_2 concentration would be around 200 ppm higher (Maier-Reimer et
286 al., 1996). During the last glacial maximum, changes in the efficiency of the BCP may have
287 played an important role in lowering atmospheric CO_2 (Galbraith and Skinner, 2020; Sigman et
288 al., 2010). Biological feedbacks may accompany anthropogenic climate change (Sabine &
289 Tanhua, 2010, Hauck et al., 2015, Moore et al., 2018), but there is significant spread in model
290 projections (Laufkötter et al., 2015, 2016; Frölicher et al., 2016). To date, observed timeseries
291 are too short to provide evidence for long-term biologically-driven trends in the ocean carbon
292 cycle (Henson et al., 2016). Thus, the ocean carbon sink for anthropogenic carbon over the
293 industrial era is currently understood as a physical and chemical process (Figure 2, right). The
294 contemporary (or 'net') air-sea CO_2 flux (F_{net}) is the sum of F_{nat} and F_{ant}. The surface ocean
295 partial pressure of CO_2, pCO_2, CO_2 flux and interior ocean inventory of anthropogenic carbon
296 (C_{ant}) are shown in Figure 3.

297   The ocean surface layer carbon content equilibrates with the atmosphere on time-scales
298 of months. The ocean continually removes C_{ant} from the atmosphere because the ocean
299 circulation transports C_{ant}-laden waters away from the surface layer and into the ocean interior,
300 while the water that returns to the surface tends to have low C_{ant} content. Thus, the ocean
301 circulation is essential to continued CO_2 uptake. At the global scale, the ocean overturns
302 relatively slowly, on timescales of 1000 years. Because of this, 75% of all anthropogenic carbon
303 attributable to the industrial age remains in the upper 1000m (Gruber et al., 2019a). Because
304 carbon is highly soluble in ocean water, the fundamental limit on the rate of anthropogenic
305 carbon uptake by the ocean is the rate of overturning, as it determines how fast waters with C_{ant}
306 uptake capacity are exposed to the surface.

307   Since the beginning of the industrial era, the uptake of C_{ant} by the land carbon sink has
308 been largely offset by emissions associated with land use change. The ocean has therefore been
309 the primary cumulative net C_{ant} sink over this period (Friedlingstein et al., 2019; 2020). Looking
310 forward, the behavior of the ocean carbon sink is expected to continue playing a critical role in
311 determining how much anthropogenic carbon remains in the atmosphere (Randerson et al., 2015,
312 Zickfeld et al., 2016, Schwinger and Tjiputra, 2018).

313   The following sections describe the approaches used to study the ocean carbon sink. A
314 mechanistic understanding of this sink is essential for diagnosing its state and for making reliable
315 future predictions. This requires quantification of carbon stocks and fluxes at higher spatio-
316 temporal resolution than is available from interior data alone. Air-sea fluxes on monthly to
317 decadal timescales are quantified using surface ocean observations and ocean models of varying

318 complexity. Agreement between independent estimates for mean fluxes and temporal variability
319 indicates growing confidence in global-scale mechanistic understanding. Yet, key uncertainties
320 remain and must be resolved to support better predictions for future ocean carbon sink and to
321 allow for reduced diagnostic uncertainty for the global carbon cycle as it evolves. Substantial
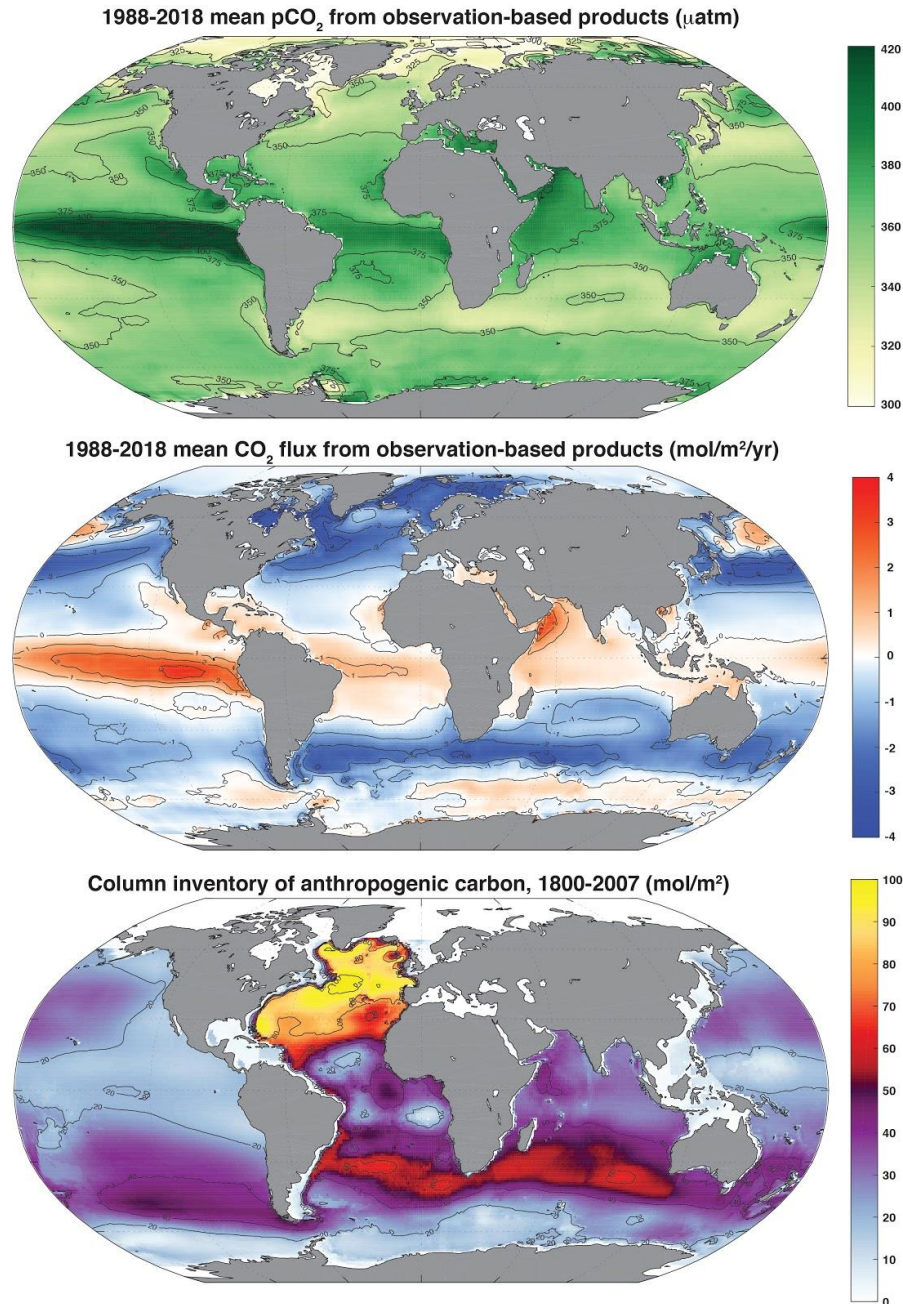322 advances in observing systems, quantification of land-to-ocean fluxes of carbon, and models of

1988-2018 mean pCO$_2$ from observation-based products (μatm)

1988-2018 mean CO$_2$ flux from observation-based products (mol/m²/yr)

Column inventory of anthropogenic carbon, 1800-2007 (mol/m²)

Figure 3: Surface ocean pCO$_2$ (top); and air-sea CO$_2$ flux (F$_{net}$), positive flux to the atmosphere (middle), 1988-2018, mean of 6 observation-based products (Fay et al., in prep); column inventory of anthropogenic carbon (C$_{ant}$, bottom), 1800-2007 (Sabine et al., 2004, Gruber et al., 2019).

323   ocean circulation are needed to reduce these uncertainties. In addition, as nations implement
324   substantial reductions in carbon emissions, we need to assess the near-term response of the ocean
325   carbon sink to reduced atmospheric pCO_2 growth rates.

326   ***4.1   Bottom-up Estimates of Anthropogenic Carbon Accumulation In The Ocean From***
327   ***Interior Observations***

328   Based on a bottom-up accounting using interior ocean data, Gruber et al. (2019a) find a
329   total ocean C_{ant} accumulation of 152 ± 20 Pg C for the industrial era through 2007. By
330   combining evidence from top-down and bottom-up approaches, Khatiwala et al. (2013) find an
331   inventory of 160 ± 26 Pg C in 2010. Consistent with previous inventories (Sabine et al., 2004),
332   these studies find that the ocean has cumulatively absorbed excess carbon equivalent to 45% of
333   industrial-era fossil fuel emissions until 2010, or 30% of the total emissions including LUC. The
334   column inventory of ocean C_{ant} accumulation from Gruber et al. (2019a) is shown in Figure 3
335   (bottom).

336   The amount of C_{ant} estimated for 2010 (160 ± 26 Pg C) represents only about ~0.4% of
337   the ocean carbon stock, indicating the significant challenge of directly observing the temporal
338   change in carbon stock over time. Direct measurements are only possible in areas with rapid
339   change in dissolved inorganic carbon (DIC; e.g. Tanhua and Keeling, 2012). Instead, it is more
340   practical to infer ocean storage of C_{ant} against the large natural background, and then to calculate
341   the change in storage over time. A few different methods have been used to estimate the storage
342   of C_{ant}, either based on observations of biogeochemistry variables, or by transient tracers (see
343   Sabine and Tanhua (2010) for a review).

344   On a global scale, different methods converge within the uncertainties, but significant
345   differences persist regionally (e.g. Waugh et al., 2006, Khatiwala et al., 2009). Multivariate
346   techniques (e.g. Friis et al., 2005, Clement and Gruber, 2018) can be used to disentangle
347   variability and calculate decadal-scale trends. A global estimate of the storage of anthropogenic
348   carbon finds an increase of 34 ± 4 Pg C between 1994 and 2007 (Gruber et al., 2019a), indicating
349   a mean F_{ant} uptake of -2.6 ± 0.3 Pg C (negative flux into the ocean) annually over this time
350   frame. This relatively accurate (~12%) estimate provides an important benchmark for the ocean's
351   role in sequestering anthropogenic carbon, and acts as a direct constraint on the net magnitude of
352   the land flux given low uncertainty on fossil fuel emissions and atmospheric carbon
353   accumulation. The magnitude of the uptake implies that the ocean is continuing to take up
354   anthropogenic carbon at a rate proportional to anthropogenic carbon emissions.

355   A critical element to the success of global estimates of anthropogenic carbon stocks and
356   changes in carbon storage is the GLODAP data product (Key et al., 2004), which collects all
357   carbon-relevant interior ocean data into a product that has undergone the extensive quality
358   control (Tanhua et al., 2010) required to quantify small changes over a large background. This
359   data product is now being released on an annual basis and the GLODAPv2.2020 version contains
360   data from over 1.2 million water samples collected during 946 cruises (Olsen et al., 2020).

361

4.2   Bottom-up Estimates of Ocean-Atmosphere CO_2 Fluxes from Observations of Surface Ocean pCO_2

In order to understand the ocean carbon sink on annual to interannual timescales relevant to climate change policy, more frequent estimates of the sink are required than those produced from decadal timescale interior ocean observations. These data come from observations of the surface ocean partial pressure of CO_2 (pCO_2), and are used to directly estimate net air-sea CO_2 fluxes (F_{net}). The reported variable is surface ocean fugacity of CO_2 (fCO_2) which equals the partial pressure of CO_2 corrected for the non-ideal behavior of the gas (Pfeil et al., 2013). The fugacity of CO_2 is 0.3-0.4% smaller than the partial pressure of CO_2 (Zeebe and Wolf-Gladrow, 2001). For simplicity, we use the terminology pCO_2 to refer to these data for the remainder of this paper. Over the past decade, the number of publicly available observations of pCO_2 has increased rapidly from 6 million in the first release of the Surface Ocean CO_2 Atlas (SOCAT) database (Pfeil et al., 2013, Bakker et al., 2014, 2016, 2020) in 2011 to 28 million in 2020 (www.socat.info). These observations and their automated organization into a consistent database have enabled scientists to create a variety of new observationally-based estimates of the ocean carbon sink that use correlated data (sea surface temperature, salinity and height, chlorophyll, mixed layer depth) to drive upper ocean extrapolation techniques and machine-learning algorithms so as to fill the observational gaps (Rödenbeck et al., 2014; 2015, Landschützer et al., 2013; 2014; 2020; Denvil-Sommer et al., 2019, Gregor et al., 2019).

As the SOCAT database currently offers pCO_2 data for only ~2% of all 1° x 1° locations across the surface ocean, the extrapolation is quite significant. Nonetheless, comparisons of the extrapolated, observationally-based products to independent data indicate relatively low bias and convergence of the independent estimates (Gregor et al., 2019). Root mean square errors (RMSE) range from 10 to 35 µatm. The fact that bias and RMSE comparisons are largely consistent across the variety of approaches suggests that it is data sparsity rather than extrapolation methodology that is now a fundamental limitation on further error reduction (Gregor et al., 2019). Additional tests of the machine-learning based extrapolation approaches using an Earth System Model testbed indicate that they generally have low bias and are skillful in representing the amplitude and timing of seasonality across the global ocean. However, higher and lower frequency variations are more poorly represented because of inadequate sampling on these timescales (Gloege et al., 2020, Stamell et al., 2020). Several challenges remain in using these data, including the uneven distribution of data over time, methodological differences in the calculation of air-sea flux from pCO_2 (Fay et al., 2021, Woolf et al., 2019, Zavarsky and Marandino, 2019), and the potential need for adjustments to pCO_2 data to account for near-surface temperature and salinity gradients (Watson et al., 2020).

Despite the significant extrapolation and remaining uncertainties, it is a major advance for ocean carbon cycle science to have spatially-resolved, data-based estimates of air-sea CO_2 fluxes on monthly timescales. This allows for new investigation into the magnitudes and mechanisms of interannual and decadal variability in the ocean carbon sink, and a key point of comparison to ocean models that were previously the only basis for this analysis. Models are discussed in the next section, and results are compared in the following.

4.3   Bottom-Up Estimates of Ocean-Atmosphere CO_2 Fluxes from Ocean Models

405   Global ocean biogeochemical hindcast models estimate interior ocean carbon cycling
406 and, from this, air-sea CO_2 fluxes. Models simulate the carbon distribution in the ocean with
407 currents, water mass formation and mixing, and for biological carbon turn-over. The bottle-neck
408 for ocean carbon uptake in the models, as in the real world, is the carbon transport across the
409 mixed layer depth. As a result, the models' carbon uptake is sensitive to simulated physics
410 (Doney et al., 2004; Goris et al., 2018; Huber and Zanna, 2017). Models can also provide air-sea
411 flux estimates prior to the 1990s when surface pCO_2 observations were rare.

412   Models are routinely evaluated against observations or observation-derived estimates
413 that characterize the physical and biogeochemical state of the ocean for the last several decades
414 (Doney et al., 2004; Schourup-Kristensen et al., 2014; Aumont et al., 2015; Schwinger et al.,
415 2016; Stock et al., 2020). For the suite of models used in the Global Carbon Budget, comparison
416 of pCO_2 at observed locations from SOCAT reveals the models' ability to capture variability and
417 trends on annual (RMSE <10 µatm) and decadal timescales (RMSE <10 µatm). However, large
418 model-data mismatches on the seasonal timescale also exist (RMSE of 20–80 µatm; Hauck et al.,
419 2020). Despite concurrence on annual and decadal timescales, ocean carbon sink estimates
420 diverge (Hauck et al., 2020), indicating the available data do not fully constrain the models'
421 emergent carbon sink.

422   Global ocean biogeochemical models are routinely used to quantify the ocean sink in the
423 GCB. For example, for 2019, they find that the ocean sink accounted for 22% of 2019
424 anthropogenic CO_2 emissions (Friedlingstein et al., 2020). Models have also shed light on
425 processes behind observed variability such as the weakening of the Southern Ocean carbon sink
426 in response to increased westerlies (LeQuéré et al., 2007), and to explore the role of stationary
427 Rossby waves in subduction of anthropogenic carbon (Langlais et al., 2017). As a component of
428 Earth System Models, ocean models are the single tool for future projections. In the future, on
429 timescales from decadal to centennial, models project a decreased carbon sink efficiency due to
430 changes in the air-sea pCO_2 gradient, ocean circulation and reduced buffer capacity (Schwinger
431 et al., 2014, Randerson et al., 2015, Zickfeld et al., 2016, Schwinger and Tjiputra, 2018, Ridge
432 and McKinley, 2020b).

433 ### *4.4   Reconciling Air-Sea Flux Estimates from Different Methods*

434   We must accurately quantify the ocean sink and understand its mechanisms so that the
435 sink can be monitored as it evolves, and so that reliable projections can be developed. The best
436 window into our current understanding is the degree to which the above-mentioned independent
437 estimates of the present-day sink's magnitude agree. We discuss the degree of agreement in this
438 section, where a negative flux refers to a flux from atmosphere to ocean, and we discuss
439 mechanistic understanding in the next section.

440   Surface ocean carbon observations indicate the net air-sea flux of carbon into the ocean
441 ($F_{net}\sim$ -1.6 Pg C yr^{-1}), while interior measurements offer estimates of the anthropogenic uptake
442 and storage ($F_{ant}\sim$ -2.6 Pg C yr^{-1}). Dynamic hindcast models as used in the GCB estimate the
443 total of anthropogenic perturbations, that is the sum of anthropogenic uptake (F_{ant}) and
444 anthropogenic climate change induced natural carbon fluxes ($F_{nat, ns}$). Closure terms of significant
445 net magnitude (~1 Pg C yr^{-1}) are required to bridge the gap between F_{net} and F_{ant}.

446   To reconcile flux estimates from pCO_2-based data products with ocean models and
447 estimates from interior data, it is well established that an adjustment due to the riverine input of

448 natural carbon that outgasses from the ocean ($F_{nat,riv}$) must be applied (Sarmiento and Sundquist,
449 1992; Aumont et al., 2001; Lacroix et al., 2020). Unfortunately, high quality direct estimates of
450 $F_{nat,riv}$ do not exist, and so the closure between surface flux estimates of F_{net} and F_{ant} remains a
451 significant uncertainty. Lacking better evidence, values typically used are between 0.45 and 0.78
452 Pg C yr^{-1} (Jacobson et al., 2007, Resplandy et al., 2018), with uncertainty estimates that are
453 approximately 100% of these mean values. Anthropogenic changes to the riverine input of
454 carbon are an additional closure term not usually considered with no temporally-resolved
455 estimates available and one estimate for 2000-2010 suggesting it to be small (0.1 Pg C yr^{-1},
456 Regnier et al., 2013). No estimates on anthropogenic changes to the outgassing of the riverine
457 carbon in the ocean are available.

458　　　　It has also been proposed that climate change is having an effect on the natural carbon
459 cycle ($F_{nat,ns}$, Le Quéré et al., 2010; Gruber et al., 2019a). The magnitude of this non-steady state
460 component of the natural carbon cycle is still highly uncertain. $F_{nat,ns}$ has been estimated with one
461 model for the period 1981-2007 (Le Quéré et al., 2010) and with a back-of-the-envelope
462 calculation for the period 1994-2007 (Gruber et al., 2019a), suggesting a reduction of F_{ant} by 10
463 to 15%. Gruber et al. (2019a) estimate $F_{nat, ns}$ by assuming that the accumulation of
464 anthropogenic carbon in the ocean follows a strictly linear scaling with the atmospheric load.
465 However, this assumption is known to hold only when the atmospheric growth is strictly
466 exponential, which has not been the case (Raupach et al., 2014, Ridge and McKinley 2020b), and
467 thus the resulting estimate of +0.38 Pg C yr^{-1} is likely an upper-bound. Another approach for
468 estimating $F_{nat, ns}$ is to use ocean models that represent the natural carbon cycle, and to make a
469 reasonable assumption that the total carbon cycle response to climate variability is dominated by
470 the natural component. With this assumption, models indicate $F_{nat, ns}$ for 1994-2007 of +0.06 to
471 +0.31 Pg C yr^{-1} (DeVries et al., 2019; McKinley et al., 2020). Better quantification of this term is
472 clearly needed.

473　　　　Numbers for the ocean sink efficiency relative to emissions vary between 22% and 45%
474 in the literature (Friedlingstein et al., 2020; Khatiwala et al., 2013; Sabine et al., 2004). These
475 seemingly contradicting numbers are explained by different components of the ocean sink
476 compared to different components of the emissions. Quantitatively the most important choice is
477 the denominator used. For studies of the interior ocean cumulative ocean sink, efficiency is
478 calculated relative to anthropogenic fossil emissions: 45% for the industrial era through 2010
479 (Khatiwala et al., 2013), and 41% for the industrial era through 2007 (Sabine et al., 2004). GCB
480 estimates compare the ocean sink to total anthropogenic CO_2 emissions, which includes
481 emissions to the atmosphere from land-use change. From the GCB, a lower number with an
482 efficiency of 22% compared to total anthropogenic emissions is estimated for 2010-2019. The
483 GCB's approach also includes climate perturbation effects ($F_{nat,ns}$), which reduces the magnitude
484 of the ocean sink.

485　　　　The choice to compare studies of interior ocean accumulation to fossil fuel emissions is
486 motivated by the fact that these numbers are cumulative over the industrial era, and over this
487 time, the land use source and land sink have been in approximate balance. Thus, this approach
488 also circumvents the higher uncertainties associated with land-use changes emissions and the
489 land sink. The GCB's approach, on the other hand, acknowledges that fossil fuel and land-use
490 change emissions increase the atmospheric CO_2 concentration indistinguishably, and this
491 determines the magnitudes of the ocean and land carbon sink.

492 ### *4.5   Recent Evidence for Decadal Variability of the Ocean Carbon Sink*

493   In the mid-2000s, studies using ocean hindcast models suggested a slowing of the ocean
494   carbon sink from the mid-1990s and attributed this change to processes in the Southern Ocean
495   (Lovenduski et al., 2007; 2008; Le Quéré et al., 2007). In the following decade, the release of
496   both the LDEO pCO_2 database and the development of the international SOCAT database
497   allowed for new analyses of trends in air-sea CO_2 fluxes directly from observations (Le Quéré et
498   al., 2009; McKinley et al., 2011; Fay and McKinley 2013). Additionally, a variety of
499   extrapolations of these data to global monthly coverage were developed (Rödenbeck et al.,
500   2015), and a recovery of the ocean carbon sink following the low near the year 2000 was noted
501   (Fay and McKinley, 2013; Landschützer et al., 2015; DeVries et al., 2017; Gruber et al., 2019b).
502   The Southern Ocean was generally identified as a key regional driver of these trends. A number
503   of studies agreed that the stagnation of the Southern Ocean carbon sink in the 90s was related to
504   a trend towards a more positive Southern Annular Mode (SAM) index associated with stronger
505   westerly winds leading to more upwelling of natural carbon and hence dampened net air-to sea
506   CO_2 flux (Le Quéré et al., 2007; Lovenduski et al., 2007; Lenton and Matear, 2007; Hauck et al.,
507   2013).

508   Increasing nutrient concentrations in surface waters of all sectors of the Southern Ocean
509   provide further evidence of strengthened upwelling during the late 1990s (Iida et al., 2013; Ayers
510   and Strutton, 2013; Hoppema et al., 2015; Pardo et al., 2017; Panassa et al., 2018). However, the
511   same driving mechanisms cannot explain the reinvigoration of the sink in the 2000s, as the trends
512   towards a more positive SAM and stronger winds in the 2000s continued. Asymmetric changes
513   in atmospheric circulation (Landschützer et al., 2015), a weaker upper ocean overturning
514   circulation (DeVries et al., 2017) and regional wind variability (Keppler and Landschützer,
515   2019) were proposed as possible explanations, but no consensus was reached on the driving
516   mechanisms of the reinvigoration. Several studies concluded that ocean models were
517   substantially underestimating the magnitude of decadal variability in the ocean carbon sink (De
518   Vries et al., 2019; Gruber et al., 2019b).

519   In the last few years, more observation-based estimates have become available (Denvil-
520   Sommer et al., 2019, Gregor et al., 2019), and now the size of the ensemble of observation-based
521   estimates and of hindcast models is more comparable. With similar size ensembles for both
522   observation-based and hindcast models, estimates of decadal variability are more similar in
523   magnitude and phase, and not as large as the initial observation-based products had suggested
524   (McKinley et al., 2020; Hauck et al., 2020). Both the ensemble of hindcast models and
525   observation-based products indicate a larger ocean carbon sink in the early 1990s, then a slowing
526   of the sink through about 2000, and then a strong and steady recovery through 2018 (Figure 4).
527   In both the products and models, flux variability is largely homogenous across the globe
528   (McKinley et al., 2020). The mechanism driving this variability is still unknown.

529   By representing the surface ocean as a single abiotic box that exchanges water with the
530   deep ocean at a constant rate, McKinley et al. (2020) are able to reproduce the variability of the
531   ocean carbon sink with two external forcings (Figure 4). The two external forcings are the
532   observed atmospheric pCO_2 and surface ocean temperature anomalies caused by eruptions of
533   large volcanoes (El Chichon, 1982; Mt Pinatubo, 1991). This result emerges because the
534   globally-averaged air to sea pCO_2 gradient - the fundamental driver of the flux - is only 6-10
535   µatm, and thus anomalies in the atmospheric growth rate of a few µatm over several years can
536   rapidly modify the global air-sea gradient. Large volcanic eruptions, such as Mt Pinatubo in

537 1991, cause a rapid surface ocean cooling, which increases solubility and creates an uptake pulse
538 (Eddebbar et al., 2019). Then, as the ocean warms from this rapid cooling, solubility is lowered
539 and the sink is damped for 5-7 years beyond the eruption (Figure 4).

540   This model of McKinley et al. (2020) is arguably simple. Yet, it can reproduce the ocean
541 carbon uptake that occurs in the ensemble mean of much more complex models and observation-
542 based products. What does this mean? It can be interpreted simply as Henry's Law operating at
543 the global scale, wherein the partial pressure in the water is moving toward equilibration with the
544 partial pressure in the air. Since the atmospheric pCO_2 continues to increase, the ocean continues
545 to adjust toward equilibrium. In other words, McKinley et al. (2020) demonstrate that the ocean
546 carbon sink temporal variability today is likely dominated by the external forcing from an ever-
547 growing atmospheric pCO_2 concentration. This perspective is consistent with recent analysis that
548 shows heat uptake and interior redistribution in the ocean is far more sensitive to the details of
549 the ocean circulation than is the pattern and magnitude of carbon uptake and storage (Bronselaer
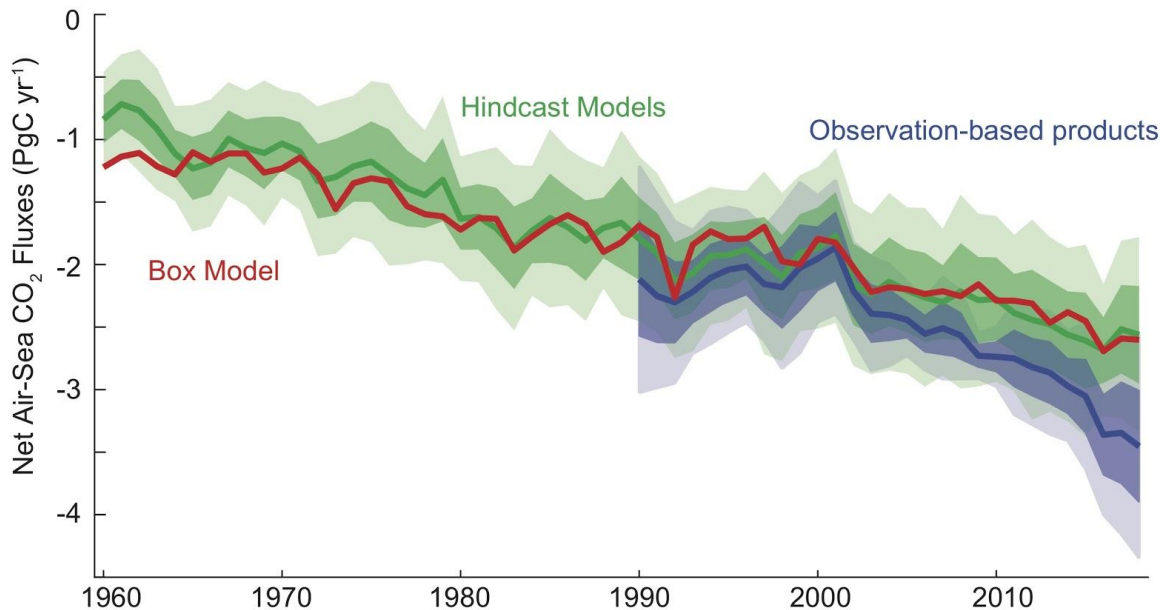550 and Zanna, 2020).

Figure 4. Air-sea CO_2 flux of carbon ($F_{ant} + F_{nat,ns}$) from observationally-based products
(blue), hindcast models (green) and upper ocean diagnostic box model (red); negative flux
into the ocean. Global ensemble means (bold), with 1 sigma and 2 sigma of individual
members (shading). Hindcast ocean models from Global Carbon Budget 2020 (Friedlingstein
et al., 2020). Observationally-based product pCO_2 fields have missing ocean areas filled with
a full-coverage climatology (Landschützer et al., 2020) and air-sea flux calculated as average
of 3 wind reanalyses (CCMP, ERA5, JRA55) with a quadratic parameterization (Wanninkhof
2014, Fay et al., 2021); to this F_{net} estimate, $F_{riv,nat}= 0.62$ Pg C yr^{-1} (Jacobson et al., 2007,
Resplandy et al., 2018) is added. The upper ocean diagnostic box model (McKinley et al.,
2020) is forced with observed atmospheric pCO_2 and surface ocean temperature changes
associated with the eruptions of three large volcanoes (Agung 1963, El Chichon 1982, and
Mt. Pinatubo 1991; Eddebbar et al., 2019).

551

4.6 Advancing Understanding of the Current and Future Ocean Carbon Sink

In order to continue to quantify the global carbon cycle, the constraint provided by the relatively low-uncertainty estimates for decadal anthropogenic carbon accumulation must be maintained. To better quantify fluxes on monthly to decadal timescales, increased observational capacity at the surface and higher fidelity models are needed. In order to be prepared to support climate management efforts in the near-term, the likely behavior of the ocean sink under emissions mitigation must receive increased attention.

Observations of ocean interior carbon require measurements with high accuracy and precision due to the small perturbations on a large background signal. For example, in 2010, the C_{ant} content was ~160 Pg C out of a total inorganic carbon content of ~39,000 Pg C. For the surface ocean flux estimates, the high spatiotemporal variability in pCO_2 and a low average deviation from air-sea equilibrium concentration needed to drive the observed net flux, i.e. a net flux of ~2.5 Pg C yr^{-1} over a total flux of ~90 Pg C yr^{-1}, indicates that accuracy and data coverage are possibly the most important components of the observing system. There is a seasonal bias in the observing system, with fewer observations being made in winter at high latitudes. This is particularly important for observations of surface fluxes, which tend to be high in winter, but less so for the interior ocean observations where seasonality tends to be low below the winter mixed layer.

4.6.1 Expanding autonomous observations:

Although ship-based observations remain a central resource for the carbon observing system, these are expensive and tend to be seasonally biased. Driven by these demands, there is a continuous development of sensors for inorganic carbon system measurements with at least some of these attributes; increased precision and accuracy, lower power consumption and lower instrument drift (Johnson et al., 2016; Sabine et al., 2020; Seelmann et al., 2019; Sutton et al., 2014). Similarly, there is a continuous development of autonomous platforms capable of carrying sensors for ocean carbon. These include moorings (Sutton et al., 2014), profiling floats (e.g. BGC Argo, Claustre et al., 2020), underwater gliders (Rudnick, 2016), and autonomous surface vehicles powered by wind or waves (Sabine et al., 2020). These developments are rapidly changing the capability to monitor ocean carbon with higher spatial and temporal resolution. For instance, observations from Biogeochemical (BGC) Argos floats enable the calculation of surface pCO_2 (from pH and alkalinity estimates) with reasonable accuracy and precision, ~11 μatm (Takeshita et al., 2018; Williams et al., 2017). Although not as good as the 2 μatm target for the ship-based observations, this system has shown potential to fill spatiotemporal gaps in the observations, with important implications for the carbon flux estimates. For example, Bushinsky et al. (2019) report on significantly lower uptake of carbon in the Southern Ocean by including winter time pCO_2 from BGC-Argo floats using a neural network interpolation.

4.6.2 Improved constraints on carbonate chemistry:

Although individual components of the ocean carbon observing system have high technical readiness levels, the new capabilities have not yet been integrated with existing, well-tested technologies to provide an observing system that can quantify ocean carbon uptake to within 10%. One key need is an improved understanding of the ocean inorganic carbonate system. There are four measurable inorganic carbon variables in the ocean - total alkalinity (TA), total dissolved inorganic carbon (DIC), pH and fCO_2. By measuring two out of those, the complete

595   inorganic carbon system can, in theory, be calculated. Small errors in the dissociation constants,
596   the boron-salinity ratio, and small contribution to the total alkalinity from unknown bases, can
597   cause significant discrepancies in directly measured and calculated carbon variables (Fong and
598   Dickson, 2019, Takeshita et al., 2020). A recent study by Álvarez et al. (2020) shows that
599   inconsistencies between calculated and measured pH has decreased during the last decade, and
600   they conclude that improved standard operating procedures for measurements and calculation of
601   pH are urgently needed. An improved understanding of these issues is essential to fully utilize
602   data from, for instance, BGC Argo floats equipped with pH sensors.

603   *4.6.3   High-quality, timely data:*

604   As noted above, the anthropogenic perturbation in the global ocean is more than an order of
605   magnitude smaller than the background natural state. Thus, if we are to track the changing
606   anthropogenic carbon uptake by the ocean, we must maintain very high standards for accuracy
607   and precision of carbon system data. New autonomous technologies offer great promise for
608   expanding the observing system, but cannot be incorporated into the observing system if this
609   substantially increases overall uncertainties. For the foreseeable future, ship-based measurements
610   will continue to be required to calibrate and validate autonomous observations. Cross-over
611   evaluations should occur both with deployment and post-deployment (Fay et al., 2018). At the
612   same time, ocean carbon data should be ingested into publicly-released databases (SOCAT,
613   GLODAP) in a timely manner that supports at least annual diagnoses of the ocean carbon sink. It
614   is essential that these data be carefully quality controlled. As the timescales at which the user
615   community requires these diagnoses become shorter, these data will need to be available more
616   quickly.

617   *4.6.4   Improved quantification of closure terms to link estimates of surface flux and interior C_{ant}*
618   *accumulation:*

619   In order to reduce uncertainties in the global and regional ocean carbon cycle, we need to
620   understand how interior-based estimates of F_{ant} and surface flux estimates of F_{net} are
621   quantitatively linked. A key barrier to this is the significant magnitude and high uncertainty in
622   current estimates for natural fluxes of carbon in rivers ($F_{nat,riv}$) and interannual variability in the
623   natural carbon cycle ($F_{nat,\ ns}$).

624   *4.6.5   Constraining mechanisms of surface flux variability:*

625   Though recent work has identified the important role of external forcing from atmospheric pCO_2
626   and volcanoes in driving ensemble-mean estimates of recent variability of the ocean carbon sink,
627   individual models and individual observation-based products deviate from the mean of the
628   ensembles (Hauck et al., 2020, McKinley et al., 2020). These deviations are due to internal
629   variability of the ocean circulation and biology in each individual ensemble member. We do not
630   currently have understanding of which of these individual estimates best represent the real ocean.
631   To understand the actual total variability of the real ocean carbon sink (total = forced + internal),
632   we need to select the observation-based products and models of highest fidelity. More stringent
633   application of observational constraints can allow for focused analysis of the mechanisms driving
634   variability in the highest-fidelity models and help improve others.

635   Another approach for combining observations and models is through data-assimilation
636   that constrains the model ocean state and fluxes using observations, and closes data gaps by
637   model dynamics rather than extrapolation. While assimilation applications so far have not
638   provided annually updated global ocean sink estimates with full spatial and temporal

639   resolution (e.g., Mikaloff Fletcher et al., 2006; DeVries 2014; Verdy and Mazloff, 2017;
640   DeVries et al., 2019), the first spatially and temporally resolved global data-assimilated models
641   are starting to become available (Carroll et al., 2020).

642   *4.6.6   Potential change in the natural carbon cycle:*

643   Climate change induced modifications of the ocean, such as ocean acidification, warming and
644   ecosystem composition could significantly influence the transport of particulate and dissolved
645   organic carbon from the surface to the interior ocean, i.e. the "biological pump". The efficiency
646   of this transport is a key factor regulating the atmospheric CO_2 concentration and is thought to
647   play a role in regulating glacial / deglacial atmospheric CO_2 (e.g. Galbraith and Skinner, 2020).
648   For instance, Marsay et al. (2015) suggest that a warmer ocean might lead to reduced
649   sequestration of CO_2 by the biological pump. Complex interactions in the marine ecosystem will
650   affect carbon export in a changing climate in ways that are difficult to predict and currently
651   inadequately quantified (Laufkötter et al., 2015, 2016, Frölicher et al., 2016).

652   *4.6.7   The future ocean sink under scenarios of emission mitigation:*

653   On centennial timescales under high emissions scenarios, slowing of the overturning circulation
654   and reduced buffer capacity will significantly slow the rate of ocean carbon uptake (Randerson et
655   al., 2015, Ridge and McKinley 2020b). But how will the ocean sink evolve under the
656   increasingly more likely scenario of emission mitigation (Hausfather and Peters, 2020)? Given
657   that the long-term growth and interannual variability of the ocean sink observed to date is driven
658   by the exponential growth of atmospheric pCO_2 (Joos, 1996, Raupach et al., 2014, McKinley et
659   al,. 2020, Ridge and McKinley, 2020b), the ocean sink can be expected to slow in parallel to
660   slowing in the growth rate of atmospheric pCO_2. In effect, the anthropogenic carbon stuck in the
661   near-surface ocean will begin to equilibrate with the atmosphere and the sink will be
662   significantly reduced in response to the mitigation of emissions. This will occur simply due a
663   change in the growth of atmospheric pCO_2 - no change in the ocean circulation or buffer capacity
664   is required (Ridge and McKinley, 2020b). Slowing of the ocean sink will feedback on the
665   atmosphere, reducing the effectiveness of mitigation actions and increasing climate warming.

666   Though a series of idealized studies have established the general fact that the ocean sink
667   will be reduced with mitigation (Joos et al., 1996, Raupach et al., 2014, Zickfeld et al., 2016,
668   Schwinger and Tjiputra, 2018, MacDougall et al., 2020, Ridge and McKinley, 2020b), the
669   spatially and temporally resolved response of the ocean sink to emission mitigation has received
670   little attention. Thus, we do not know how rapidly the ocean sink will slow, nor where surface
671   flux changes will be most substantial. We do not know what will be required from our
672   monitoring systems to detect these changes.

673   Current uncertainties in ocean models suggest despite the fact that the current ensemble
674   of models largely agrees as to the recent evolution of the sink (Figure 4), there may be
675   substantial divergence in feedback strength and ocean sink response to emission mitigation.
676   Since the majority of the anthropogenic carbon is held in the ocean's thermocline (Gruber et al.,
677   2019a), the circulation here is critical to the ocean sink's near-term response to mitigation
678   (Iudicone et al., 2016, Rodgers et al., 2020, Ridge and McKinley 2020b). There is substantial
679   spread in the regional distribution of ocean carbon uptake in current models (McKinley et al.,
680   2016, Hauck et al., 2020), and major differences in representations of seasonality (Mongwe et
681   al., 2018), which illustrates knowledge gaps with respect to physical and biological processes
682   and their representations in models. In addition, circulation in these critical upper-ocean regions

683 is not consistently represented in state-of-the-art models (Bronselaer and Zanna, 2020).
684 Uncertainties in the ocean sink under mitigation need first to be assessed, and then they need to
685 be reduced by model development efforts so that robust projections can be made. Especially in
686 these first decades of climate management via emission mitigation, there will be great public
687 interest in how emission cuts are changing atmospheric CO_2. Scientists need to be prepared to
688 explain ocean carbon sink changes as they occur.

689 **5   The Terrestrial Carbon Cycle**

690   The terrestrial carbon cycle is characterized by large, spatially diffuse fluxes that should
691 generally balance on multi-year time scales. Its primary stocks and fluxes are summarized in
692 Figure 5. The Gross Primary Production (GPP) was estimated to be 123 Pg C yr^{-1} from an
693 analysis of direct flux observation made by a network of eddy covariance towers (Beer et al.,
694 2010). Roughly one third of this (40.8 Pg C yr^{-1}) is produced in the tropical forests, and one
695 quarter (31.3 Pg C yr^{-1}) in the tropical savannas, making the tropics by far the largest contributor
696 to global GPP. Temperate and boreal forest are estimated to have a GPP of only 9.9 Pg C yr^{-1}
697 and 8.3 Pg C yr^{-1}. When integrated over the globe, the GPP of croplands contributes an estimated
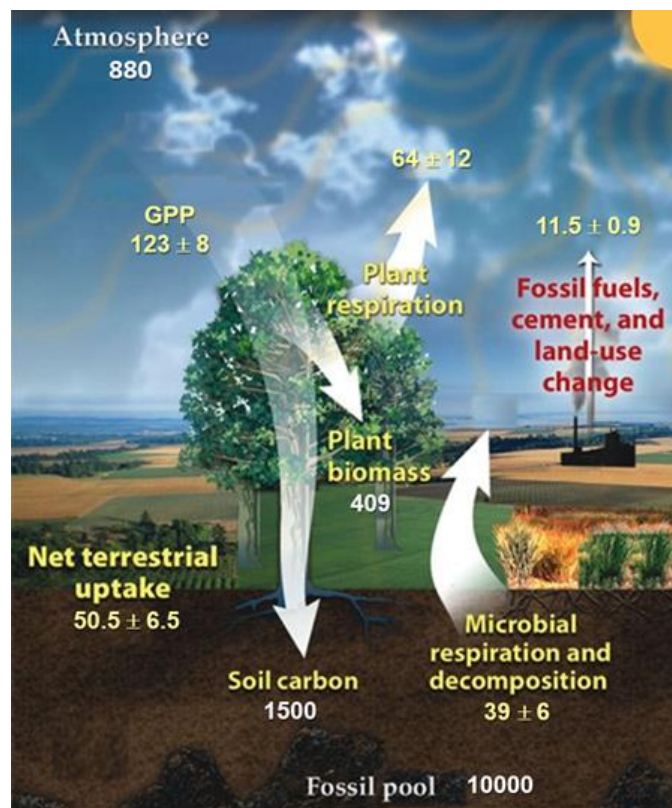698 14.8 Pg C yr^{-1}.

Figure 5: the land carbon cycle, showing the primary fluxes and reservoirs. The sources for
the fluxes, shown in yellow, are listed in Table 2. Stock estimates are shown in white.
Atmospheric carbon stocks were calculated assuming 410 ppm CO_2 and 1.884 ppm methane.
Plant biomass stocks were taken from Spawn et al. (2020). Soil carbon stocks are from
Scharlemann et al. (2014). Fossil pool stocks are from Ajani et al. (2013). (Adapted from
U.S. Department of Energy Genomic Science program - https://genomicscience.energy.gov).

699   Welp et al. (2011), using oxygen isotopes, suggest that this value of Global GPP may be
700   too low and would be closer to 150 -175 Pg C yr^{-1}. However, Anav et al. (2015) argue that Welp
701   et al. used a limited number of observations and a simple model that included gross
702   photosynthesis, but neglected photorespiration by land plants . They note that plants immediately
703   respire away 20-40% of the carbon fixed by photosynthesis. When photorespiration is included,
704   they note that these GPP values are more in line with those obtained from other methods.

705   Global Autotrophic Respiration is estimated at 64 (±12) Pg Cyr^{-1} (Ito, 2020). This is the
706   term that is also called maintenance respiration and consists mainly of dark respiration. Precise
707   determination is difficult as it also involves a substantial below ground component. It is expected
708   to vary with biome and climate (Ito, 2020). Estimates of Net Primary Production (NPP), GPP
709   minus autotrophic respiration, are generally assumed to be of the order of 50% of GPP (i.e. Ito,
710   2020), but Ciais et al. (2020) suggest values in the range of 44-57 Pg C yr^{-1}. They suggest that
711   decomposition of organic matter or soil (heterotrophic) respiration (SHR) produces 39 Pg C yr^{-1}
712   within an interquartile range of 33-46 Pg C yr^{-1}. This estimate is lower than conventionally
713   assumed but agrees with recent large-scale estimates based on site soil respiration measurements
714   (e.g. Jian et al., 2020). An additional flux to the atmosphere of 8.3 ± 9 Pg C yr^{-1} is due to a series
715   of processes listed Table 2. The remainder of GPP-NPP-SHR and these additional losses
716   constitutes how much carbon is currently taken up by the land, and yields a value of the Net
717   Ecosystem Exchange (NEE) of 2.2 ± 0.6 Pg C yr^{-1}. This value is derived from a combination of
718   methods such as close analysis of stock changes, flux measurements and inventories at the
719   continental scale obtained during the Regional Carbon Cycle Assessment and Processes
720   (RECCAP) Project. It is clear from the above description that the terrestrial carbon cycle is
721   complex, composed of many, sometimes interacting elements, that often are not easy to
722   quantify.

Table 2: Land Carbon Fluxes (Note: numbers without uncertainties are assumed to have uncertainties comparable to their stated values.)

Quantity	Flux (P C yr^{-1})	Reference
Gross Primary Production (GPP)	123 ± 8	1
Net Primary Production	~50.5 (44 - 57)	2
Autotrophic Respiration	~64 ± 12	3
Soil Heterotrophic Respiration	39 (33 - 46)	2
Outgassing by Rivers, Lakes and Estuaries	0.8 to 2.3	2
Fires	1.6	2
Consumption of Harvested Crops	1.5	2
Land Use Change	1.1	2
Grazing	1.0	2
Biogenic Reduced Carbon	0.8	2
Decay and Burning of Wood Products	0.7	2
[1]Beer et al. (2010); [2]Ciais et al. (2020); [3]Ito (2020)		

5.1 Bottom-up Estimates of CO₂ Emissions from Land

723

724   Fluxes of carbon between the land biosphere and atmosphere have traditionally been
725   inferred from changes in land carbon stocks. To create a "bottom-up" estimate of the CO_2
726   emissions or uptake due to deforestation, reforestation, disturbance, or land use change requires
727   information about the area affected, the corresponding carbon stock per unit area, and the
728   fraction of carbon exchanged with the atmosphere due to the observed change. In practice, all
729   three of these properties are challenging to quantify accurately (e.g., Saatchi et al., 2011;
730   Ramankutty et al., 2007; Pearson et al., 2017), but all have benefited from new in situ and remote
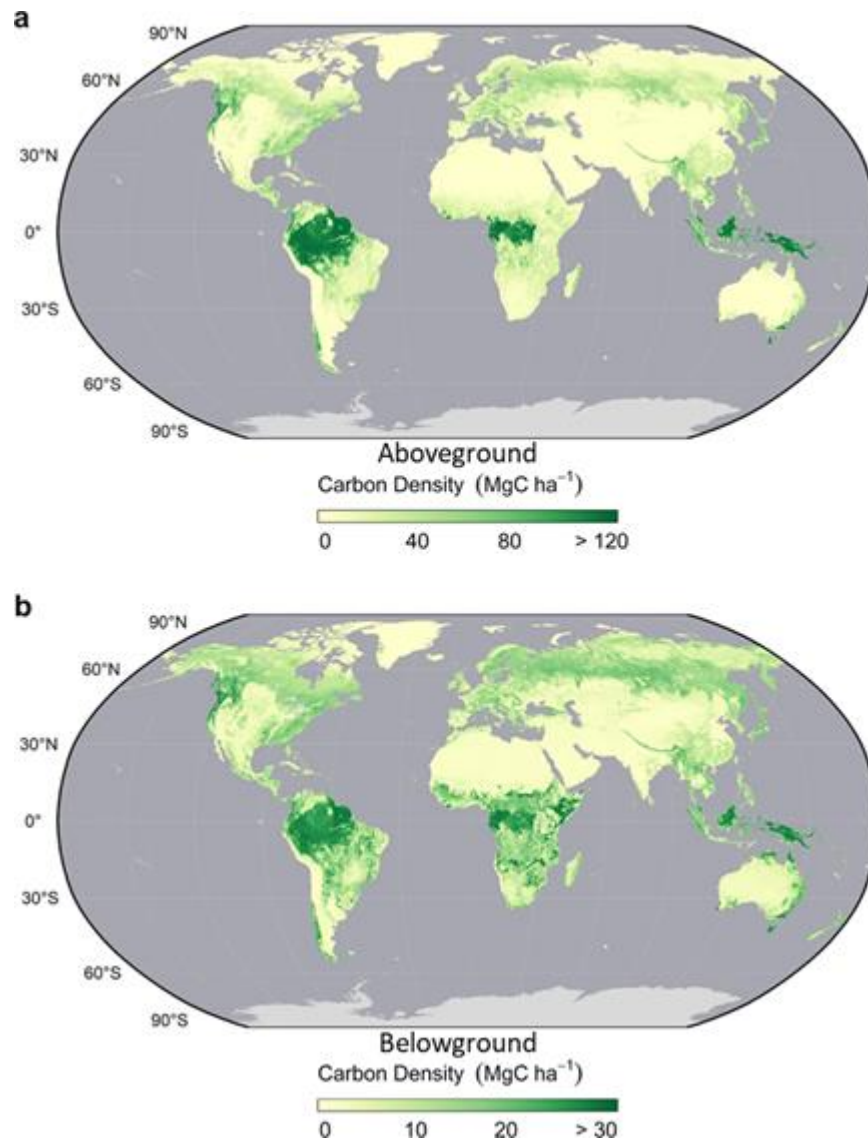731   sensing measurement techniques and more advanced bottom-up modeling techniques.

Figure 6. Maps of above and belowground living biomass carbon densities. (a) Aboveground
biomass carbon density (AGBC) and (b) belowground biomass carbon density (BGBC).
Maps have been aggregated at 5 km spatial resolution (Spawn et al., 2020).

732   Improved estimates of the area affected by the change have been facilitated by the
733   availability of high-resolution space-based remote sensing observations from sensors such as
734   LandSat, Moderate Resolution Spectroradiometer (MODIS) and Sentinel-2. Until recently,
735   estimates of the carbon stocks per unit area associated with above-ground and below ground
736   biomass still relied primarily on in situ measurements collected from a limited number of
737   dedicated research plots at regular intervals (e.g. Pan et al., 2011). However, the increasing
738   availability of above-ground biomass estimates derived from light detection and ranging (Lidar)
739   and radio detection and ranging (radar) sensors on airborne and space-based platforms is
740   providing improved spatial coverage and temporal sampling frequency. Soil carbon inventories
741   still rely exclusively on in situ measurements, that are often characterized by limited spatial
742   coverage and infrequent (decadal) repeat intervals (Ciais et al., 2014).

743   Figure 6 shows a map of global biomass (Spawn et al., 2020). This map was produced by
744   combining and harmonizing several satellite products and site information. This involved using
745   the satellite products of biomass with land cover with machine learning techniques to produce
746   aerial estimates, and link this to below ground carbon density information (see Spawn et al.,
747   2020 for more detail). These estimates yield a total living biomass of 409 Pg C, composed of an
748   above ground biomass of 287 Pg C and a below ground biomass carbon density of 122 Pg C.
749   Note that this is several orders of magnitude smaller than the ocean carbon reservoir, and in fact
750   more comparable to the amount of total anthropogenic carbon stored in the ocean (160 Pg C).

751   CO_2 exchanged between the land and the atmosphere can be measured in situ using
752   networks of eddy covariance flux towers, such as those deployed by FLUXNET (Baldocchi et
753   al., 2001). The global network of eddy covariance sites have grown substantially over the past 25
754   years, with some records spanning that full period. These data provide unique constraints on the
755   CO_2 fluxes from a broad range of vegetation types, climate regions and disturbance types.
756   Globally, this network still has large gaps, particularly in the tropics, and each flux tower has a
757   limited spatial footprint. Thus, early efforts to upscale results from local to regional scales often
758   introduced large uncertainties (Baldocchi, 2003; Jung et al., 2009; Beer et al., 2010; Xiao et al.,
759   2012; Keenan and Williams, 2018).

760   More recent methods that combine flux tower data with other remote sensing data in
761   machine learning algorithms to produce upscaled fluxes (see Jung et al., 2020 for a review) yield
762   global GPP estimates that agree well with those obtained from other methods, while providing
763   insights into the processes controlling the carbon cycle of the land biosphere and their changes
764   over time, particularly in the temperate Northern latitudes. Using radar derived estimates of
765   biomass and soil carbon data from the harmonized world soil database and other sources
766   combined with flux estimates of the global product of Beer et al. (2010), Carvalhais et al. (2014)
767   calculated residence times of carbon. They found that the sensitivity of the residence time to soil
768   moisture and temperature did not agree with the sensitivity of a set of DGVMs, while the overall
769   pattern of increasing residence time at higher latitudes was reproduced. The following sections
770   summarize recent results from bottom-up inventories that combine plot-based in situ
771   measurements and remote sensing observations to constrain the carbon uptake and emissions
772   from the land biosphere.

773   *5.2   Indications of a Declining Tropical Land Sink from Bottom-up Inventories*

774   The carbon sink associated with intact tropical forests has been a major focus of bottom-
775 up inventory methods like those described above. For example, Pan et al. (2011) estimated the
776 intact tropical forest carbon sink to be approximately 1.2 Pg C yr^{-1} over 1990–2007 using an in
777 situ inventory derived from up-scaled plot measurements. Hubau et al. (2020) present a more up-
778 to-date assessment of the carbon sink in African and Amazon forest and conclude that while the
779 African sink strength showed no trend (0.66 Mg C ha^{-1} yr^{-1}), the Amazon forest sink slowed
780 down –0.034 Mg C ha^{-1} yr^{-2} between 1983 and 2010, citing Brienen et al. (2015). The results
781 presented in Figure 7 show that this trend has persisted. Hubau et al. (2020) attribute the
782 downward trend in the sink strength by intact forest primarily to increased mortality of live
783 biomass. Disentangling the compound effects of CO_2 fertilization (i.e. the increased rate of
784 photosynthesis resulting from increased levels of CO_2 in the atmosphere), increased temperature
785 and drought, they imply that chronic long-term environmental change factors, temperature and
786 CO_2, rather than simply the direct effects of drought, underlie longer-term trends in tropical
787 forest tree mortality. Temperature increases enhance respiration and a reduce growth by
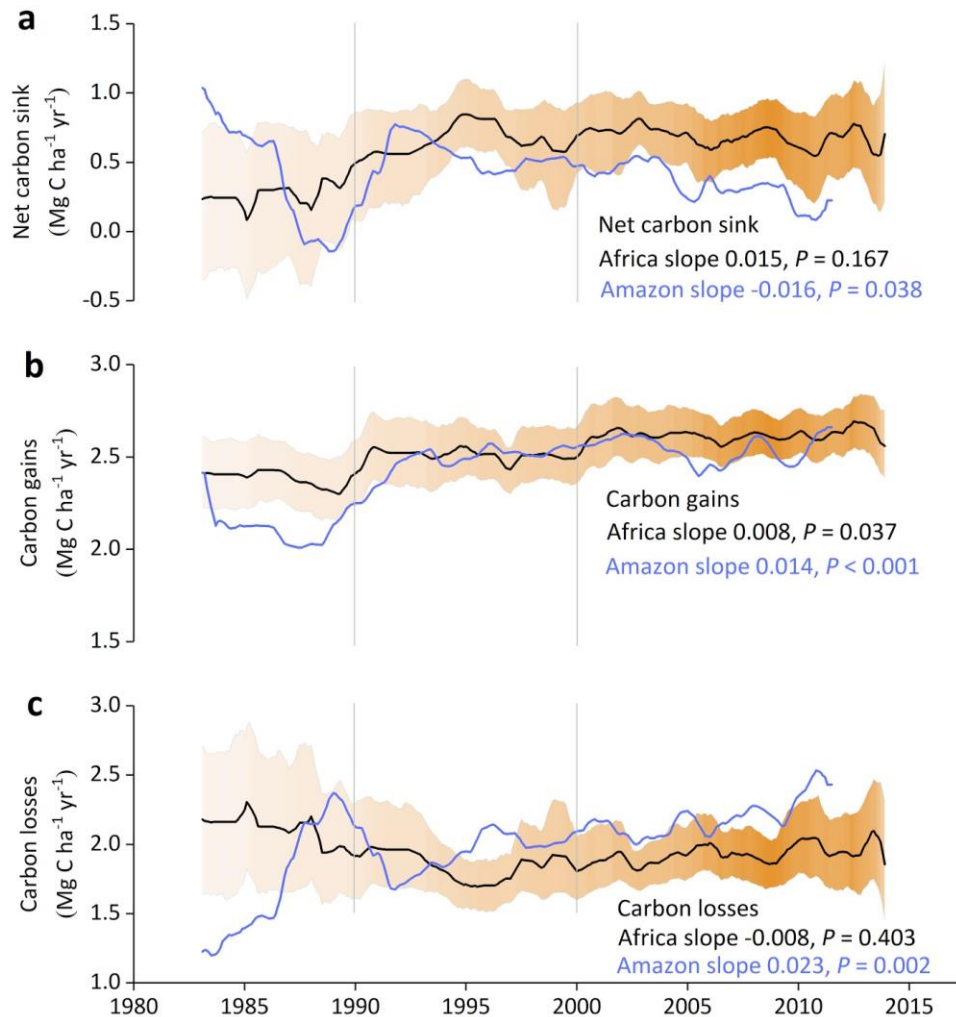788 increasing the vapor pressure deficit (VPD).

Figure 7. Time series of carbon dynamics from structurally-intact old-growth tropical forests in Africa and Amazonia from 1985 through 2015 (Data: Hubau et al., 2020).

789   While it is difficult to show the impact of climate extremes such as strong El Niños using
790 in situ inventory data alone, bottom-up inventories of above ground biomass stocks compiled
791 from microwave remote sensing observations provide a temporally denser record of such
792 impacts. For example, contrary to Hubau et al. (2020), Wigneron et al. (2020) show that there
793 was a strong legacy effect after the 2015-2016 El Niño event in both African and Amazon forest
794 (0.9 and 0.5 Pg C loss in 2014-2017 respectively). For the overall tropics, Fan et al. (2019) use
795 Vegetation Optical Depth (VOD) data from microwave sensors to show how changes in the
796 above ground biomass of the forest of Tropical Africa and Tropical Asia contributed strongly to
797 the interannual variability in CO_2 growth rates, while for semi-arid regions, those of Tropical
798 America were the most important.

799   The net balance of tropical forest biomass remains the sum of the carbon gain from intact
800 forest minus land use change, which is mostly deforestation. Estimates of deforestation in the
801 Amazon fell from about 15000-20000 $km^2\,yr^{-1}$ in the 1990s to about 6000 km^2yr^{-1} in 2016-2017,
802 but have recently peaked again
803 (http://terrabrasilis.dpi.inpe.br/app/dashboard/deforestation/biomes/legal_amazon/rates) to
804 around 10000 km^2yr^{-1}. Preliminary analysis suggests that this increase would cause 12-14
805 teragrams of carbon (Tg C) to be released annually, compared to 8-10 Tg C over the period
806 2005-2015. The strong El Niño of 2015-2016 caused an estimated release of almost 19 Tg C,
807 (https://www.globalfiredata.org/regional.html#amazonas) of which, 75% was due to forests.

808   Another possible cause of mortality could be a decrease in photosynthesis or GPP.
809 Quantitative estimates of these quantities are now available from space-based observations of
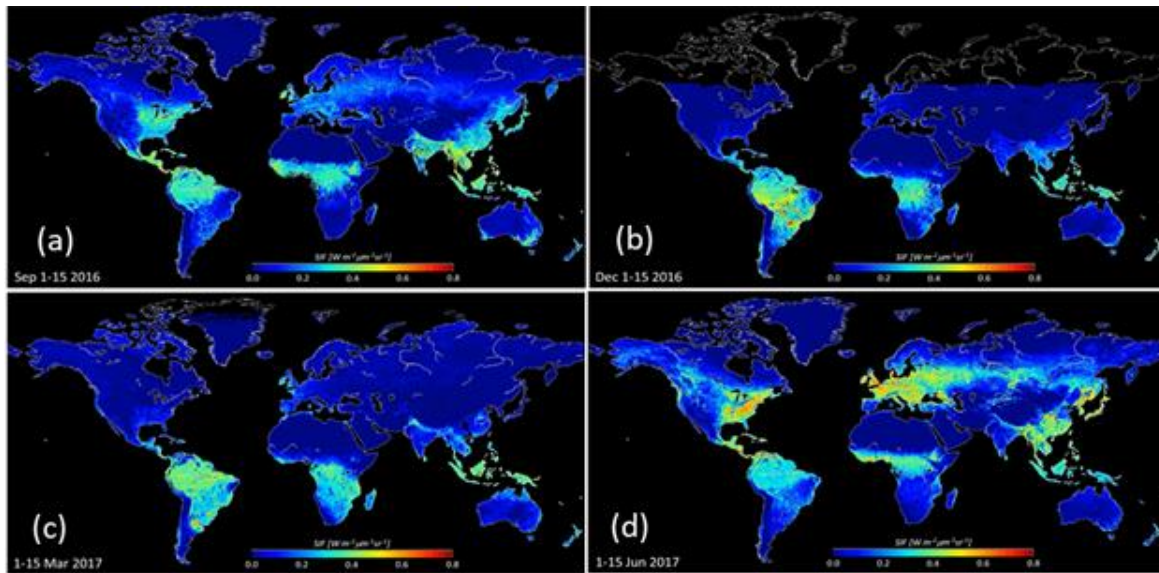810 solar induced chlorophyll fluorescence (SIF). As plants absorb sunlight to perform

Figure 8. OCO-2 observations of SIF for (a) 1-15 September 2016; (b) 1-15 December 2016; (c) 1-15 March 2017, and 1-15 June 2017. Blue indicates low SIF and therefore low photosynthetic activity. The warmer colors indicate higher SIF and higher photosynthetic activity (Ying Sun, Personal communication,2018).

811 photosynthesis, a faction of that light ($< 2\%$) is re-emitted at longer wavelengths (fluorescence),
812 which can be detected in the cores of strong solar Fraunhofer lines by high resolution space-

813 based spectrometers (Frankenberg et al., 2014; Sun et al., 2018). SIF is a rapidly-responding
814 indicator of light use efficiency that has been adopted as a functional proxy for GPP (Figure 8).
815 Koren et al. (2018) find that SIF was strongly suppressed over areas with anomalously high
816 temperatures and reduced availability of soil moisture. SIF fell below its climatological range
817 starting from the end of the 2015 dry season (October), but returned to normal levels by February
818 2016 when atmospheric conditions returned to normal. Importantly, the impacts of the El Niño
819 were not uniform across the Amazon basin.

820 The eastern part of the Amazon experienced a much larger (10–15%) reduction in SIF
821 than the western part (2–5%). Koren et al. estimated the integrated loss of GPP across the
822 Amazon basin relative to eight previous years to be 0.34 – 0.48 Pg C in the three-month period
823 October-December 2015. Ciais et al. (2020) calculated a small sink of 0.06 Pg C yr^{-1} using a
824 combination of top down and bottom up inventories for the whole of South America, albeit with
825 a large uncertainty of 0.29 Pg C yr^{-1}. Thus, in contrast with the African sink, which shows no
826 trend, the Amazon forest sink strength appears to be gradually declining, and that extreme events
827 imposed on this trend cause additional losses.

828 ### 5.3 Evidence for a Global Greening from Bottom-up Inventories

829 In a recent analysis of land use change over 1982-2016, Song et al. (2018) show that
830 global tree cover has increased by 2.24 million km^2 (+7.1%) relative to the 1982 value. This
831 overall net gain is the result of a net loss in the tropics being outweighed by a net gain in the
832 extra tropics. Global bare ground cover has decreased by 1.16 million km^2 (−3.1%), most notably
833 in agricultural regions of tropical and subtropical Asia. Of all land changes, 60% are associated
834 with direct human activities and 40% with indirect drivers such as climate change.

835 Several factors are thought to impact vegetation greening, including rising atmospheric
836 CO_2 concentrations, climate change, nitrogen deposition and land- use changes. Supporting the
837 conclusions of Song et al., using long-term satellite records, Piao et al. (2020) find a significant
838 global greening of vegetated areas since the 1980s, which they suggest has continued past 2010
839 (Figure 9). The most pronounced greening is observed in China and India and is due to
840 afforestation and in particular agricultural intensification. They also analyzed a set of DGVMs
841 that suggest CO_2 fertilization is the main driver of global vegetation greening. In addition,
842 warming was the major cause of greening in boreal and Arctic biomes. However, in contrast to
843 this result and in line with Hubau et al., they find that CO_2 fertilization had negative effects on
844 greening in the tropics. Overall, they suggest that the greening contributed to mitigation of global
845 warming through enhanced land carbon uptake and evaporative cooling, but could also lead to
846 decreased albedo, which could potentially cause local warming.

847   Piao et al. (2020) find widespread greening occurred since the 1980's north of 50ºN.
848   Warming was considered the major cause of greening in boreal and Arctic biomes. However, a
849   small, but persistent browning was seen at 3% of the high latitudes between 1982 and 2014. Such
850   browning trends are caused by trends in disturbances such as fires, harvesting and insect

851   defoliation (Beck and Goetz, 2011). North American boreal forests exhibit browning areas nearly
852   20 times larger than the Eurasian boreal forests. Importantly, dramatic increases in fire
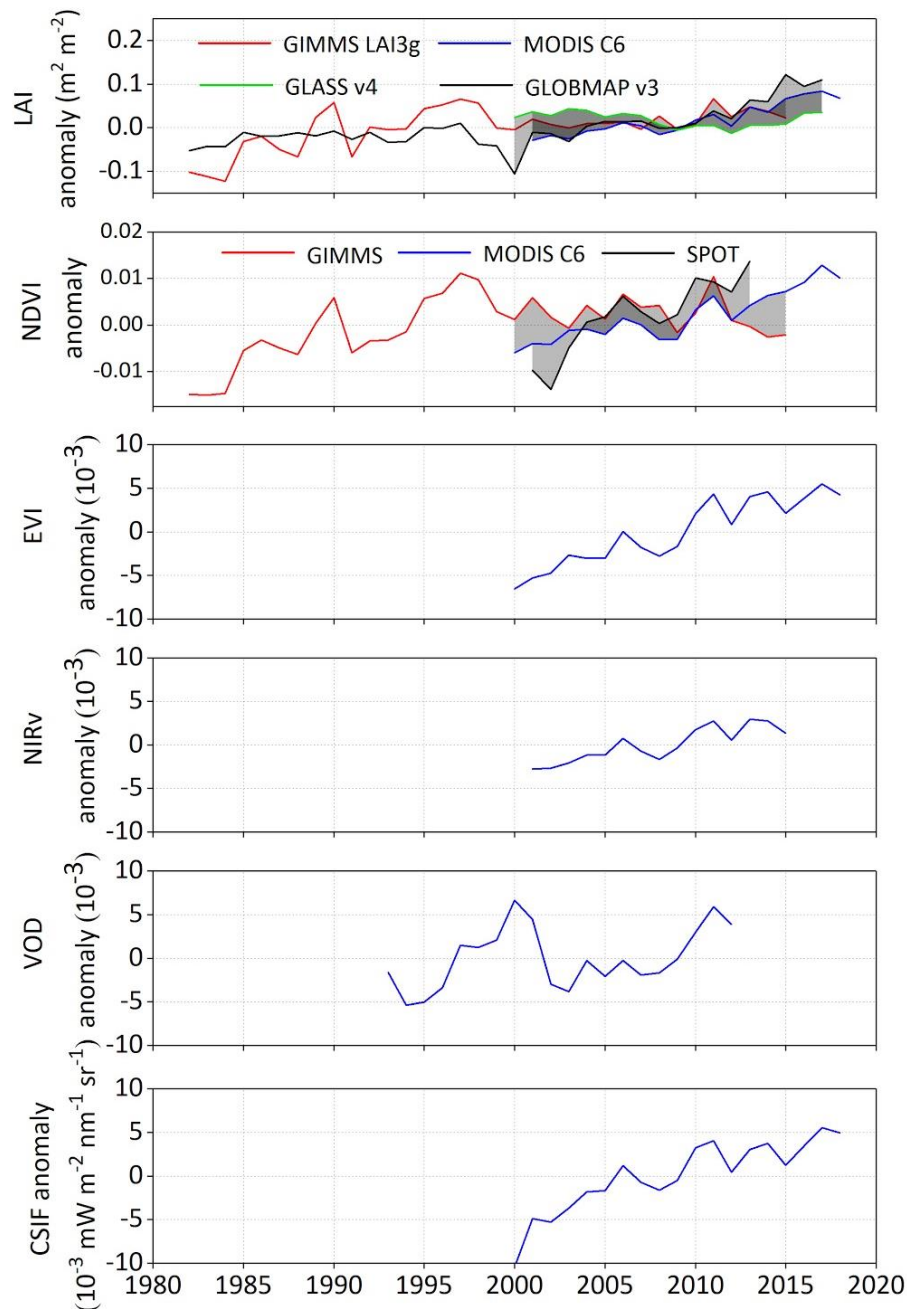
Figure 9. Changes in satellite- derived global vegetation indices, including anomalies in the normalized difference vegetation index (NDVI), Enhanced Vegetation Index (EVI), near-infrared reflectance of vegetation (NIRV), vegetation optical depth (VOD) and contiguous solar- induced fluorescence (CSIF) (Data: Piao et al., 2020.)

853   disturbances and insect infestation such as those from the bark beetle have also been seen in
854   browning areas, partially offsetting the decades long greening trend.

855   While the CO_2 emissions and uptake by agriculture and other land use practices are still
856 highly uncertain, there is growing evidence that these activities are contributing to the global
857 greening trend. Zeng et al. (2014) analyzed the impact of the Agricultural Green Revolution,
858 which enhanced crop yields through hybridization, irrigation and fertilization, on the amplitude
859 of the atmospheric CO_2 seasonal cycle. They use a DGVM to analyze CO_2 observations and
860 atmospheric inversions for the 50-year period extending from 1961 to 2010. Between the
861 decades 1961-1970 and 2001-2010, they attribute the observed the ~15% increase in the CO_2
862 seasonal amplitude to a peak growing season that now starts ~10 days earlier and lasts about two
863 weeks longer, with the land biosphere absorbing ~0.5 Pg more carbon at its peak in July than it
864 did at the beginning of the period. They find that the increased CO_2 seasonal amplitude
865 originates primarily from two regions: the midlatitude cropland between 25º N and 60º N and the
866 high-latitude natural vegetation between 50º N and 70º N. Zeng et al. note that the leading role of
867 mid-latitude cropland in CO_2 uptake is reinforced by recent space-based observations of SIF,
868 which show that at the peak of the growing season, cropland is substantially more productive
869 than surrounding dense forests with similar climate conditions. These conclusions are reinforced
870 by other studies of the relationship between SIF and crop productivity (Guan et al., 2016; 2017;
871 He et al., 2020).

5.4   *Current Status and Next Steps in Bottom-up Land Carbon Observations and Analysis*

873   The overall picture that emerges from recent observations of aboveground biomass stocks
874 is that the classical sinks in the tropical humid forests are slowly losing their sink strength, with
875 these changes amplified by deforestation. In extra-tropical areas, greening has taken place due to
876 afforestation and increased agriculture. At Arctic latitudes, browning, i.e. a loss of vegetation
877 activity, is increasing. These trends provide the fragile background for a still slowly increasing
878 land uptake. The underlying causes for these increases are complex and consist of interacting
879 processes of CO_2 fertilization, nutrient and water availability compounded by climate variability.
880 On top of this, the impact of human activities including deforestation and intensifying agriculture
881 are additional complications.

882   This myriad of interacting processes complicates predictions of the future trajectory of
883 the terrestrial sink. Until now, the sink has grown in harmony with the increase in fossil fuel
884 emissions with the result that the atmospheric fraction has remained remarkably constant over
885 the past 40 years or so. Theoretical and empirical evidence, such as that described here in this
886 paper, suggest that this may stop at some point in the future. Theoretically it is unlikely that the
887 global vegetation will continue to grow indefinitely. Water and nutrient shortages will
888 impede increased growth (Wang et al., 2020). Similarly, the balance between GPP, as
889 determined by plant photosynthetic properties, and the heterotrophic respiration is expected to
890 shift. It has long been known that on short time scales, the efficiency of photosynthesis decreases
891 beyond a critical temperature, while that of heterotrophic respiration continues to increase
892 (Doughty et al., 2008; Mau et al., 2018). This behavior has recently been experimentally
893 confirmed by Duffy et al. (2021) using FLUXNET data. How this works out at longer time
894 scales, when heterotrophic carbon limitation on microbial decomposition may also start playing a
895 role is virtually unknown (Soong et al., 2021). It is likely that the first signs of a deceleration of
896 the terrestrial carbon sink, and a decoupling with the fossil fuel increase are already there, and
897 that the atmospheric fraction will increase.

898 One factor that has impeded progress in the analysis of trends inferred from aboveground
899 biomass stocks is they are not well represented in the current generation of DGVMs. For
900 example, Sitch et al. (2015) use an ensemble of nine DGVMs to study global and regional
901 processes and trends in the land sink for a period extending from 1990 - 2009. They conclude
902 that for this period, the global land sink is increasing, led by CO_2 fertilization of plant
903 production, with the largest increases seen in the natural ecosystems of the tropics. They find no
904 significant trend in northern land regions. This is largely inconsistent with the observations
905 presented above.

906 Another cause for concern is the recent finding that the effects of CO_2 fertilization appear
907 to decline due to nutrient limitations and water availability (Wang et al., 2020). Like the results
908 presented above, this conclusion is, largely based on satellite and ground-based data analysis of
909 NDVI and SIF, and cannot be reproduced by the current generation of DGVMs. A decline in the
910 effectiveness of CO_2 fertilization of the order as suggested by Wang et al. (2020) gives cause for
911 concern of the efficiency of the terrestrial sink going forward. To date, both the land and ocean
912 sink have increased steadily over time such that the airborne fraction has remained relatively
913 stable since the 1960s (Raupach et al., 2014). If the land biospheric processes responsible for
914 maintaining the airborne fraction are disrupted by human activities or climate variability and
915 change, this could compromise our ability to predict the coupled evolution of the land carbon
916 cycle and its interactions with an evolving climate.

917 Fortunately, advances in bottom-up observation capabilities and modeling tools are
918 coming on line to facilitate more comprehensive and responsive monitoring and analysis of the
919 land carbon cycle. Ground-based estimates of stocks and fluxes will continue to provide the most
920 accurate and site-specific information. However, remote sensing observations from airborne and
921 space-based active and passive sensors and modeling tools will play an increasingly important
922 role for upscaling these results to yield useful constraints on regional to global scales.

923 Xiao et al. (2019) review the evolution of remote sensing observations of terrestrial
924 carbon stocks over the past 50 years, spanning the electromagnetic spectrum from the visible,
925 infrared, and microwave. They then review the methods being used to analyze the observations
926 to yield quantitative estimates of carbon stocks and fluxes, including vegetation indices, SIF,
927 light use efficiency models, DGVMs, as well as data driven (including machine learning)
928 techniques. Xiao et al. discuss the use of these data and analysis techniques to quantify the
929 impacts of disturbances and to quantify uncertainties in carbon stock estimates, noting advances
930 achieved by integrating in situ and remote sensing observations into progressively more
931 advanced, process-based carbon cycle models. Looking forward, they predict substantial
932 improvements in our ability to track above ground biomass stocks, through the use of merged
933 datasets, such as the NASA Harmonized LandSat and Sentinel 2 (HLS) products, ultra-high
934 resolution imaging products from QuickBird, IKONOS, and UAVs, lidar measurements from
935 GEDI, future active microwave products from NASA's NISAR (Rosen et al., 2016), TanDEM-L
936 and BIOMASS missions (Quegan et al., 2019).

937 While in situ and space-based measurements of aboveground biomass play a critical role
938 in efforts to monitor trends in managed and natural forest, they are not sufficient for monitoring
939 the rapid turnover of carbon stocks in croplands and grasslands. Until recently, high resolution
940 imaging observations and moderate resolution estimates of vegetation indices provided the
941 primary tools for scaling up plot-based observations to national and continental scales. Recently,
942 these capabilities have been augmented by space-based observations of SIF. SIF relates the

943 emission of excess radiative energy from the photosynthesis process of leaves at two
944 wavelengths 685 nm and 740 nm to photosynthesis, or GPP. Estimates of SIF from GOME,
945 GOME2, GOSAT, OCO-2 and TROPOMI are increasingly being used to monitor crop and
946 grassland productivity and crop yield prediction (He et al., 2020; Peng et al., 2020; Parazoo et
947 al., 2020; Qiu et al., 2020; Yin et al., 2020). Future SIF observations from the ESA
948 FLuorescence EXplorer (FLEX), Japan's GOSAT-GW, NASA's GeoCarb, and the Copernicus
949 CO2M missions promise substantial improvements in resolution.

950 To fully exploit these new measurements to describe long term trends in the terrestrial
951 carbon cycle, the in situ and remote sensing measurements must be reconciled so that their
952 climate data records can be combined to increase their spatial and temporal resolution and
953 coverage. The protocol for cross-validating aboveground biomass products described by
954 Duncanson et al. (2019) and the effort by the Forest Observation Initiative to develop a global in
955 situ forest biomass databases for validating remote sensing observations (Schepaschenko et al.,
956 2018) are positive steps in this direction. While the current generation of DGVMs and other
957 terrestrial biosphere models are evolving rapidly and provided key insights into the
958 processes driving the land carbon cycle, these modeling tools are still yielding widely diverging
959 results the uptake of CO_2 by the land biosphere and its trends (i.e. Fisher et al., 2014; Sitch et al.,
960 2015; Keenan and Williams, 2018; Parazoo et al., 2020). These limitations have raised concerns
961 about their use in CO_2 emission inventory development activities (Grassi et al., 2018; Petrescu et
962 al., 2020). Pioneering model intercomparison efforts such as the Carbon-Land Model
963 Intercomparison Project (C-Lamp; Randerson et al., 2009) are being followed up by the
964 International Land Model Benchmarking (ILAMB) project (see https://www.ilamb.org/) to
965 address these concerns and accelerate the development of these critical tools.

966 **6   The Atmospheric Carbon Cycle**

967 Until recently, the concentrations of atmospheric CO_2 and other greenhouse gases were
968 measured in situ by instruments deployed at surface stations, tall towers or on aircraft.
969 Continuous measurements of atmospheric CO_2 were initiated in 1958 by Charles David
970 Keeling of the Scripps Institution of Oceanography, when he established stations at Mauna Loa,
971 Hawaii and the South Pole. These measurements are now being collected at a global network that
972 includes the U.S. National Oceanic and Atmospheric Administration (NOAA) Global
973 Greenhouse Gas Reference Network (GGGRN), the European Integrated Carbon Observation
974 System (ICOS) network and other partners of the World Meteorological Organization Global
975 Atmospheric Watch (WMO GAW) program. These in situ measurements provide the most

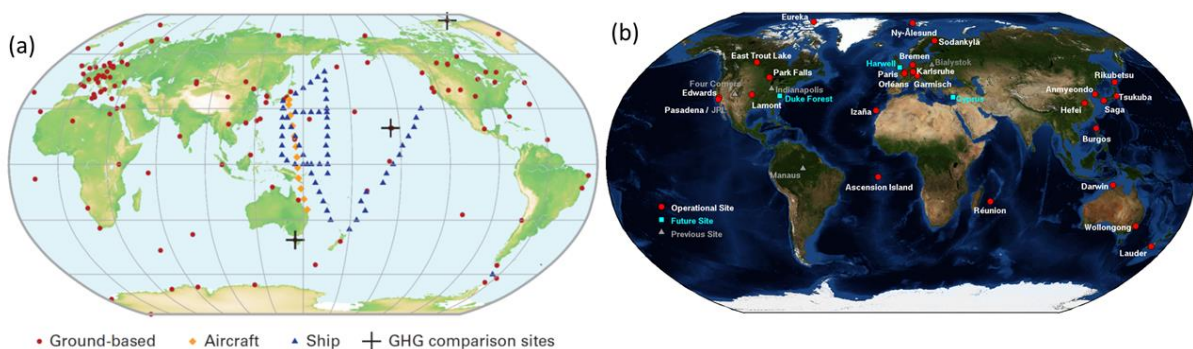• Ground-based   • Aircraft   ▲ Ship   + GHG comparison sites

Figure 10: Spatial distribution of stations in the ground-based atmospheric CO_2 monitoring network. The vast majority of the stations are in North America and western Europe. (a) In situ CO_2 measurements are collected routinely at the WMO Global Atmospheric Watch Stations (from WMO Greenhouse Gas Bulletin, 25 Nov. 2019). (b) Solar-looking remote sensing observations of CO_2 are collected at Total Carbon Column Observing Network (TCCON) stations.

976   accurate estimates of the CO_2 concentrations and their trends on global scales. They also
977   quantify chemical and isotopic tracers, such as carbon-14 (^{14}C), which help to discriminate fossil
978   fuel from biogenic contributions to the observed CO_2 trends. Perhaps the most important asset of
979   the ground based in situ measurements is the length of their climate data records, which now
980   extend over 70 years. While the ground-based networks have grown over time, the spatial
981   resolution and coverage of in situ measurements are still far too limited to identify and quantify
982   the natural and anthropogenic emission sources emitting CO_2 into the atmosphere and the natural
983   "sinks" absorbing it at the surface on spatial scales ranging large urban areas to nations. The
984   coverage is particularly sparse in Arctic, boreal and tropical land regions and over most ocean
985   basins (Figure 10).

986   Recent advances in space based remote sensing capabilities are providing new insights
987   into the current state of the atmospheric carbon cycle as well as the primary processes controlling
988   its interactions with the land and ocean carbon reservoirs. With the launch of Japan's
989   Greenhouse gases Observing SATellite, GOSAT in 2009, and NASA's Orbiting Carbon
990   Observatory in 2014, space-based remote sensing measurements are complementing the ground-
991   based and airborne CO_2 measurements with much greater spatial resolution and coverage,
992   yielding tens of thousands of observations over the sunlit hemisphere each day. These two
993   satellites have recently been joined by their sister missions, GOSAT-2 and OCO-3, providing
994   additional coverage and resolution. These space-based sensors collect high-resolution spectra of
995   reflected sunlight within molecular oxygen (O_2) and CO_2 bands that can be analyzed to yield
996   precise, spatially resolved estimates of the column-averaged CO_2 dry air mole fraction, XCO_2.
997   The principal challenge of this technique is the need for unprecedented levels of precision and
998   accuracy for a space-based atmospheric trace gas measurement. While intense local sources,
999   such as large coal-fired power plants or large urban areas can increase the near surface CO_2
1000   concentrations by more than 10%, these variations decay rapidly with altitude, such that they
1001   rarely yield XCO_2 variations larger than 1-2 ppm (0.25 to 0.5%) on the spatial scale of a satellite
1002   footprint (1 to 100 km^2). Natural sinks of CO_2, such as forests or ocean basins, produce even
1003   smaller changes in XCO_2.

1004   In addition to XCO_2, these sensors collect simultaneous observations of SIF, providing
1005   additional constraints on the CO_2 uptake by the land biosphere. The primary challenge of this
1006   approach is the need for unprecedented precision and accuracy to resolve the small ($< 0.25\%$ or 1
1007   ppm) XCO_2 variations associated with surface sources and sinks of CO_2. While these space-
1008   based measurements are not as accurate as those collected by ground-based and airborne
1009   systems, they complement those observations with improved coverage and spatial resolution.

1010   Atmospheric CO_2 estimates collected by ground-based, airborne, and space-based sensors
1011   are now being assimilated into atmospheric inverse models, along with meteorological data and
1012   space based global measurements of the land biosphere to provide new insights into the carbon
1013   cycle. These models illustrate the spatial and temporal relationships between SIF and the
1014   seasonal CO_2 drawdown in the northern hemisphere spring (Eldering et al., 2017; Byrne et al.,
1015   2018; Yin et al., 2020; Qui et al., 2020). They have also been used to quantify the atmospheric
1016   signature of the land biosphere's response to the record-setting 2015-2016 El Niño (Chatterjee et
1017   al., 2017; Liu et al., 2017; Palmer et al., 2019). The high spatial and temporal resolution of these
1018   atmospheric CO_2 observations, combined with their global coverage, should facilitate the
1019   development of improved diagnostic models for studying processes operating in the present-day
1020   carbon cycle. This evolving land-ocean-atmosphere carbon monitoring system also fosters the

1021   development of more comprehensive and reliable prognostic models for predicting the evolution
1022   of the carbon cycle as it responds to climate change.

1023   From a carbon monitoring perspective, these atmospheric measurements are now
1024   providing quantitative constraints on CO_2 emission and uptake at policy relevant spatial and
1025   temporal scales. CO_2 estimates retrieved from GOSAT and OCO-2 measurements clearly show
1026   persistent positive anomalies associated with the anthropogenic emissions over East Asia,
1027   Western Europe and eastern North America (Hakkarainen et al., 2016; 2019; Wang et al., 2018).
1028   On smaller scales, space-based XCO_2 estimates are being used to quantify CO_2 emissions from
1029   large urban areas (Hedelius et al., 2018; Wu et al., 2018; Wu et al., 2020) and individual power
1030   plants (Nassar et al., 2017; Reuter et al., 2019). Estimates of CO_2 emissions and uptake derived
1031   from atmospheric measurements of XCO_2 are not as source specific as traditional bottom-up
1032   statistical methods, which infer CO_2 emissions from fuel use, power generation statistics, etc.
1033   However, they complement those methods by providing an integral constraint on the total
1034   amount of CO_2 added to or removed from the atmosphere by all natural and anthropogenic
1035   processes.

1036   The availability of high spatial resolution atmospheric emissions products within a few
1037   weeks of acquisition could help to identify and track rapidly-evolving emission hotspots that are
1038   often missed in the bottom-up statistical inventories. As these tools are integrated into a more
1039   comprehensive carbon management system, they could also help carbon managers to assess the
1040   effectiveness of their carbon management strategies, and help to identify emerging emission
1041   reduction opportunities.

1042   ***6.1   The Tropical Land Carbon Cycle Did Not Recover as Expected from 2015–2016 El Niño***

1043   As noted above, bottom-up inventories indicate that the strength of the tropical forest sink
1044   is gradually declining over time. This conclusion is reinforced by atmospheric CO_2 observations.
1045   Gatti et al. (2014), using in situ observations of atmospheric CO_2, determined that the Amazon
1046   basin lost 0.48 ± 0.18 Pg C yr^{-1} during a dry year (2010), but was carbon neutral (0.06 ± 0.1 Pg C
1047   yr^{-1}) when measurements were taken during a wet year (2011). Correcting for carbon losses, they
1048   derived a basin net biome exchange that was carbon neutral during the dry year. During the wet
1049   year, vegetation was a net carbon sink of 0.25 ± 0.14 Pg C yr^{-1}. The latter value compares well
1050   with the bottom-up estimates by Hubau et al. (2020).

1051   The availability of time-resolved global measurements of atmospheric CO_2 at high spatial
1052   resolution is providing a more comprehensive description of impacts of severe weather and
1053   climate on the exchange of carbon between land and ocean reservoirs and the atmosphere on
1054   regional scales. These emerging capabilities were recently demonstrated in studies of the record-
1055   setting 2015-2016 El Niño. GOSAT and OCO-2 measurements collected over the central and
1056   eastern tropical Pacific basin were combined to quantify 0.5 ppm XCO_2 decreases associated
1057   with reductions in outgassing in the tropical Pacific Ocean during March through July of 2015
1058   (Chatterjee et al., 2017). These reduced CO_2 values were then replaced by 0.5 to 2 ppm increases
1059   in XCO_2 associated with reduced uptake and increased emissions of CO_2 by tropical forests in
1060   South America, Africa and tropical Asia (Liu et al., 2017; Heymann et al., 2017; Palmer et al.,
1061   2019; Crowell et al., 2019; Figure 11).
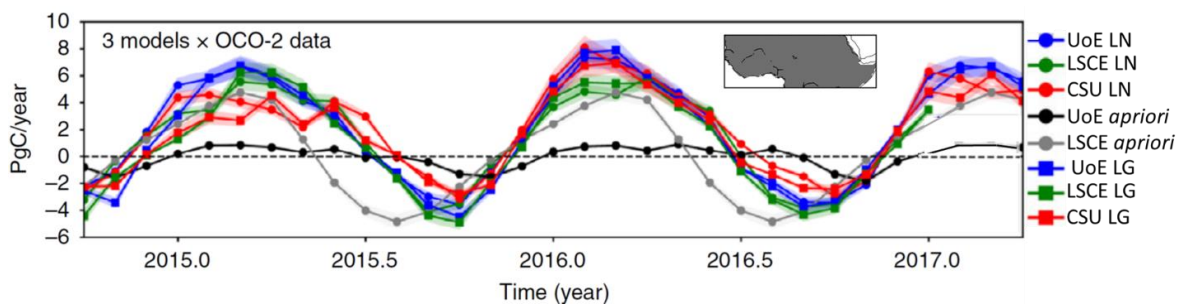
Figure 11. CO_2 fluxes from tropical northern Africa inferred from the University of Edinburgh (UoE), LSCE and Colorado State University (CSU) models constrained by in situ CO_2 measurements as well as XCO_2 data from GOSAT and OCO-2. Positive fluxes indicate CO_2 emissions from the land surface to the atmosphere. LN and LG denote OCO-2 XCO_2 measurements taken using nadir and glint observing modes, respectively. The geographical region is shown in the inset. Fluxes inferred from OCO-2 data have larger amplitudes and a larger seasonal cycle than those from in situ data. An extended mission will provide new opportunities to validate these results and track their changes (Adapted from Palmer et al., 2019).

1062   Liu et al., (2017) find that the pan-tropical biosphere released an additional 2.36 ± 0.34
1063   Pg C into the atmosphere, or about 78% of the global total. Emissions originated throughout the
1064   tropics with 0.91 ± 0.24, 0.85 ± 0.21, and 0.60 ± 0.31 Pg C from tropical South America, tropical
1065   Africa, and tropical Asia, respectively. Although the enhanced emissions from these three
1066   regions were comparable, *different* processes appeared to dominate in each region. Fire
1067   emissions dominated over tropical Asia. Both increased respiration and fires associated with
1068   historically high temperatures dominated over tropical Africa. Increased CO_2 over the Amazon
1069   was attributed to GPP reductions associated with drought. These results support the hypothesis
1070   that El Niño related increases in CO_2 growth rates are primarily due to tropical land carbon
1071   fluxes, but they show that specific mechanisms can differ from continent to continent.
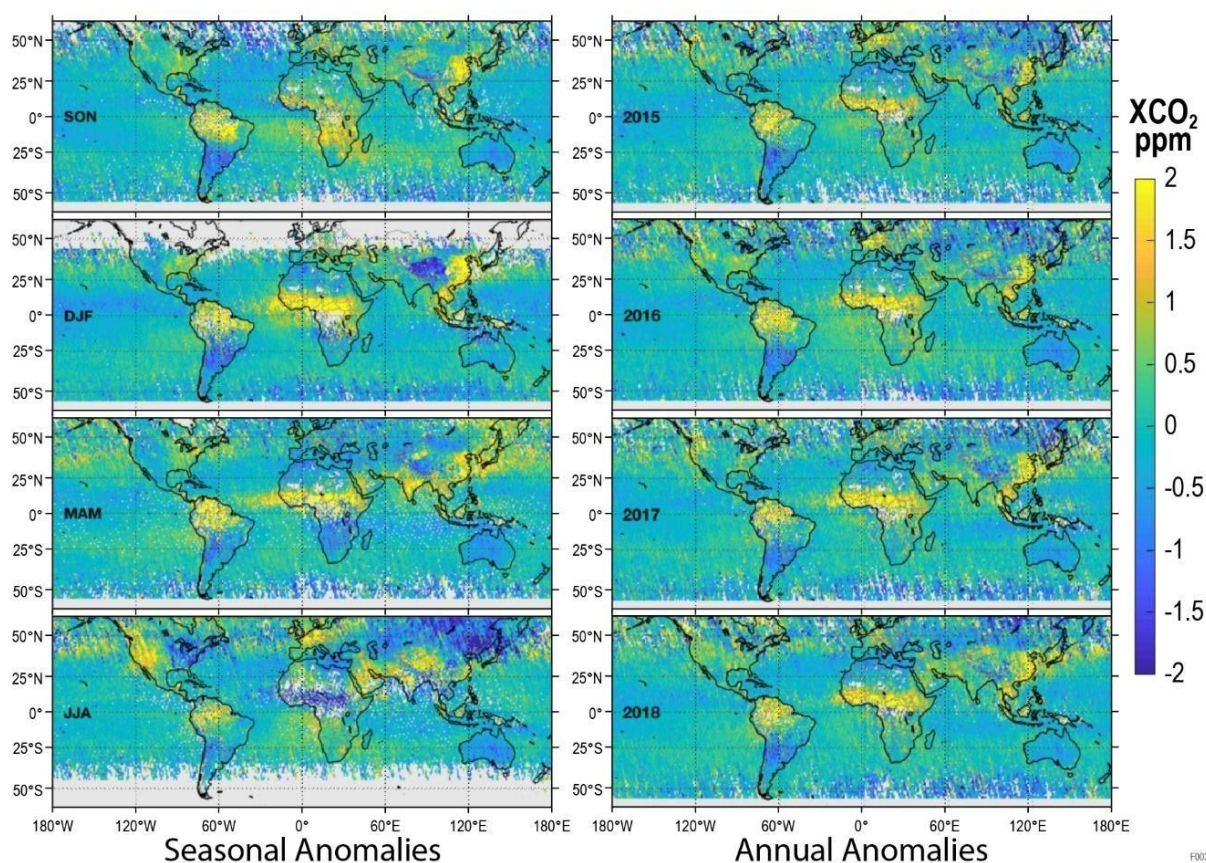
Figure 12. OCO-2 XCO_2 estimates indicate that some regions have persistently high
(positive) or low (negative) spatial anomalies that persist from season to season (left,
integrated over the four-year period) and from year to year (right). A longer data record is
needed to determine whether the tropical anomalies reflect short-term climate variations or
long-term climate trends. (Adapted from Hakkarainen et al., 2019).

1072   Palmer et al., (2019) use three different models to analyze *in situ* CO_2 measurements
1073   along with XCO_2 and SIF observations from Japan's Greenhouse gases Observing SATellite
1074   (GOSAT) and OCO-2 (Figure 11). Like Liu et al., in 2015–2016, they find that the largest CO_2
1075   emissions over western Ethiopia and western tropical Africa, where there are large soil organic
1076   carbon stores and substantial land use change. While the amplitude of the XCO_2 anomalies that

1077   produced these sources may have been overestimated in the early OCO-2 XCO$_2$ products used in
1078   this investigation (version 7), they clearly reveal important components of the tropical carbon
1079   budget that is largely missing from in carbon flux inverse models constrained by *in situ*
1080   measurements alone.

1081   As the 2015-2016 El Niño transitioned to a weak La Niña in 2017, and then to more
1082   neutral conditions in 2018, OCO-2 XCO$_2$ and SIF estimates indicate that tropical forests, once
1083   thought to be significant net sinks of CO$_2$ (Pan et al., 2011; Sellers et al., 2018) may now be
1084   persistent net sources (Hakkarainen et al., 2019; Palmer et al., 2019; Crowell et al., 2019).
1085   Hakkarainen et al. (2019) processed OCO-2 Version 9 (V9) XCO$_2$ data to remove the seasonal
1086   cycle and reveal spatially persistent anomalies. They find positive XCO$_2$ anomalies over tropical
1087   forests with amplitudes as high as 2 ppm above the background (Figure 12). The spatial extent of
1088   the Amazon anomaly was slightly greater during the 2015–2016 El Niño than in 2017, but the
1089   positive XCO$_2$ anomalies there have persisted from season to season and from year to year
1090   throughout the OCO-2 mission. The Amazon is now a persistent *source* of CO$_2$, rather than a
1091   sink. Positive anomalies over topical Africa and Southeast Asia are seen on annual time scales.
1092   However, in Figure 11, tropical African fluxes are negative during June-July-August (JJA),
1093   indicating that this region becomes a weak sink during that season (Palmer et al., 2019). These
1094   conclusions are supported by some satellite-based aboveground biomass studies (Baccini et al.,
1095   2017; Wigneron et al., 2020), but are inconsistent with plot-based studies (Pan et al., 2011;
1096   Hubau et al., 2020), which conclude that tropical forests are absorbing less CO$_2$, but are still a
1097   net sink of carbon.

1098   Additional insight into the tropical land carbon cycle can be obtained by comparing
1099   XCO$_2$ anomalies to observations of SIF. Specifically, the largest positive CO$_2$ anomalies derived
1100   from the space-based XCO$_2$ estimates are seen in regions where SIF observations indicate the
1101   highest photosynthetic activity (Figure 8). This suggests that in spite of significant growth,
1102   tropical forests are now emitting more CO$_2$ than they absorb, when integrated over the annual
1103   cycle. This may have always been the case, but it may also be due to increased respiration,
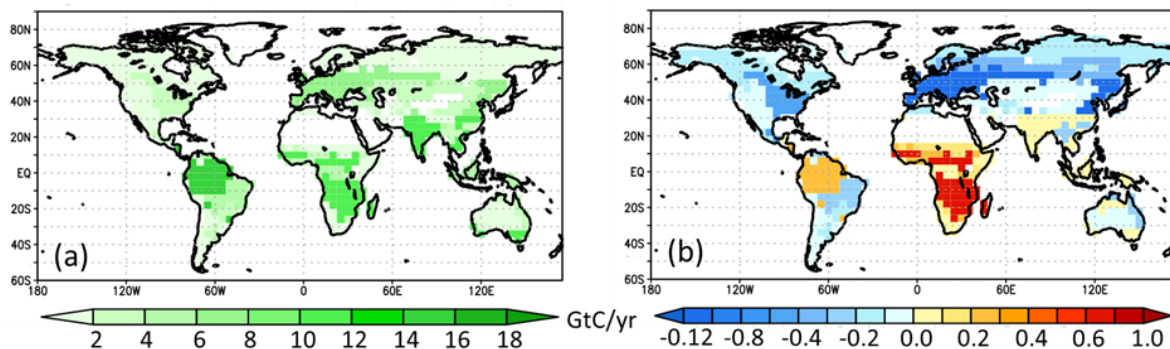1104   drought stress, fires, and other processes.

Figure 13. (a) GPP from OCO-2 SIF and (B) Net Biospheric Exchange (NBE) from XCO$_2$
and SIF, both expressed in gigatons of carbon per year (Pg C yr^{-1}) for 2015-2018. Negative
NBE indicates sinks while positive values indicate sources. NBE is typically < 5% of the
GPP, but is positive in the tropics where we see the highest GPP, in sharp contrast to existing
models (Junjie Liu, Personal communication, 2019).

1105   These conclusions are reinforced by experiments that assimilate XCO_2 and SIF results
1106 into atmospheric inverse models (Liu et al., 2017; 2020; Palmer et al., 2019; Chevallier et al.,
1107 2019; Crowell et al., 2019). Even in the Amazon and tropical Africa, where the GPP exceeds 10
1108 Pg C yr^{-1} (Figure 13a), the net biospheric exchange (NBE) can still be positive (Figure 13b). This
1109 contradicts results from carbon flux inversion models constrained by in situ data, alone, which
1110 indicate that, at least until recently, these tropical forests were significant net sinks of CO_2
1111 (Hubau et al., 2020).

6.2 *New Insights into the Extratropical Land Biosphere from Space*

1113   Unlike for the tropics, the XCO_2 anomalies and retrieved CO_2 fluxes from northern
1114 temperate and boreal forests are generally more consistent with expectations. During the NH
1115 summer (JJA in Figure 12), we see negative XCO_2 anomalies. Annual average flux inversion
1116 experiments show moderately strong GPP and negative NBE (Figure 13). The OCO-2 XCO_2 and
1117 SIF measurement therefore indicate that these forests have continued to be significant net CO_2
1118 sinks as the CO_2 seasonal cycle amplitude has grown in response to warming. While mid- and
1119 high-latitude CO_2 fluxes derived from inverse models constrained by OCO-2 XCO_2 and SIF
1120 estimates are generally consistent with those from earlier flux inversion experiments constrained
1121 by *in situ* CO_2 data alone (Lucht et al., 2002; Graven et al., 2013; Byrne et al., 2018), there are
1122 substantial differences in amplitude and phase in some regions (Reuter et al., 2017; Crowell et
1123 al., 2019; Palmer et al., 2019; Chevallier et al., 2019).

1124   Space-based observations of XCO_2 and SIF provide unique opportunities to study the
1125 relationships between the land and atmospheric carbon cycles and the hydrological cycle. Yin et
1126 al. (2020) combine SIF with atmospheric CO_2 observations to quantify the effects of large-scale
1127 flooding on cropland carbon sequestration. Widespread flooding during spring and early summer
1128 of 2019 delayed crop planting across the U.S. Midwest. As a result, satellite observations of SIF
1129 from OCO-2 and the TROPOspheric Monitoring Instrument (TROPOMI) reveal a shift of 16
1130 days in the seasonal cycle of photosynthetic activity relative to 2018, along with a 15% lower
1131 peak photosynthesis. Yin et al. find that the 2019 anomaly produced an estimated GPP reduction
1132 of -0.21 Pg C in June and July that was partially compensated in August and September with a
1133 +0.14 Pg C increase. The growing season integral corresponds to a 4% reduction in cropland
1134 GPP for the Midwest, but a 3% increase for areas where cropland occupies less than 10% of the
1135 land. Using an atmospheric transport model, they show that a decline of ~0.1 Pg C in the net
1136 carbon uptake in June and July is consistent with observed ~10 ppm CO_2 enhancements in the
1137 midday boundary layer from the Atmospheric Carbon and Transport - America (ACT-America)
1138 aircraft and the ~1 ppm increases in XCO_2 seen by OCO-2.

1139   In another study, Gonsamo et al. (2019) combined OCO-2 SIF observations with soil
1140 moisture (SM) observations from NASA's Soil Moisture Active Passive (SMAP) mission to
1141 study the impact of environmental limiting factors on terrestrial ecosystem productivity of
1142 drylands and croplands. For drylands (dry sub-humid, semi-arid, and arid zones) and the majority
1143 of croplands, soil water content is typically low and topsoil moisture is critical for plant growth.
1144 As expected, SMAP SM retrievals show positive daily relationships with OCO-2 SIF for
1145 drylands and croplands of the tropics and Australia, where SM is limiting plant growth and
1146 concurrent data records are sufficient to make statistical inferences. Negative relationships
1147 between SIF and SM were observed in forested areas of mid-latitude dry sub humid zones with
1148 high average annual SM. In these regions, SIF showed a positive relationship with air

1149   temperature. They find strong evidence that the OCO-2 SIF is accurately capturing monthly
1150   SMAP SM dynamics, particularly for regions with distinct seasonality of rainfall such as Sub-
1151   Saharan North Africa, Indian subcontinent, and southern Africa.

1152 *6.3 Lessons Learned from Space-based XCO_2 Estimates over the Ocean*

1153   In general, XCO_2 anomalies over the ocean were expected to be much smaller than those
1154   over land, but they have still yielded some surprises in first-generation space-based observations
1155   of CO_2. For example, the earliest version of the OCO-2 product, version 7 (v7) revealed large (2-
1156   3 ppm) positive XCO_2 anomalies over the midlatitude ocean (20 – 50 S) in the southern
1157   hemisphere during the Austral winter. These anomalies were initially suspicious because they
1158   were not seen in the XCO_2 observations from the Total Carbon Column Observing Network
1159   (TCCON) stations at Lauder, New Zealand or Wollongong, or Reunion Island (Wunch et al.,
1160   2017). However, they could not be dismissed immediately because there are few CO_2
1161   measurements over the ocean at the latitudes where they had their largest amplitudes. Retrieval
1162   algorithm validation efforts subsequently traced these anomalies to a bias introduced by a thin
1163   layer of volcanic aerosol in the stratosphere that had been neglected in the retrieval algorithm
1164   (O'Dell et al., 2018). This bias was corrected in the version 8 (v8) and later versions of the OCO-
1165   2 products by explicitly retrieving the stratospheric aerosol optical depth.

1166   While the v8 and version 9 (v9) OCO-2 XCO_2 products were generally more reliable
1167   over the ocean at mid latitudes (O'Dell et al. 2018; Kiel et al., 2019), they included a new
1168   anomaly that compromised their acceptance by the ocean carbon cycle community. In contrast to
1169   existing carbon cycle models, which assume that ocean-atmospheric CO_2 fluxes are correlated
1170   with ocean surface pCO_2 values, Figure 12 shows persistent negative XCO_2 anomalies over the
1171   tropical Pacific and Indian Oceans, where surface ocean pCO_2 is high (Figure 3, top). The lowest
1172   persistent spatial anomalies in XCO_2 are seen in regions that receive the highest rainfall (1000 -
1173   3000 mm/year), suggesting a possible correlation. Comparisons of OCO-2 XCO_2 estimates with
1174   TCCON XCO_2 observations indicate that the OCO-2 estimates are systematically low over the
1175   topical Pacific and Indian Oceans (S. Kulawik personal communication, 2019), but this does not
1176   expain the apparent spatial correlation of the deepest anomalies with the rain bands. These
1177   spatial correlations are not entirely surprising. Atmospheric CO_2 dissolves in cloud and
1178   raindrops, reducing the pH of rain to values between 5 and 6 even for regions well away from
1179   anthropogenic nitrate and sulfate acid rain sources (Willey et al., 2000; Bogan et al., 2009; Liu et
1180   al., 2010). Liu et al. (2010) estimate that precipitation transports ~0.2 Pg C yr^{-1} (0.35 to 0.7 Pg
1181 CO_2) from the atmosphere to the ocean. This process is not seen in carbon cycle models because
1182   most assume that rain contains no inorganic carbon, and falls with a pH of 7.0. If these OCO-2
1183 XCO_2 anomalies can be validated, this assumption will have to be revisited.

1184 *6.4 The Continuing Need for in situ Measurements of CO_2 and other Greenhouse Gases*

1185   While this first generation of space-based measurements of CO_2 have provided new
1186   insights into land, ocean, and atmospheric carbon cycles, they have also revealed some key
1187   limitations of this approach, and the continuing need to maintain and expand the ground-based
1188   and airborne atmospheric greenhouse measurement networks. First, while CO_2 and CH_4 can now
1189   be measured from space with the accuracies need to quantify surface sources and sinks, other
1190   critical greenhouse gases including nitrous oxide (N_2O), chlorofluorocarbons (CFCs),
1191   hydrochlorofluorocarbons (HCFCs), hydrofluorocarbons (HFCs), perfluorocarbons (PFCs), and

1192   sulfur hexafluoride (SF_6) cannot be measured to adequate accuracy. For these gases, as well as
1193 CO_2 and CH_4, in situ measurements continue to provide the most reliable means for tracking
1194   their concentrations on hemispheric to global scales. These measurements therefore continue to
1195   be a critical element of any global stocktake of these gases, like that mandated by the UNFCCC
1196   Paris Agreement. Other species that are useful for discriminating fossil fuel from biospheric CO_2
1197   emissions, such as carbon-14 (^{14}C) can also only be measured in situ (Miller et al., 2012; 2020).

1198   While spatial coverage is a critical asset of space-based atmospheric CO_2 measurements,
1199   there are situations where in situ measurements complement the coverage provided by these data.
1200   For example, remote sensing observations of near-surface CO_2 can only be collected in regions
1201   that are sufficiently free of clouds and aerosols. In situ measurements are therefore essential in
1202   persistently cloudy regions like those occupied by the intertropical convergence zone (ITCZ),
1203   and the Asian summer monsoon. In situ measurements are also needed at high latitudes during
1204   the winter, where clouds, low sun angles, and the low reflectivity of snow and ice covered
1205   surfaces at shortwave infrared wavelengths reduce the number and quality of remote sensing
1206   observations of CO_2. In addition, in situ data from instruments on airborne platforms
1207   complement the vertically-integrated remote sensing results with information about the vertical
1208   profile of CO_2, which can provide critical insight into net flux of CO_2 into the atmosphere.
1209   Finally, because the air-sea flux of CO_2 is determined mainly by the pCO_2 gradient between the
1210   ocean surface layer and the atmospheric surface boundary layer, in situ observations of near-
1211   surface atmospheric CO_2 concentrations are critical over the ocean.

1212   Finally, because both surface in situ and remote sensing observations are more accurate
1213   than space-based remote sensing measurements, these data are critical for validating the remote
1214   sensing measurements. Currently, space-based XCO_2 estimates are validated against ground-
1215   based remote sensing observations collected by the Total Carbon Column Observing Network
1216   (TCCON), which, in turn, are validated against airborne in situ measurements, to provide a
1217   transfer standard to the WMO atmospheric greenhouse gas standard (Wunch et al., 2017). This
1218   validation approach has yielded valuable information about surface and atmospheric properties
1219   that introduce bias and scatter in the space-based remote sensing measurements. However, while
1220   this network now includes 27 stations in 14 countries, it still provides little coverage of the
1221   tropics and high latitudes, some of the most dramatic features are seen in the space-based remote
1222   sensing data.

1223   While the number of ground-based and airborne in situ and remote sensing reference
1224   stations have grown slowly over the past decade, new measurement capabilities are coming on
1225   line that promise substantial increases in coverage. The up-looking remote sensing measurements
1226   being collected by the TCCON spectrometers are being complemented by measurements from
1227   smaller, less costly, and more portable Bruker EM27/SUN systems. These spectrometers are now
1228   being deployed as networks in urban settings (Hedelius et al., 2018) and in remote locations
1229   (Frey et al., 2019). In situ vertical profiles of CO_2, CH_4 and other gases are now being collected
1230   at altitudes as high as 25 km by AirCore instruments deployed on low-cost weather balloons
1231   (Karion et al., 2010). Additional in situ profiles and upper tropospheric measurements are now
1232   being made by commercial aircraft in Japan's Comprehensive Observation Network for Trace
1233   gases by Airliner (CONTRAIL) and Europe's In-service Aircraft for a Global Observing System
1234   (IAGOS).

7   Discussion

When integrated over the industrial age, the land sink has roughly balanced the land use source. The ocean has therefore been the only *de facto* cumulative net sink of fossil carbon from the atmosphere (Friedlingstein et al., 2019; 2020). However, since 1958, when continuous atmospheric CO_2 measurements have been available, CO_2 emissions from fossil fuel combustion have increased by about a factor of four, from less than 2.5 Pg C yr^{-1} to almost 10 Pg C yr^{-1} in 2019. During this period, the land sink has taken up an increasing fraction of anthropogenic emissions. Together, sinks in ocean and on land have absorbed enough anthropogenic CO_2 to limit the fraction that has remained in the atmosphere to a remarkably constant value around 45% (Raupach et al., 2014). This implies that, to first order, the uptake capacity of the ocean and land sinks has increased in step with the emissions (Friedlingstein et al., 2020). There has been debate as to whether increases in the atmospheric fraction, i.e. declines in sink efficiency, are already observable (Canadell et al., 2007; Knorr 2009; Raupach et al., 2014). Even if an increasing atmospheric fraction is not yet detectable, process-level understanding and regional trends indicate that the atmospheric fraction should increase as climate change progresses. While the exact timing and magnitude of changes in the land and ocean sinks remains unclear, the likelihood is high that substantial climate-carbon feedbacks will occur during this century. Any upward change in the atmospheric fraction, or reduction in sink capacity, will decrease the allowable fossil carbon that can still be burned without violating the temperature targets specified in the Paris agreement.

For the ocean, despite remaining uncertainties and missing closure terms, distinct methodologies for quantifying the ocean sink agree that the sink has increased over the industrial era, including in recent decades. Since the uptake of atmospheric CO_2 on annual to decadal time scales is primarily controlled by the pCO_2 gradient at its surface, the carbon sink is expected to grow steadily as long as near-exponential growth of atmospheric pCO_2 continues. However, if anthropogenic emissions are reduced, atmospheric pCO_2 will grow more slowly, and thus there will be a reduced ocean carbon sink even if the ocean circulation and chemical buffer capacity do not change. To understand these likely changes, it is essential that ocean carbon studies start to focus more attention on the near-term response to emission mitigation scenarios (Hausfather and Peters, 2020). If emissions are not mitigated, current climate models suggest that by the middle to late 21st century, a slowing ocean overturning rate and reduced chemical capacity in the ocean will reduce the rate of growth in the ocean sink.

To develop an integrated ocean carbon observing system that can track the evolution of the ocean sink on the annual to interannual timescales most relevant to climate change policy, we need to sustain existing and continue to develop improved observation systems for the surface and interior ocean. Ocean carbon instruments deployed on autonomous platforms are revolutionizing ocean carbon measurement spatial and temporal resolution and coverage, but reduced uncertainties in the carbonate constants are needed to fully exploit these data. High-quality shipboard observations will continue to be required. We also need improved ocean hindcast models and better understanding of uncertainties in observation-based data products derived through statistical extrapolation of sparse surface ocean pCO_2 data.

For the land carbon cycle, the picture is more complicated and appears to already be changing. Classical sinks in the tropical humid forests are slowly losing their strength and these changes are amplified by the losses associated with deforestation, forest degradation and extreme climate events. In the extra tropics, bottom-up measurements show evidence for a mid-latitude

1280   greening associated with afforestation and increased agriculture, accompanied by increased
1281   browning in some parts of the Arctic. Overall, these trends provide the fragile background for a
1282   slowly increasing land uptake of CO_2. Over the next century, carbon-climate feedback is
1283   expected to play a larger role in the Arctic, although the magnitude and timing of those changes
1284   is subject to considerable debate (Schuur et al., 2015).

1285   Space-based remote sensing observations are helping to revolutionize our ability to
1286   monitor the land and atmospheric carbon cycles to anthropogenic forcing and a changing
1287   climate. From a bottom-up perspective, microwave and lidar measurements are providing higher
1288   spatial and temporal resolution estimates of above ground biomass stocks. SIF measurements are
1289   providing a more responsive estimate of light use efficiency and CO_2 uptake by plants. From a
1290   top-down perspective, space-based remote sensing estimates of XCO_2 are complementing
1291   ground-based and aircraft in situ measurements with much greater spatial and temporal
1292   resolution and coverage. These space-based measurements sometimes reinforce, amplify or
1293   contradict the results inferred from ground-based in situ measurements, painting a somewhat
1294   controversial picture of the evolution of the land carbon cycle. For example, in the tropics, both
1295   space-based microwave estimates of above ground biomass (Wigneron et al., 2020) and top-
1296   down atmospheric inverse models constrained by space-based estimates of XCO_2 (Liu et al.,
1297   2017; 2020; Palmer et al., 2019; Crowell et al., 2019) indicate that the humid tropical forests
1298   never fully recovered from the 2015-2016 El Niño, and have transitioned from net sinks to net
1299   sources of CO_2. Meanwhile, at mid- and high latitudes, bottom-up and top-down models
1300   constrained by space-based remote sensing measurements largely reinforce the in situ results,
1301   showing a long term increase in the amplitude of the seasonal cycle (Graven et al., 2013; Byrne
1302   et al., 2018; 2020; Liu et al., 2020) and that mid-latitude and boreal forests are strong net sinks of
1303 CO_2 when averaged over the seasonal cycle. More generally, the space based measurements are
1304   also providing more information about rapid changes in the land carbon cycle associated with
1305   severe weather, such as droughts (Gonsamo et al., 2019; Castro et al., 2020) and floods (Yin et
1306   al., 2020). They are also beginning to provide estimates of CO_2 emissions from fossil fuel
1307   combustion and other human activities (Hakkarainen et al., 2016; 2019; Wang et al., 2018;
1308   Hedelius et al., 2018; Wu et al., 2018; 2020; Reuter et al., 2019).

1309   In spite of these advances, the reliability of the space-based remote sensing results are
1310   still a subject of substantial debate within the land carbon cycle community. This is especially
1311   true for the tropics, where CO_2 fluxes derived from the space-based XCO_2 estimates differ in
1312   both sign and magnitude from the results of earlier flux inversion experiments constrained by
1313   bottom-up stock or flux estimates or ground-based in situ measurements of atmospheric CO_2.
1314   This apparent inconsistency suggests one of three possibilities. First, the space-based XCO_2
1315   estimates might still include biases that compromise the accuracy of the top-down flux estimates.
1316   Recent efforts to validate the space-based XCO_2 estimates using measurements from TCCON
1317   and other standards (Wunch et al., 2017) indicate biases with amplitudes less than one third as
1318   large as the observed tropical XCO_2 anomalies. However, there are few TCCON stations or other
1319   validation capabilities in the tropics. Second, fluxes constrained by surface in situ
1320   measurements, alone, may tell an incomplete story of the land carbon cycle in sparsely sampled
1321   regions. The spatial resolution and coverage provided by surface in situ measurements of carbon
1322   stocks, fluxes, or atmospheric CO_2 are still very limited, especially in the tropics and boreal
1323   regions, where the largest flux differences are seen. Both top-down and bottom-up methods may
1324   yield unreliable results where there are few measurements. Third, flux estimates based on the
1325   much denser space-based XCO_2 measurements may be tracking changes in the natural carbon

1326 cycle on time and space scales too short to be resolved by the in situ measurements of stocks or
1327 CO_2 concentrations. There is increasing evidence from atmospheric CO_2 measurements and
1328 modeling studies and other carbon cycle observations, that the tropical land carbon cycle is
1329 evolving rapidly in response to human activities (deforestation and degradation, biomass
1330 burning, land use change) and climate change (drought, heat stress, flooding). Satellite
1331 observations of aboveground biomass (Baccini et al., 2017) also support this conclusion.

1332 All three of these possibilities may be valid to some extent. To address these questions
1333 and improve our understanding of the land carbon cycle in the tropics and at high latitudes, we
1334 need additional ground-based and aircraft validation measurements in these areas, advances in
1335 the space-based measurement calibration, retrieval algorithms, and validation techniques to
1336 further reduce regional scale biases and a longer, continuous space-based data record that clearly
1337 resolves the carbon cycle impacts of short-term climate anomalies from long-term secular
1338 climate trends.

8   Conclusions

1340 Our understanding of the carbon cycle and its response to natural and anthropogenic
1341 forcing has grown steadily over the past two decades as more advanced carbon cycle
1342 measurement systems have been deployed and their results have been analyzed with more
1343 sophisticated diagnostic and prognostic carbon cycle models. These results reveal a strongly
1344 coupled, dynamic system that responds on daily, to seasonal, to interannual time scales across
1345 spatial scales spanning individual fields, forest plots or coal-fired power plants on land or
1346 individual eddies in the ocean to entire continents or ocean basins. While surface or ocean
1347 interior in situ measurements still provide the most precise and accurate results, these data are
1348 now being complemented by a broad range of ground and ocean-based, airborne and space based
1349 remote sensing observations that extend their spatial resolution and coverage. The growing
1350 international collaborations between the top-down and bottom-up carbon cycle measurement and
1351 modeling communities, with their continued focus on a rigorous peer review process is
1352 contributing to the transparency of the carbon emission inventory process, an increasingly urgent
1353 requirement of any carbon management system.

1354 While these observations and models have provided new insights into this system, they
1355 have also revealed measurement gaps and modeling limitations that must be addressed to
1356 develop a true global carbon monitoring system that can track changes in both natural and
1357 anthropogenic sources and sinks of CO_2 on policy relevant time and space scales. For example,
1358 space-based remote sensing observations of atmospheric CO_2 and land and ocean surface
1359 properties can expand the coverage and resolution of surface-based in situ measurements.
1360 However, passive remote sensing observations are largely precluded in persistently cloudy
1361 regions such as tropical rain forests, or mid- and high-latitude forests during the fall, winter and
1362 spring. These regions are often centers of action in the carbon cycle, but are also among the most
1363 challenging to observe systematically with surface-based in situ measurement systems. Remote
1364 sensing observations provide little insight into the carbon budget of the interior ocean, but here
1365 networks of autonomous in situ sensors are providing new tools for gathering data. Like remote
1366 sensing observations, their data typically has larger uncertainties and biases than conventional
1367 shipboard in situ measurements. Thus, a robust ocean carbon observing system will require
1368 continued shipboard observations for calibration and validation.

1369   Top-down atmospheric CO_2 inventories are now complementing bottom-up statistical
1370 inventory methods by providing an integral constraint on total CO_2 emitted into the atmosphere
1371 and absorbed at the surface on scales ranging from large urban areas to nations. However, the
1372 inventory community has been slow to adopt top-down methods because they are much less
1373 source specific, and thus provide less direct, actionable information to policy makers than the
1374 bottom-up inventories. Optimal methods for combining top-down and bottom up emissions
1375 estimates are essential to both improve the accuracy and ensure the transparency urban to
1376 national scale inventories should be a high priority in any carbon management system. An effort
1377 to integrate top-down and bottom-up methods could also yield significant scientific benefits by
1378 fostering the development of more reliable models for diagnosing the current state of the carbon
1379 cycle, and for more accurately predicting the carbon cycle response to a changing climate.

1380   The world's space agencies are actively working to coordinate ambitious plans for an
1381 expanded space-based remote sensing capability that supports atmospheric CO_2 measurements,
1382 high resolution maps of land surface type and biomass and ocean biological productivity. These
1383 efforts are being led by the Committee on Earth Observation Satellites (CEOS) and Coordination
1384 Group on Meteorological Satellites (CGMS) through their Joint Working Group on Climate
1385 (WGClimate) Greenhouse Gas Task team. In parallel, national agencies such as the U.S. NOAA
1386 and Japan's National Institute for Environmental Studies (NIES) and European organizations,
1387 such ICOS and IAGOS, are working with international organizations including WMO GAW and
1388 the Global Climate Observing System and the Global Ocean Observing System (GCOS, GOOS)
1389 to coordinate the deployment of ground-based, ocean and airborne in situ sensors. These
1390 programs are receiving less attention and much less resources than the space-based measurement
1391 systems, but are equally critical to a global carbon monitoring system. The modeling systems
1392 needed to ingest and analyze the data collected by these expanding measurement systems are
1393 also advancing, but efforts to organize carbon cycle modeling efforts are also receiving less
1394 attention from the carbon cycle science community and their stakeholders. Ambitious efforts to
1395 track changes in the emission and uptake of CO_2 associated with human activities and the carbon
1396 cycle's response to climate change, such as the global stocktakes mandated by the UNFCCC
1397 Paris agreement, will require both expanded capabilities and much more coordination among all
1398 of these groups.

1399 **9   Open Research**

1400   This is a review of other published work. No new data has been created or archived
1401 specifically for this manuscript. Original data are available through the citations listed here.
1402 Figures have been redrawn to avoid copyright conflicts.

1403 **10 Acknowledgments**

11   References

1421   Ajani, J. I., Keith, H., Blakers, M., Mackey, B. G. and King, H. P. (2013). Comprehensive
1422   carbon stock and flow accounting: A national framework to support climate change
1423   mitigation policy. *Ecological Economics,* **89**, 61-72. doi:10.1016/j.ecolecon.2013.01.010

1424   Álvarez, M., Fajar, N. M., Carter, B. R., Guallart, E. F., Pérez, F. F., Woosley, R. J. and Murata,
1425   A. (2020). Global Ocean Spectrophotometric pH Assessment: Consistent Inconsistencies.
1426   *Environ. Sci. Technol.,* **54**, 10977-10988. doi:10.1021/acs.est.9b06932

1427   Anav, A., Friedlingstein, P., Beer, C., Ciais, P., Harper, A., Jones, C., Murray-Tortarolo, G.,
1428   Papale, D., Parazoo, N. C., Peylin, P., Piao, S., Sitch, S., Viovy, N., Wiltshire, A. and
1429   Zhao, M. (2015). Spatiotemporal patterns of terrestrial gross primary production: A
1430   review. *Rev. Geophys.,* **53**, 785–818. doi:10.1002/2015RG000483

1431   Andrew, R. M. (2020). A comparison of estimates of global carbon dioxide emissions from fossil
1432   carbon sources. *Earth Syst. Sci. Data,* **12**, 1437–1465. doi:10.5194/essd-12-1437-2020

1433   Aumont, O., Orr, J.C., Monfray, P., Ludwig, W., Amiotte-Suchet, P. and Probst, J.-L. (2001).
1434   Riverine-driven interhemispheric transport of carbon. *Global Biogeochemical Cycles.* **15**,
1435   393–405. doi:10.1029/1999GB001238

1436   Aumont, O., Ethé, C., Tagliabue, A., Bopp, L. and Gehlen, M. (2015). PISCES-v2: An ocean
1437   biogeochemical model for carbon and ecosystem studies. *Geosci. Model Dev.,* **8**, 2465–
1438   2513. doi:10.5194/gmd-8-2465-2015

1439   Ayers, J.M. and Strutton, P.G. (2013). Nutrient variability in Subantarctic Mode Waters forced
1440   by the Southern Annular Mode and ENSO: Subantarctic mode water nutrients.
1441   *Geophysical Research Letters,* **40**, 3419–3423. doi:10.1002/grl.50638

1442   Baccini, A., Walker, W., Carvalho, L., Farini, M., Sulla-Menashe, D. and Houghton, R. A.
1443   (2017). Tropical forests are a net carbon source based on aboveground measurements of
1444   gain and loss. *Science.* **358**, 230–234. doi:10.1126/science.aam5962

1445   Bakker, D. C. E., Pfeil, B., Smith, K., Hankin, S., Olsen, A., Alin, S. R., Cosca, C., Harasawa, S.,
1446   Kozyr, A., Nojiri, Y., O'Brien, K. M., Schuster, U., Telszewski, M., Tilbrook, B., Wada,
1447   C., Akl, J., Barbero, L., Bates, N. R., Boutin, J., Bozec, Y., Cai, W.-J., Castle, R. D.,
1448   Chavez, F. P., Chen, L., Chierici, M., Currie, K., de Baar, H. J. W., Evans, W., Feely, R.
1449   A., Fransson, A., Gao, Z., Hales, B., Hardman-Mountford, N. J., Hoppema, M., Huang,
1450   W.-J., Hunt, C. W., Huss, B., Ichikawa, T., Johannessen, T., Jones, E. M., Jones, S. D.,
1451   Jutterström, S., Kitidis, V., Körtzinger, A., Landschützer, P., Lauvset, S. K., Lefévre, N.,
1452   Manke, A. B., Mathis, J. T., Merlivat, L., Metzl, N., Murata, A., Newberger, T., Omar, A.
1453   M., Ono, T., Park, G.-H., Paterson, K., Pierrot, D., Ríos, A. F., Sabine, C. L., Saito, S.,

1454   Salisbury, J., Sarma, V. V. S. S., Schlitzer, R., Sieger, R., Skjelvan, I, Steinhoff, T.,
1455   Sullivan, K. F., Sun, H., Sutton, A. J., Suzuki, T., Sweeney, C., Takahashi, T., Tjiputra,
1456   J., Tsurushima, N., van Heuven, S. M. A. C., Vandemark, D., Vlahos, P., Wallace, D. W.
1457   R., Wanninkhof, R. and Watson, A. J. (2014). An update to the Surface Ocean CO_2 Atlas
1458   (SOCAT version 2). *Earth Syst. Sci. Data,* **6**, 69-90. doi:10.5194/essd-6-69-2014

1459 Bakker, D. C. E., Pfeil, B., Landa, C. S., Metzl, N., O'Brien, K. M., Olsen, A., Smith, K., Cosca,
1460   C., Harasawa, S., Jones, S. D., Nakaoka, S. I., Nojiri, Y., Schuster, U., Steinhoff, T.,
1461   Sweeney, C., Takahashi, T., Tilbrook, B., Wada, C., Wanninkhof, R., Alin, S. R.,
1462   Balestrini, C. F., Barbero, L., Bates, N. R., Bianchi, A. A., Bonou, F., Boutin, J., Bozec,
1463   Y., Burger, E. F., Cai, W. J., Castle, R. D., Chen, L., Chierici, M., Currie, K., Evans, W.,
1464   Featherstone, C., Feely, R. A., Fransson, A., Goyet, C., Greenwood, N., Gregor, L.,
1465   Hankin, S., Hardman-Mountford, N. J., Harlay, J., Hauck, J., Hoppema, M., Humphreys,
1466   M. P., Hunt, C. W., Huss, B., Ibanhez, J. S. P., Johannessen, T., Keeling, R., Kitidis, V.,
1467   Kortzinger, A., Kozyr, A., Krasakopoulou, E., Kuwata, A., Landschutzer, P., Lauvset, S.
1468   K., Lefevre, N., Lo Monaco, C., Manke, A., Mathis, J. T., Merlivat, L., Millero, F. J.,
1469   Monteiro, P. M. S., Munro, D. R., Murata, A., Newberger, T., Omar, A. M., Ono, T.,
1470   Paterson, K., Pearce, D., Pierrot, D., Robbins, L. L., Saito, S., Salisbury, J., Schlitzer, R.,
1471   Schneider, B., Schweitzer, R., Sieger, R., Skjelvan, I., Sullivan, K. F., Sutherland, S. C.,
1472   Sutton, A. J., Tadokoro, K., Telszewski, M., Tuma, M., van Heuven, S. M. A. C.,
1473   Vandemark, D., Ward, B., Watson, A. J. and Xu, S. (2016). A multi-decade record of
1474   high-quality fCO_2 data in version 3 of the Surface Ocean CO_2 Atlas (SOCAT). *Earth*
1475   *Syst. Sci. Data*, 8, 383-413. doi:10.5194/essd-8-383-2016

1476 Bakker, D. C. E., Alin, S. R., Bates, N., Becker, M., Castaño-Primo, R., Cosca, C. E., Cronin,
1477   M., Kadono, K., Kozyr, A., Lauvset, S. K., Metzl, N., Munro, D. R., Nakaoka, S.,
1478   O'Brien, K. M., Ólafsson, J., Olsen, A., Pfeil, B., Pierrot, D., Smith, K., Sutton, A. J.,
1479   Takahashi, T., Tilbrook, B., Wanninkhof, R., Andersson, A., Atamanchuk, D., Benoit-
1480   Cattin, A., Bott, R., Burger, E. F., Cai, W.-J., Cantoni, C., Collins, A., Corredor, J. E.,
1481   Cronin, M. F., Cross, J. N, Currie, K. I., De Carlo, E. H., DeGrandpre, M. D., Dietrich,
1482   C., Emerson, S., Enright, M. P., Evans, W., Feely, R. A., García-Ibáñez, M. I., Gkritzalis,
1483   T., Glockzin, M., Hales, B., Hartman, S. E., Hashida, G., Herndon, J., Howden, S. D.,
1484   Humphreys, M. P., Hunt, C. W., Jones, S. D., Kim, S., Kitidis, V., Landa, C. S,
1485   Landschützer, P., Lebon, G. T., Lefèvre, N., Lo Monaco, C., Luchetta, A., Maenner
1486   Jones, S., Manke, A. B., Manzello, D., Mears, P., Mickett, J., Monacci, N. M., Morell, J.
1487   M., Musielewicz, S., Newberger, T., Newton, J., Noakes, S., Noh, J.-H., Nojiri, Y.,
1488   Ohman, M., Ólafsdóttir, S., Omar, A. M., Ono, T., Osborne, J., Plueddemann, A. J.,
1489   Rehder, G., Sabine, C. L, Salisbury, J. E., Schlitzer, R., Send, U., Skjelvan, I.,
1490   Sparnocchia, S., Steinhoff, T., Sullivan, K. F., Sutherland, S. C., Sweeney, C., Tadokoro,
1491   K., Tanhua, T., Telszewski, M., Tomlinson, M., Tribollet, A., Trull, T., Vandemark, D.,
1492   Wada, C., Wallace, D. W. R., Weller, R. A., and Woosley, R. J. (2020). Surface Ocean
1493 CO_2 Atlas Database Version 2020 (SOCATv2020) (NCEI Accession 0210711), NOAA
1494   National Centers for Environmental Information. doi:10.25921/4xkx-ss49

1495 Baldocchi, D., Falge, E., Gu, L., Olson, R., Hollinger, D., Running, S. W., Anthoni, P.,
1496   Bernhofer, C., Davis, K. J., Evans, R., Fuentes, J., Goldstein, A., Katul, G., Law, B., Lee,
1497   X., Malhi, Y., Meyers, T., Munger, W., Oechel, W., Paw, U. K. T., Pilegaard, K.,
1498   Schmid, H. P., Valentini, R., Verma, S., Vesala, T., Wilson, K. and Wofsy, S. (2001).

FLUXNET: A new tool to study the temporal and spatial variability of ecosystem-scale carbon dioxide, water vapor, and energy flux densities. *Bull. Amer. Meteor. Soc.*, **82**, 2415–2434. doi:10.1175/1520-0477

Baldocchi D. D. (2003). Assessing the eddy covariance technique for evaluating carbon dioxide exchange rates of ecosystems: past, present and future. *Global Change Biology*, **9**, 479–492. doi:10.1046/j.1365-2486.2003.00629.x

Ballantyne, A. P., Alden, C. B., Miller, J. B., Tans, P. P. and White, J. W. C. (2012). Increase in observed net carbon dioxide uptake by land and oceans during the past 50 years. *Nature*, **488**, 70–72. doi:10.1038/nature11299

Beck, S. A. and Goetz, S. J. (2011). Satellite observations of high northern latitude vegetation productivity changes between 1982 and 2008: ecological variability and regional differences. *Environ. Res. Lett.*, **6**, 045501. doi:10.1088/1748-9326/6/4/045501

Beer, C., Reichstein, M., Tomelleri, E., Ciais, P., Jung, M., Carvalhais, N., Rödenbeck, C., Arain, M. A., Baldocchi, D., Bonan, G., B., Bondeau, A., Cescatti, A., Lasslop,G., Lindroth, A., Lomas, M., Luyssaert, S., Margolis, H., Oleson, K. W., Roupsard, O., Veenendaal, E., Viovy, N., Williams, C., Woodward, F., I. and Papale, D. (2010). Terrestrial gross carbon dioxide uptake: global distribution and covariation with climate. *Science,* **329**, 834–838. doi:10.1126/science.1184984

Bennedsen, M., Hildebrand, E. and Koopman, S. (2019). Trend analysis of the airborne fraction and sink rate of anthropogenically released CO_2. *Biogeosciences*, **16**, 3651–3663. doi:10.5194/bg-16-3651-2019

Boden T. A., Marland G. and Andres R. J. (2017). Global, Regional, and National Fossil-Fuel CO_2 Emissions. Carbon Dioxide Information Analysis Center, Oak Ridge National Laboratory, U.S. Department of Energy, Oak Ridge, Tenn., U.S.A. doi:10.3334/CDIAC/00001_V2017

Bogan, R. A. J., Ohde, S., Arakaki, T., Mori, I. and McLeod, C. W. (2009). Changes in rainwater pH associated with atmospheric carbon dioxide after the Industrial Revolution. *Water, Air, and Soil Pollution*, **196**, 263-271. doi:10.1007/s11270-008-9774-0

Bolin, B., Björkström, A., Holmén, K. and Moore, B. (1983). The simultaneous use of tracers for ocean circulation studies. *Tellus B*, **35B**, 206–236. doi:10.1111/j.1600-0889.1983.tb00025.x

BP Statistical Review of World Energy 2020. available at https://www.bp.com/en/global/corporate/energy-economics/statistical-review-of-world-energy/co2-emissions.html, last access 1 February 2021.

Brienen, R. J.W., Phillips, O. L., Feldpausch, T. R., Gloor, E., Baker, T. R., Lloyd, J., Lopez-Gonzalez, G., Monteagudo-Mendoza, A., Malhi, Y., Lewis, S. L., Vásquez Martinez, R., Alexiades, M., Álvarez Dávila, E., Alvarez-Loayza, P., Andrade, A., Aragão, L. E. O. C., Araujo-Murakami, A., Arets, E. J. M. M., Arroyo, L., Aymard, C. A. G., Bánki, O.S., Baraloto, C., Barroso, J., Bonal, D., Boot, R. G. A. , Camargo, J. L. C., Castilho, C. V., Chama, V., Chao, K. J., Chave, J., Comiskey, J. A., Cornejo Valverde, F., da Costa, L., de Oliveira, E. A., Di Fiore, A., Erwin, T. L., Fauset, S., Forsthofer, M., Galbraith, D. R., Grahame, E. S., Groot, N., Hérault, B., Higuchi, N., Honorio Coronado, E. N., Keeling,

H., Killeen, T. J., Laurance, W. F., Laurance, S., Licona, J., Magnussen, W. E., Marimon, B. S., Marimon-Junior, B. H., Mendoza, C., Neill, D. A., Nogueira, E. M., Núñez, P., Pallqui Camacho, N. C., Parada, A., Pardo-Molina, G., Peacock, J., Peña-Claros, M., Pickavance, G. C., Pitman, N. C. A., Poorter, L., Prieto, A., Quesada C. A., Ramírez, F., Ramírez-Angulo, H., Restrepo, Z., Roopsind, A., Rudas, A., Salomão, R. P., Schwarz, M., Silva, N., Silva-Espejo, J. E., Silveira, M., Stropp, J., Talbot, J., ter Steege, H., Teran-Aguilar, J., Terborgh, J., Thomas-Caesar, R., Toledo, M., Torello-Raventos, M., Umetsu, R. K., van der Heijden, G. M. F., van der Hout, P., Guimarães, Vieira I. C., Vieira, S. A., Vilanova, E., Vos ,V. A. and Zagt, R. J. (2015). Long-term decline of the Amazon carbon sink. *Nature,* **519**(7543), 344-348. doi:10.1038/nature14283

Bronselaer,B., and Zanna, L. (2020), Heat and carbon coupling reveals ocean warming due to circulation changes. *Nature,* **584**, 227–233. doi:10.1038/s41586-020-2573-5

Bushinsky, S. M., Landschützer, P., Rödenbeck, C., Gray, A. R., Baker, D., Mazloff, M. R., Resplandy, L., Johnson, K. S., and Sarmiento, J. L. (2019). Reassessing Southern Ocean air-sea CO_2 flux estimates with the addition of biogeochemical float observations. *Global Biogeochemical Cycles*, **33**(11), 1370-1388, doi:10.1029/2019GB006176

Byrne, B., Wunch, D., Jones, D. B. A., Strong, K., Deng, F., Baker, I., Köhler, P., Frankenberg, C., Joiner, J., Arora, V. K., Badawy, B., Harper, A. B., Warneke, T., Petri, C., Kivi, R. and Roehl, C. M. (2018). Evaluating GPP and respiration estimates over northern midlatitude ecosystems using solar-induced fluorescence and atmospheric CO_2 measurements. *Journal of Geophysical Research: Biogeosciences*, **123**(9), 2976–2997. doi:10.1029/2018JG004472

Byrne, B., Liu, J., Lee, M., Baker, I., Bowman, K. W., Deutscher, N. M., Feist, D. G., Griffith D. W. T., Iraci, L. T., Kiel, M., Kimball, J. S., Miller, C. E., Morino, I., Parazoo, N. C., Petri, C., Roehl, C. M., Sha, M. K., Strong, K., Velazco, V. A., Wennberg, P. O. and Wunch, D. (2020). Improved constraints on northern extratropical CO2 fluxes obtained by combining surface-based and space-based atmospheric CO_2 measurements. *Journal of Geophysical Research: Atmospheres*, **125**, e2019JD032029. doi:10.1029/2019JD032029

Canadell, J. G., Le Quéré, C., Raupach, M. R., Field, C. B. , Buitenhuis, E., Ciais, P., Conway, T. J., Gilett, N. P., Houghton, J. T. and Marland, G. (2007). Contributions to accelerating atmospheric CO_2 growth from economic activity, carbon intensity, and efficiency of natural sinks. *Proceedings of the National Academy of Sciences*, **104**, 18,866 – 18,870. doi:10.1073/ pnas.0702737104

Carroll, D., Menemenlis, D., Adkins, J. F., Bowman, K. W., Brix, H., Dutkiewicz, S., Fenty, I., Gierach, M. M., Hill, C., Jahn, O., Landschützer, P., Lauderdale, J. M., Liu, J., Manizza, M., Naviaux, J. D., Rodenbeck, C., Schimel, D. S., Van der Stocken, T. and Zhang, H. (2020). The ECCO-Darwin data-assimilative global ocean biogeochemistry model: Estimates of seasonal to multi-decadal surface ocean pCO_2 and air-sea CO_2 flux. *J. Adv. Model. Earth Syst.*, **12**, e2019MS001888. doi:10.1029/2019MS001888

Carvalhais, N., Forkel, M., Khomik, M., Bellarby, J., Jung, M., Migliavacca, M. Mu, M., Saatchi, S., Santoro, M., Thurner, M., Weber, U., Ahrens, B., Beer, C., Cescatti, A., Randerson, J. T. and Reichstein, M. (2014). Global covariation of carbon turnover times with climate in terrestrial ecosystems. *Nature*, **514**(7521) 213-7. doi:10.1038/nature13731

1584 Castro, A. O., Chen, J., Zang, C. S., Shekhar, A., Jimenez, J. C., Bhattacharjee, S., Kindu, M.,
1585   Morales, V. H. and Ramming, A. (2020). OCO-2 Solar-Induced Chlorophyll
1586   Fluorescence Variability across Ecoregions of the Amazon Basin and the Extreme
1587   Drought Effects of El Nino (2015-2016), *Remote Sensing*, **12**(7), 1202.
1588   doi:10.3390/rs12071202

1589 Chatterjee, A., Gierach, M. M., Sutton, A. J., Feely, R. A., Crisp, D., Eldering, A., Gunson, M.
1590   R., O'Dell, C. W., Stephens, B. B. and Schimel, D. S. (2017). Influence of El Niño on
1591   atmospheric CO_2 over the tropical Pacific Ocean: Findings from NASA's OCO-2
1592   mission. *Science,* **358**, eaam5776. doi:10.1126/science.aam5776

1593 Chevallier, F., Ciais, P., Conway, T. J., Aalto, T., Anderson, B. E., Bousquet, P., Brunke, E. G.,
1594   Ciattaglia, L., Esaki, Y., Frohlich, M., Gomez, A. J., Gomez-Pelaez, A. J., Haszpra, L.,
1595   Krummel, P., Langenfelds, R., Leuenberger, M., Machida, T., Maignan, F., Matsueda,
1596   H., Morgui, J. A., Mukai, H., Nakazawa, T., Peylin, P., Ramonet, M., Rivier, L., Sawa,
1597   Y., Schmidt, M., Steele, P., Vay, S. A., Vermeulen, A. T., Wofsy, S. and Worthy, D.
1598   (2010). CO_2 surface fluxes at grid point scale estimated from a global 21-year reanalysis
1599   of atmospheric measurements. *Journal of Geophysical Research: Atmospheres*, **115**,
1600   D21307. doi:10.1029/2010JD013887

1601 Chevallier, F., Remaud, M. O'Dell, C. W., Baker, D., Peylin, P. and Cozic, A. (2019). Objective
1602   evaluation of surface and satellite driven CO_2 atmospheric inversion. *Atmospheric
1603   Chemistry and Physics*, **19**, 14233–14251. doi:10.5194/acp-19-14233-2019

1604 Ciais, P., Dolman, A. J., Bombelli, A., Duren, R., Peregon, A., Rayner, P. J., Miller, C., Gobron,
1605   N., Kinderman, G., Marland, G., Gruber, N., Chevallier, F., Andres, R. J., Balsamo, G.,
1606   Bopp, L., Bréon, F.-M., Broquet, G., Dargaville, R., Battin, T. J., Borges, A.,
1607   Bovensmann, H., Buchwitz, M., Butler, J., Canadell, J. G., Cook, R. B., DeFries, R.,
1608   Engelen, R., Gurney, K. R., Heinze, C., Heimann, M., Held, A., Henry, M., Law, B.,
1609   Luyssaert, S., Miller, J., Moriyama, T., Moulin, C., Myneni, R. B., Nussli, C.,
1610   Obersteiner, M., Ojima, D., Pan, Y., Paris, J.-D., Piao, S. L., Poulter, B., Plummer, S.,
1611   Quegan, S., Raymond, P., Reichstein, M., Rivier, L., Sabine, C., Schimel, D., Tarasova,
1612   O., Valentini, R., Wang, R., van der Werf, G., Wickland, D., Williams, M. and Zehner,
1613   C. (2014). Current systematic carbon-cycle observations and the need for implementing a
1614   policy-relevant carbon observing system, *Biogeosciences*, **11**, 3547–3602.
1615   doi:10.5194/bg-11-3547-2014

1616 Ciais, P., Yao, Y., Gasser, T., Baccini, A., Wang, Y., Lauerwald, R., Peng, S., Bastos, A., Li, W.,
1617   Raymnd, P. A., Canadell, J. G., Peters, G. P., Andres, R. J., Chang, J., Yue, C., Dolman,
1618   A. J., Haverd, V., Hartman, J., Laruelle, G., Konings, A. G., King, A. W., Liu, Y.,
1619   Luyssaert, S., Maignan, F., Patra, P. K., Peregon, A., Regnier, P., Pongratz, J., Poulter,
1620   B., Shvidenko, A., Valentini, R., Wang, R., Broquet, G., Yin, Y., Zscheischler, J.,
1621   Guenet, B., Goll, D., S., Ballantyne, A.-P., Yang, H., Qiu, C. and Zhu, D. (2020).
1622   Empirical estimates of regional carbon budgets imply reduced global soil heterotrophic
1623   respiration. *National Science Review*, **0**, nwaa145,1-14. doi:10.1093/nsr/nwaa145

1624 Clement, D., and Gruber, N. (2018). The eMLR(C*) Method to determine decadal changes in the
1625   global ocean storage of anthropogenic CO_2. *Global Biogeochemical Cycles,* **32**, 654-679.
1626   doi:10.1002/2017gb005819

1627   Claustre, H., Johnson, K. S., and Takeshita, Y. (2020). Observing the global ocean with
1628   Biogeochemical-Argo, *Annual Review of Marine Science*, **12**, 23-48.
1629   doi:10.1146/annurev-marine-010419-010956

1630   Crowell, S., Baker, D., Schuh, A., Basu, S., Jacobson, A., Chevallier, F., Liu, J., Deng, F., Feng,
1631   L., McKain, K., Chatterjee, A., Miller, J., Stephens, B., Eldering, A., Crisp, D., Schimel,
1632   D., Nassar, R., O'Dell. C., Oda, T., Sweeney, C., Palmer, P., and Jones, D. (2019). The
1633   2015-2016 carbon cycle as seen from OCO-2 and the global in situ network. *Atmospheric*
1634   *Chemistry and Physics*, **19**, 7347–7376. doi:10.5194/acp-19-7347-2019

1635   Denman, K.L., G. Brasseur, A. Chidthaisong, P. Ciais, P.M. Cox, R.E. Dickinson, D.
1636   Hauglustaine, C. Heinze, E. Holland, D. Jacob, U. Lohmann, S Ramachandran, P.L. da
1637   Silva Dias, S.C. Wofsy and X. Zhang, (2007). Couplings between changes in the climate
1638   system and biogeochemistry. In: Climate Change 2007: The Physical Science Basis.
1639   Contribution of Working Group I to the Fourth Assessment Report of the
1640   Intergovernmental Panel on Climate Change [Solomon, S., Qin ,D., Manning, M., Chen,
1641   Z., Marquis, M., Avery, K. B., Tignor, M. and Miller, H. L. (eds.)]. Cambridge
1642   University Press, Cambridge, United Kingdom and New York, NY, USA.

1643   Denvil-Sommer, A., M. Gehlen, M. Vrac, and C. Mejia (2019). LSCE-FFNN-v1: A two-step
1644   neural network model for the reconstruction of surface ocean pCO_2 over the global ocean.
1645   *Geosci. Model Dev.*, **12**(5), 2091–2105. doi:10.5194/gmd-12-2091-2019

1646   DeVries, T. (2014). The oceanic anthropogenic CO_2 sink: Storage, air-sea fluxes, and transports
1647   over the industrial era, *Global Biogeochemical Cycles*, **28**(7), 631–647.
1648   doi:10.1002/2013GB004739

1649   DeVries, T., Holzer, M. and Primeau, F. (2017). Recent increase in oceanic carbon uptake driven
1650   by weaker upper-ocean overturning. *Nature,* **542**, 215–218. doi:10.1038/nature21068

1651   DeVries, T., Le Quéré, C., Andrews, O., Berthet, S., Hauck, J., Ilyina, T., Landschützer, P.,
1652   Lenton, A., Lima, I. D., Nowicki, M., Schwinger, J., Séférian, R. (2019). Decadal trends
1653   in the ocean carbon sink. *Proceedings of the National Academy of Sciences,* 201900371.
1654   doi:10.1073/pnas.1900371116

1655   Dlugokencky, E. J., Hall, B.D., Montzka, S.A., Dutton, G., Muhle, J. and Elkins, J.W. (2018).
1656   Long-lived greenhouse gases [in "State of the Climate in 2017"]. *Bulletin of the American*
1657   *Meteorological Society*, **99**(8), S46-S48. doi:10.1175/2018BAMSStateoftheClimate.1

1658   Doney S.C., Lindsay, K., Caldeira, K., Campin, J.-M., Drange, H., Dutay, J. C., Follows, M.,
1659   Gao, Y., Gnanadesikan, A., Gruber, N., Ishida, A., Joos, F., Madec, G., Maier-Reimer,
1660   E., Marshall, J. C., Matear, R. J., Monfray, P., Mouchet, A., Najjar, R., Orr, J. C.,
1661   Plattner, G.-K., Sarmiento, J., Schlitzer, R., Slater, R., Totterdell, I. J., Weirig, M. F.,
1662   Yamanaka, Y. and Yool, A. (2004). Evaluating global ocean carbon models: The
1663   importance of realistic physics. *Global Biogeochemical Cycles,* **18** (3), GB3017.
1664   doi:10.1029/2003GB002150

1665   Doughty, C. E. and Goulden, M. L. (2008). Are tropical forests near a high temperature
1666   threshold? *Journal of Geophysical Research: Biogeosciences,* **113**, G00B07.
1667   doi:10.1029/2007JG000632

1668   Duffy, K., A., Schwalm, C. R., Arcus, V. L., Koch, G. W., Liang, L. L. and Schipper, L. A.
1669   (2021). How close are we to the temperature tipping point of the terrestrial biosphere?
1670   *Science Advances*, **7**, eaay1052.

1671   Duncanson, L., Armston, J., Disney, M., Avitabile, V., Barbier, N., Calders, K., Carter, S.,
1672   Chave, J., Herold, M., Crowther, T. W., Falkowski, M., Kellner, J. R., Labrière, N.,
1673   Lucas, R., MacBean, N., McRoberts, R. E., Meyer, V., Naesset, E., Nickeson, J. E., Paul,
1674   K. I., Phillips, O. L., Réjou-Méchain, M., Román, M., Roxburgh, S., Saatchi, S.,
1675   Schepaschenko, D., Scipal, K., Siqueira, P. R., Whitehurst, A. and Williams, M.
1676   (2019). The importance of consistent global forest aboveground biomass product
1677   Validation. *Surveys in Geophysics volume,* **40**, 979–999. doi:10.1007/s10712-019-09538-
1678   8

1679   Eddebbar, Y. A., Rodgers, K. B., Long, M. C., Subramanian, A. C., Xie S.-P. and Keeling, R. F.
1680   (2019). El Niño-like physical and biogeochemical ocean response to tropical eruptions.
1681   *Journal of Climate*, **32**(9), JCLI–D–18–0458.1, doi:10.1175/JCLI-D-18-0458.1

1682   Eldering, A.,Wennberg, P. O., Crisp, D., Schimel, D., Gunson, M. R., Chatterjee, A., Liu J.,
1683   Schwandner, Y. Sun, C.W. O'Dell, C. Frankenberg, T. Taylor, B. Fisher, G.B. Osterman,
1684   D. Wunch, F., Hakkarainen, J. and Tamminen, J. (2017). The Orbiting Carbon
1685   Observatory-2 early science investigations of regional carbon dioxide fluxes. *Science* ,
1686   **358**, eaam5745. doi:10.1126/science.aam5745

1687   Enting, I.G., Trudinger, C.M. and Francey, R.J. (1995). A synthesis inversion of
1688   the concentration and δ^{13}C atmospheric CO_2. *Tellus*, **47B**, 35-52. doi:10.1034/j.1600-
1689   0889.47.issue1.5.x

1690   Fan, L., Wigneron, J.-P., Ciais, P., Chave, J., Brandt, M., Fensholt, R., Saatchi, S. S. Bastos, A.,
1691   Al-Yaari, A., Hufkens, K., Qin, Y., Xiao, X., Chen, C., Myneni, R. B., Rernandez-
1692   Moran, R., Mialon, A., Rodriguez-Fernandez, N. J., Kerr, Y., Tian, F. and Peñuelas, J.
1693   (2019). Satellite-observed pantropical carbon dynamics. *Nature Plants,* **5**, 944–951.
1694   doi:10.1038/s41477-019-0478-9

1695   Fay, A. R., McKinley, G. A. (2013). Global trends in surface ocean pCO_2 from in situ data.
1696   *Global Biogeochemical Cycles*, **27**, 541–557. doi:10.1002/gbc.20051

1697   Fay, A.R., Gregor, L., Landschützer, P. McKinley, G.A., Gruber, N., Gehlen, M., Iida, Y.,
1698   Laruelle, G. G., Rödenbeck, C. and Zeng J. (2021). Harmonization of global surface
1699   ocean pCO_2 mapped products and their flux calculations; an improved estimate of the
1700   ocean carbon sink. *Earth Syst. Sci. Data*, submitted 2020.

1701   Fay, A. R., Lovenduski, N. S., McKinley, G. A., Munro, D. R., Sweeney, C., Gray, A. R.,
1702   Landschützer, P., Stephens, B. B., Takahashi ,T. and Williams, N. (2018). Utilizing the
1703   Drake Passage Time-series to understand variability and change in subpolar Southern
1704   Ocean pCO_2. *Biogeosciences*, **15**(12), 3841–3855. doi:10.5194/bg-15-3841-2018

1705   Fisher, J. B., Huntzinger, D. N., Schwalm, C. R. and Sitch, S. (2014). Modeling the terrestrial
1706   biosphere. *Annual Review of Environment and Resources*, **39**, 91–123.
1707   doi:10.1146/annurev-environ-012913-093456

1708 Fong, M. B. and Dickson, A. G. (2019). Insights from GO-SHIP hydrography data into the
1709   thermodynamic consistency of CO_2 system measurements in seawater. *Marine*
1710   *Chemistry*, **211**, 52-63. doi:10.1016/j.marchem.2019.03.006

1711 Frankenberg, C., O'Dell, C., Berry, J., Guanter, L., Joiner, J., Köhler, P., Pollock, R. and Taylor,
1712   T. E. (2014). Prospects for chlorophyll fluorescence remote sensing from the orbiting
1713   carbon observatory-2. *Remote Sensing of Environment*, **147**, 1–12.
1714   doi:10.1016/j.rse.2014.02.007. ISSN 0034–4257

1715 Frey, M., Sha, M. K., Hase, F., Kiel, M., Blumenstock, T., Harig, R., Surawicz, G., Deutscher,
1716   N. M., Shiomi, K., Franklin, J. E., Bösch, H., Chen, J., Grutter, M., Ohyama, H., Sun, Y.,
1717   Butz, A., Mengistu Tsidu, G., Ene, D., Wunch, D., Cao, Z., Garcia, O., Ramonet, M.,
1718   Vogel, F. and Orphal, J. (2019). Building the COllaborative Carbon Column Observing
1719   Network (COCCON): long-term stability and ensemble performance of the EM27/SUN
1720   Fourier transform spectrometer. *Atmospheric Measurement Technologies*, **12**, 1513–
1721   1530. doi:10.5194/amt-12-1513-2019

1722 Friedlingstein, P., Jones, M. W., O'Sullivan, M., Andrew, R. M., Hauck, J., Peters, G. P., Peters,
1723   W., Pongratz, J., Sitch, S., Le Quéré, C., Bakker, D. C. E., Canadell, J. G., Ciais, P.,
1724   Jackson, R. B., Anthoni, P., Barbero, L., Bastos, A., Bastrikov, V., Becker, M., Bopp, L.,
1725   Buitenhuis, E., Chandra, N., Chevallier, F., Chini, L. P., Currie, K. I., Feely, R. A.,
1726   Gehlen, M., Gilfillan, D., Gkritzalis, T., Goll, D. S., Gruber, N., Gutekunst, S., Harris, I.,
1727   Haverd, V., Houghton, R. A., Hurtt, G., Ilyina, T., Jain, A. K., Joetzjer, E., Kaplan, J. O.,
1728   Kato, E., Klein Goldewijk, K., Korsbakken, J. I., Landschützer, P., Lauvset, S. K.,
1729   Lefèvre, N., Lenton, A., Lienert, S., Lombardozzi, D., Marland, G., McGuire, P. C.,
1730   Melton, J. R., Metzl, N., Munro, D. R., Nabel, J. E. M. S., Nakaoka, S.-I., Neill, C.,
1731   Omar, A. M., Ono, T., Peregon, A., Pierrot, D., Poulter, B., Rehder, G., Resplandy, L.,
1732   Robertson, E., Rödenbeck, C., Séférian, R., Schwinger, J., Smith, N., Tans, P. P., Tian,
1733   H., Tilbrook, B., Tubiello, F. N., van der Werf, G. R., Wiltshire, A. J. and Zaehle, S.
1734   (2019). Global Carbon Budget 2019. *Earth Syst. Sci. Data*, **11**, 1783–1838.
1735   doi:10.5194/essd-11-1783-2019

1736 Friedlingstein, P., O'Sullivan, M., Jones, M. W., Andrew, R. M., Hauck, J., Olsen, A., Peters, G.
1737   P., Peters, W., Pongratz, J., Sitch, S., Le Quéré, C., Canadell, J. G., Ciais, P., Jackson, R.
1738   B., Alin, S., Aragão, L. E. O. C., Arneth, A., Arora, V., Bates, N. R., Becker, M., Benoit-
1739   Cattin, A., Bittig, H. C., Bopp, L., Bultan, S., Chandra, N., Chevallier, F., Chini, L. P.,
1740   Evans, W., Florentie, L., Forster, P. M., Gasser, T., Gehlen, M., Gilfillan, D., Gkritzalis,
1741   T., Gregor, L., Gruber, N., Harris, I., Hartung, K., Haverd, V., Houghton, R. A., Ilyina,
1742   T., Jain, A. K., Joetzjer, E., Kadono, K., Kato, E., Kitidis, V., Korsbakken, J. I.,
1743   Landschützer, P., Lefèvre, N., Lenton, A., Lienert, S., Liu, Z., Lombardozzi, D., Marland,
1744   G., Metzl, N., Munro, D. R., Nabel, J. E. M. S., Nakaoka, S.-I., Niwa, Y., O'Brien, K.,
1745   Ono, T., Palmer, P. I., Pierrot, D., Poulter, B., Resplandy, L., Robertson, E., Rödenbeck,
1746   C., Schwinger, J., Séférian, R., Skjelvan, I., Smith, A. J. P., Sutton, A. J., Tanhua, T.,
1747   Tans, P. P., Tian, H., Tilbrook, B., van der Werf, G., Vuichard, N., Walker, A. P.,
1748   Wanninkhof, R., Watson, A. J., Willis, D., Wiltshire, A. J., Yuan, W., Yue, X. and
1749   Zaehle, S. (2020). Global Carbon Budget 2020. *Earth Syst. Sci. Data*, **12**, 3269–3340.
1750   doi:10.5194/essd-12-3269-2020

Friis, K., Körtzinger, A., Pätsch, J. and Wallace, D. W. R. (2005). On the temporal increase of anthropogenic CO_2 in the subpolar North Atlantic. *Deep-Sea Research.* **52**, 681-698. doi:10.1016/j.dsr.2004.11.017

Frölicher, T. L., Joos, F., Raible, C. C. and Sarmiento, J. L. (2013). Atmospheric CO_2 response to volcanic eruptions: The role of ENSO, season, and variability. *Global Biogeochemical Cycles*, **27**, 239-251. doi:10.1002/gbc.20028

Frölicher, T.L., Rodgers, K. B., Stock, C. A., Cheung, W. W. L. (2016). Sources of uncertainties in 21st century projections of potential ocean ecosystem stressors: Uncertainties in stressor projections. *Global Biogeochemical Cycles,* **30**, 1224–1243. doi:10.1002/2015GB005338

Galbraith, E. D., and Skinner, L. C. (2020). The biological pump during the last glacial maximum. *Annual Reviews of Marine Science* **12**, 559–586. doi:10.1146/annurev-marine-010419-010906

Gatti L.V., Gloor M., Miller J. B., Doughty C. E., Malhi Y., Domingues L. G., Basso L. S., Martinewski A., Correia C. S., Borges V. F., Freitas S., Braz R., Anderson L. O., Rocha H., Grace J., Phillips O. L., and Lloyd J. (2014). Drought sensitivity of Amazonian carbon balance revealed by atmospheric measurements. *Nature*, **506**, 76-80. doi:10.1038/nature12957

Gloege, L., McKinley, G. A., Landschützer, P., Fay, A., Frölicher, T., Fyfe, J. C., Illyina ,T., Jones, S.D., Lovenduski, N. S., Rödenbeck ,C., Rodgers K. B., Schlunegger, S. and Takano, Y. (2020). Quantifying errors in observationally-based estimates of ocean carbon sink variability. *Global Biogeochemical Cycles,* in review. doi:10.1002/essoar.10502036.1

Gonsamo, A., Chen, J. M., He, L., Sun, Y., Rogers, C. and Liu, J. (2019). Exploring SMAP and OCO-2 observations to monitor soil moisture control on photosynthetic activity of global drylands and croplands, *Remote Sensing of Environment*, **232**, 111314. doi:10.1016/j.rse.2019.111314

Goris, N., Tjiputra, J. F., Olsen, A., Schwinger, J., Lauvset S. K. and Jeansson E. (2018). Constraining projection-based estimates of the future North Atlantic carbon uptake. *Journal of Climate*, **31**(10), 3959–3978, doi:10.1175/JCLI-D-17-0564.1

Grassi, G., House, J., Kurz, W. A., Cescatti, A., Houghton, R. A., Peters, G. P., Sanz, M. J., Viñas, R. A., Alkama, R., Arneth, A., Bondeau, A., Dentener, F., Fader, M., Federici, S., Friedlingstein, P., Jain, A. K., Kato, E., Koven, C. D., Lee, D., Nabel, J. E. M. S., Nassikas, A. A., Perugini, L., Rossi, S., Sitch, S., Viovy, N., Wiltshire, A. and Zaehle, S. (2018). Reconciling global-model estimates and country reporting of anthropogenic forest CO_2 sinks. *Nature Climate Change*, **8**, 914–920. doi.org/10.1038/s41558-018-0283-x

Graven, H. D., Keeling, R. F., Piper, S. C., Patra, P. K., Stephens, B. B., Wofsy, S. C., Welp, L. R., Sweeney, C. and Tans, P. P. (2013). Enhanced seasonal exchange of CO_2 by northern ecosystems since 1960, *Science*, **341**(6150): 1085–1089. doi:10.1126/science.1239207

Gregor, L., Lebehot, A. D. Kok, S. and Scheel Monteiro, P. M. (2019). A comparative assessment of the uncertainties of global surface-ocean CO_2 estimates using a machine

learning ensemble (CSIR-ML6 version 2019a); have we hit the wall? *Geosci. Model Dev.*, **12**, 5113–5136. doi:10.5194/gmd-12-5113-2019

Gruber, N., Clement, D., Carter, B.R., Feely, R.A., Van Heuven, S., Hoppema, M., Ishii, M., Key, R.M., Kozyr, A., Lauvset, S.K., Lo Monaco, C., Mathis, J.T., Murata, A., Olsen, A., Perez, F.F., Sabine, C.L., Tanhua, T., and Wanninkhof, R. (2019a). The oceanic sink for anthropogenic CO_2 from 1994 to 2007. *Science* **363**, 1193-1199. doi:10.1126/science.aau5153

Gruber, N., Landschützer, P., and Lovendusk, N. S. (2019b). The variable Southern Ocean carbon sink. *Annual Reviews of Marine Sci*ence, **11**, 159–186. doi:10.1146/annurev-marine-121916-063407

Guan, K., Berry, J. A., Zhang, Y., Joiner, J., Guanter, L., Badgley, G. and Lobell, D. B. (2016). Improving the monitoring of crop productivity using spaceborne solar-induced fluorescence. *Global Change Biology*, **22**(2), 716–726. doi:10.1111/gcb.13136

Guan, K., Wu, J., Kimball, J. S., Anderson, M. C., Frolking, S., Li, B., Hain, C. R. and Lobell, D. B. (2017). The shared and unique values of optical, fluorescence, thermal and microwave satellite data for estimating large-scale crop yields. *Remote Sensing of Environment*, **199**, 333–349. doi:10.1016/j.rse.2017.06.043

Gurney, K. R., Liang, J., O'Keeffe, D., Patarasuk, R., Hutchins, M., Huang, J., Rao, P. and Song, Y. (2019). Comparison of global downscaled versus bottom-up fossil fuel CO_2 emissions at the urban scale in four U.S. urban areas. *Journal of Geophysical Research: Atmospheres*, **124**(5), 2823--2840. doi:10.1029/2018JD028859

Hakkarainen, J., Ialongo, I. and Tamminen, J. (2016). Direct space-based observations of anthropogenic CO_2 emission areas from OCO-2. *Geophysical Research Letters,* **43**, 11,400–11,406. doi:10.1002/2016GL070885

Hakkarainen, J., Ialongo, I., Maksyutov, S., and Crisp, D. (2019). Analysis of Four Years of Global XCO_2 Anomalies as Seen by Orbiting Carbon Observatory-2, *Remote Sensing*, **11**, 850. doi:10.3390/rs11070850

Hansis, E., Davis, S. J. and Pongratz, J. (2015). Relevance of methodological choices for accounting of land use change carbon fluxes. *Global Biogeochemical Cycles*, **29**, 1230–1246. doi:10.1002/2014GB004997

Hauck, J., Völker, C., Wang, T., Hoppema, M., Losch, M. and Wolf-Gladrow, D.A. (2013). Seasonally different carbon flux changes in the Southern Ocean in response to the southern annular mode. *Global Biogeochemical Cycles,* **27**, 1236–1245. doi:10.1002/2013GB004600

Hauck, J., Völker, C., Wolf-Gladrow, D. A., Laufkötter, C., Vogt, M., Aumont, O., Bopp, L., Buitenhuis, E. T., Doney, S. C., Dunne, J., Gruber, N., Hashioka, T., John, J., Le Quéré, C., Lima, I. D., Nakano, H., Séférian, R. and Totterdell, I. (2015). On the Southern Ocean CO_2 uptake and the role of the biological carbon pump in the 21st century. *Global Biogeochemical Cycles,* **29**, 1451–1470. doi:10.1002/2015GB005140

Hauck, J., Zeising, M., Le Quéré, C., Gruber, N., Bakker, D. C. E., Bopp, L., Chau, T. T. T., Gürses, Ö., Ilyina, T., Landschützer, P., Lenton, A., Resplandy, L., Rödenbeck, C., Schwinger, J. and Séférian, R. (2020). Consistency and challenges in the ocean carbon

1835   sink estimate for the Global Carbon Budget. *Frontiers in Marine Science,* **7**, 571720.
1836   doi:10.3389/fmars.2020.571720

1837 Hausfather, Z. and Peters, G. P. (2020). Emissions - the "business as usual" story is misleading.
1838   *Nature*, **577**(7792), 618–620, doi:10.1038/d41586-020-00177-3

1839 He, L., Magney, T., Dutta, D., Yin, Y., Köhler, P., Grossmann, K., Stutz, J., Dold, C., Hatfield,
1840   J., Guan, K., Peng, B. and Frankenberg, C. (2020). From the ground to space: Using
1841   solar-induced chlorophyll fluorescence to estimate crop productivity. *Geophysical*
1842   *Research Letters*, **47**, e2020GL087474. doi:10.1029/2020GL087474

1843 Hedelius, J. K., Liu, J., Oda, T., Maksyutov, S., Roehl, C. M., Iraci, L., Podolske, J., Hillyard, P.,
1844   Liang, J., Gurney, K., Wunch, D. and Wennberg P. (2018). Southern California megacity
1845 CO_2, CH_4, and CO flux estimates using ground- and space-based remote sensing and a
1846   Lagrangian model, *Atmospheric Chemistry and Physics,* **18**, 16271-16291.
1847   doi:10.5194/acp-18-16271-2018

1848 Henson, S. A., Beaulieu, C. and Lampitt, R. (2016). Observing climate change trends in ocean
1849   biogeochemistry: when and where. *Global Change Biology,* **22**, 1561–1571.
1850   doi:10.1111/gcb.13152

1851 Heymann, J., Reuter, M., Buchwitx, M., Schneising, O., Bovensmann, H., Burrows, J. P.,
1852   Massart, S., Kaiser, J. W., and Crisp, D. (2017). CO_2 emission of Indonesian fires in 2015
1853   estimated from satellite-derived atmospheric CO_2 concentrations. *Geophysical Research*
1854   *Lett*ers, 44, 1537-1544. doi: 10.1002/2016GL072042

1855 Hoppema, M., Bakker, K., van Heuven, S. M. A. C., van Ooijen, J. C. and de Baar, H. J. W.
1856   (2015). Distributions, trends and inter-annual variability of nutrients along a repeat
1857   section through the Weddell Sea (1996–2011). *Marine Chemistry,* **177**, 545–553.
1858   doi:10.1016/j.marchem.2015.08.007

1859 Houghton, R. A. (2003). Revised estimates of the annual net flux of carbon to the atmosphere
1860   from changes in land use and land management 1850–2000. *Tellus*, **55B**, 378–390.
1861   doi:10.1034/j.1600-0889.2003.01450.x

1862 Houghton, R. A. and Nassikas, A. A. (2017). Global and regional fluxes of carbon from land use
1863   and land cover change 1850–2015. *Global Biogeochemical Cycles*, **31**, 456–472.
1864   doi:10.1002/2016GB005546

1865 Hubau, W., Lewis, S. L., Phillips O. L., Affum-Baffoe, Beeckman, K. H., Cuni-Sanchez, A.,
1866   Ewango, C. E. N., Fauset, S., Sheil, D., Sonké, B., Sullivan, M. J. P., Sunderland,T.,
1867   Thomas, S. C., Abernethy, K. A., Adu-Bredu, S., Amani C. A., Baker, T. R., Banin, L. F.,
1868   Baya, F., Begne, S. K., Bennett, A. C., Benedet, F., Bitariho, R., Bocko, Y. E., Boeckx,
1869   P., Boundja, P., Brienen, R. J. W., Brncic, T., Chezeaux, E., Chuyong, G. B., Clark, C. J.,
1870   Collins, M., Comiskey, J. A., Coomes, D. A., Dargie, G. C., de Haulleville, T., Kamdem,
1871   M. N. D., Doucet, J. L., Esquivel-Muelbert, A., Feldpausch, T. R., Fofanah, A., Foli, E.
1872   G., Gilpin, M., Gloor, E., Gonmadje, C., Gourlet-Fleury, S., Hall, J. S., Hamilton, A. C.,
1873   Harris, D. J., Hart, T. B., Hockemba, M. B. N., Hladik, A., Ifo, S. F., Jeffery, K. J.,
1874   Jucker, T., Yakusu, E. K., Kearsley, E., Kenfack, D., Koch, A., Leal, M. E., Levesley, A.,
1875   Lindsell, J. A., Lisingo, J., Lopez-Gonzalez, G., Lovett, J. C., Makana, J. R., Malhi, Y.,
1876   Marshall, A. R., Martin, J., Martin, E. H., Mbayu, F. M., Medjibe ,V. P., Mitchard, E. T.
1877   A., Moore, S., Munishi, P. K. T., Bengone, N. N., Ojo, L., Ondo, F. E., Peh, K. S.,

Pickavance, G. C., Poulsen, A. D., Poulsen, J. R., Qie, L., Reitsma, J., Rovero, F., Swaine, M. D., Talbot, J., Taplin J., Taylor, D. D., Thomas, D. W., Toirambe, B., Mukendi, J. T., Tuagben, D., Umunay, P. M., van der Heijden, G. M. F., Verbeeck, H., Vleminckx, J., Willcock, S., Wöll, H., Woods, J. T. and Zemagho, L. (2020). Asynchronous carbon sink saturation in African and Amazonian tropical forests. *Nature, 579*, 80–87. doi:10.1038/s41586-020-2035-0

Huber, M. B. and Zanna, L. (2017). Drivers of uncertainty in simulated ocean circulation and heat uptake. *Geophysical Research Letters, 44*(3), 1402-1413. doi:10.1002/2016GL071587

Hurtt, G. C., Chini, L., Sahajpal, R., Frolking, S., Bodirsky, B. L., Calvin, K., Doelman, J. C., Fisk, J., Fujimori, S., Klein Goldewijk, K., Hasegawa, T., Havlik, P., Heinimann, A., Humpenöder, F., Jungclaus, J., Kaplan, J. O., Kennedy, J., Krisztin, T., Lawrence, D., Lawrence, P., Ma, L., Mertz, O., Pongratz, J., Popp, A., Poulter, B., Riahi, K., Shevliakova, E., Stehfest, E., Thornton, P., Tubiello, F. N., van Vuuren, D. P. and Zhang, X. (2020). Harmonization of global land use change and management for the period 850–2100 (LUH2) for CMIP6. *Geosci. Model Dev.*, **13**, 5425–5464. doi:10.5194/gmd-135425-2020

Iida, T., Odate, T., Fukuchi, M. (2013). Long-Term Trends of Nutrients and Apparent Oxygen Utilization South of the Polar Front in Southern Ocean Intermediate Water from 1965 to 2008. *PLoS ONE, 8*, e71766. doi:10.1371/journal.pone.0071766

IEA World Energy Balances, 2020 Edition. Available from https://www.iea.org/subscribe-to-data-services/world-energy-balances-and-statistics, last viewed on 2 February 2021.

IPCC 2006, 2006 IPCC Guidelines for National Greenhouse Gas Inventories, Prepared by the National Greenhouse Gas Inventories Programme, Eggleston H.S., Buendia L., Miwa K., Ngara T. and Tanabe K. (eds). Published: IGES, Japan.

IPCC 2019, 2019 Refinement to the 2006 IPCC Guidelines for National Greenhouse Gas Inventories, Calvo Buendia, E., Tanabe, K., Kranjc, A., Baasansuren, J., Fukuda, M., Ngarize S., Osako, A., Pyrozhenko, Y., Shermanau, P. and Federici, S. (eds). Published: IPCC, Switzerland.

Ito, A. (2020). Constraining size-dependence of vegetation respiration rates, *Scientific Reports*, **10**, 4304. doi:10.1038/s41598-020-61239-0

Iudicone, D., Rodgers, K. B., Plancherel, Y., Aumont, O., Ito, T., Key, R. M., Madec, G. and Ishii, M. (2016). The formation of the ocean's anthropogenic carbon reservoir. *Scientific Reports*, **6**, 35473. doi:10.1038/srep35473

Jacobson, A. R., Mikaloff Fletcher, S. E., Gruber, N., Sarmiento, J. L. and Gloor, M. (2007). A joint atmosphere-ocean inversion for surface fluxes of carbon dioxide: 1. Methods and global-scale fluxes. *Global Biogeochemical Cycles*, **21**(1), 273. doi:10.1029/1999GL900363

Janssens-Maenhout, G., Crippa, M., Guizzardi, D., Muntean, M., Schaaf, E., Dentener, F., Bergamaschi, P., Pagliari, V., Olivier, J. G. J., Peters, J. A. H. W., van Aardenne, J. A., Monni, S., Doering, U., Petrescu, A. M. R., Solazzo, E. and Oreggioni, G. D. (2019).

EDGAR v4.3.2 Global Atlas of the three major greenhouse gas emissions for the period 1970–2012. *Earth Syst. Sci. Data*, **11**, 959-1002. doi:10.5194/essd-11-959-2019

Janssens-Maenhout, G., Pinty, B., Dowell, M., Zunker, H., Andersson, E., Balsamo, G., Bézy, J. L., Brunhes, T., Bösch, H., Bojkov, B., Brunner, D., Buchwitz, M., Crisp, D., Ciais, P., Counet, P., Dee, D., Denier van der Gon, H., Dolman, H., Drinkwater, M., Dubovnik O., Engelen, R., Fehr, T., Fernandez, V., Heimann, M., Holmlund, K., Houweling, S., Husband, R., Juvyns, O., Kentarchos, A., Landgraf, J., Lang, R., Löscher, A., Marshall, J., Meijer, Y., Nakajima, M., Palmer, P. I., Peylin, P., Rayner, P., Scholze, M., Sierk, B., Tamminen, J., Veefkind, P. (2020). Toward an operational anthropogenic CO_2 emissions monitoring and verification support capacity. *Bulletin of the American Meteorological Society*, **101**(8), E1439-E1451. doi:10.1175/BAMS-D-19-0017.1

Jian, J., Vargas, R., Anderson-Teixeira, K., Stell, E., Herrmann, V., Horn, M., Kholod, N., Manzon, J., Marchesi, R., Paredes, D. and Bond-Lamberty, B. (2020). A restructured and updated global soil respiration database (SRDB-V5). *Earth Syst. Sci. Data Discuss.* [preprint], doi:10.5194/essd-2020-136, in review.

Johnson, K. S., Jannasch, H. W., Coletti, L. J., Elrod, V. A., Martz, T. R., Takeshita, Y., Carlson, R. J. and Connery, J. G. (2016). Deep-Sea DuraFET: A pressure tolerant pH sensor designed for global sensor networks. *Analytical Chemistry*, **88**, 3249-3256. doi:10.1021/acs.analchem.5b04653

Jones, C. D. and P. M. Cox (2005). On the significance of atmospheric CO_2 growth rate anomalies in 2002– 2003. *Geophysical Research Letters*, **32**, L14816. doi:10.1029/2005GL023027

Joos, F., Bruno, M., Fink, R., Siegenthaler, U., Stocker, T. F., Le Quéré, C. and Sarmiento, J. L. (1996). An efficient and accurate representation of complex oceanic and biospheric models of anthropogenic carbon uptake. *Tellus B*, **48**, 397. doi:10.1034/j.1600-0889.1996.t01-2-00006.x

Jung, M., Reichstein, M. and Bondeau, A. (2009). Towards global empirical upscaling of FLUXNET eddy covariance observations: validation of a model tree ensemble approach using a biosphere model. *Biogeosciences*, **6**, 2001–2013. doi:10.5194/bg-6-2001-2009

Jung, M., Schwalm, C. Migliavacca, M., Walther, S., Camps-Valls, G., Koirala, S., Anthoni, P., Besnard, S., Bodesheim, P., Carvalhais, N., Chevallier, F., Gans, F., Goll, D. S., Haverd, V., Koehler, P., Ichii, K., Jain, A. K., Liu, J., Lombardozzi, D., Nabel, J. E. M. S., Nelson, J. A., O'Sullivan, M., Pallandt, M., Papale, D., Peters, W., Pongratz, J., Roedenbeck, C., Sitch, S., Tramontana, G., Walker, A., Weber, U. and Reichstein, M. (2020). Scaling carbon fluxes from eddy covariance sites to globe: synthesis and evaluation of the FLUXCOM approach. *Biogeosciences*, **17**, 1343–1365. doi: 10.5194/bg-17-1343-2020

Karion, A., Sweeney, C., Tans, P. P. and Newberger, T. (2010). AirCore: An innovative atmospheric sampling system. *Journal of Atmospheric and Oceanic Technology*, **27**, 1839–1853. doi:10.1175/2010JTECHA1448.1

Keenan, T. F., and Williams, C. A. (2018). The terrestrial carbon sink. *Annual Review of Environment and Resources*. **43**, 219-243. doi:10.1146/annurev-environ- 102017-030204

1961 Keppler, L., Landschützer, P. (2019). Regional wind variability modulates the Southern Ocean
1962   carbon sink. *Scientific Reports,* **9**, 7384. doi:10.1038/s41598-019-43826-y

1963 Key, R. M., Kozyr, A., Sabine, C. L., Lee, K., Wanninkhof, R., Bullister, J. L., Feely, R. A.,
1964   Millero, F. J., Mordy, C. and Peng, T. H. (2004). A global ocean carbon climatology:
1965   Results from Global Data Analysis Project (GLODAP). *Global Biogeochemical Cycles*,
1966   **18**(4), GB4031. doi:10.1029/2004GB002247

1967 Khatiwala, S., Primeau, F. and Hall, T. (2009). Reconstruction of the history of anthropogenic
1968 CO_2 concentrations in the ocean. *Nature,* **462,** 346–349. doi:10.1038/nature08526

1969 Khatiwala, S., Tanhua, T., Mikaloff Fletcher, S., Gerber, M., Doney, C. S., Graven, H. D.,
1970   Gruber, N., Mckinley, G. A., Murata, A. and Sabine, C. (2013). Global storage of
1971   anthropogenic carbon. *Biogeosciences,* **10**, 2169-2191, 2013. doi: 10.519/bg-10-2169-
1972   2013

1973 Kiel, M., O'Dell, C. W., Fisher, B., Eldering, A., Nassar, R., MacDonald, C. G. and Wennberg,
1974   P. O. (2019). How bias correction goes wrong: measurement of XCO_2 affected by
1975   erroneous surface pressure estimates. *Atmospheric Measurement Techniques*, **12**, 2241-
1976   2259. doi: 10.5194/amt-12-2241-2019

1977 Knorr, W. (2009). Is the airborne fraction of anthropogenic CO_2 emissions increasing?
1978   *Geophysical Research Letters*, **36**, L21710. doi:10.1029/2009GL040613

1979 Koren, G., van Schaik, E., Araujo, A. C., Boersma, K. F., Gartner, A., Killaars, L., Kooreman,
1980   M. L., Kruijt, B., van der Laan-Luijkx, I. T., von Randow, C., Smith, N. E., and Peters,
1981   W. (2018). Widespread reduction in sun-induced fluorescence from the Amazon during
1982   the 2015/2016 El Nino. *Philosophical Transactions of the Royal Society of London.*
1983   *Series B: Biological Sciences*, **373**(1760), 20170408. doi:10.1098/rstb.2017.0408

1984 Lacroix, F., T. Ilyina, and J. Hartmann (2020). Oceanic CO_2 outgassing and biological
1985   production hotspots induced by pre-industrial river loads of nutrients and carbon in a
1986   global modeling approach. *Biogeosciences*, **17**(1), 55–88. doi:10.5194/bg-17-55-2020

1987 Landschützer, P., Gruber, N., Bakker, D. C. E., Schuster, U., Nakaoka, S., Payne, M. R., Sasse,
1988   T. P. and Zeng, J. (2013). A neural network-based estimate of the seasonal to inter-annual
1989   variability of the Atlantic Ocean carbon sink. *Biogeosciences,* **10**, 7793–7815.
1990   doi:10.5194/bg-10-7793-2013

1991 Landschützer, P., Gruber, N., Bakker, D. C. E. and Schuster, U. (2014). Recent variability of the
1992   global ocean carbon sink. *Global Biogeochemical Cycles*, **28**, 927–949.
1993   doi:10.1002/2014GB004853

1994 Landschützer, P., Gruber, N., Haumann, F. A., Rödenbeck, C., Bakker, D. C. E., van Heuven, S.,
1995   Hoppema, M., Metzl, N., Sweeney, C., Takahashi, T., Tilbrook, B. and Wanninkhof, R.
1996   (2015). The reinvigoration of the Southern Ocean carbon sink. *Science* **349**, 1221–1224.
1997   doi:10.1126/science.aab2620

1998 Landschützer, P., Laruelle, G. G. , Roobaert, A. and Regnier, P. (2020). A uniform pCO_2
1999   climatology combining open and coastal oceans. *Earth Syst. Sci. Data*, **12**, 2537–2553.
2000   doi:10.5194/essd-2020-90

2001 Langlais, C. E., Lenton, A., Matear, R., Monselesan, D., Legresy, B., Cougnon, E. and Rintoul,
2002   S. (2017). Stationary Rossby waves dominate subduction of anthropogenic carbon in the
2003   Southern Ocean. *Scientific Reports,* **7**, 17076. doi:10.1038/s41598-017-17292-3

2004 Laufkötter, C., Vogt, M., Gruber, N., Aita-Noguchi, M., Aumont, O., Bopp, L., Buitenhuis, E.,
2005   Doney, S. C., Dunne, J., Hashioka, T., Hauck, J., Hirata, T., John, J., Le Quéré, C., Lima,
2006   I.D., Nakano, H., Seferian, R., Totterdell, I., Vichi, M. and Völker, C. (2015). Drivers
2007   and uncertainties of future global marine primary production in marine ecosystem
2008   models. *Biogeosciences,* **12**, 6955–6984. doi:10.5194/bg-12-6955-2015

2009 Laufkötter, C., Vogt, M., Gruber, N., Aumont, O., Bopp, L., Doney, S.C., Dunne, J.P., Hauck, J.,
2010   John, J.G., Lima, I.D., Seferian, R. and Völker, C. (2016). Projected decreases in future
2011   marine export production: the role of the carbon flux through the upper ocean ecosystem.
2012   *Biogeosciences,* **13**, 4023–4047. doi:10.5194/bg-13-4023-2016

2013 Lenton, A. and Matear, R. J. (2007). Role of the Southern Annular Mode (SAM) in Southern
2014   Ocean CO_2 uptake. *Global Biogeochemical Cycles,* **21**, GB2016.
2015   doi:10.1029/2006GB002714

2016 Le Quéré, C., Rödenbeck, C., Buitenhuis, E. T., Conway, T. J., Langenfelds, R., Gomez, A.,
2017   Labuschagne, C., Ramonet, M., Nakazawa, T., Metzl, N., Gillett, N. and Heimann, M.
2018   (2007). Saturation of the Southern Ocean CO_2 Sink Due to Recent Climate Change.
2019   *Science,* **316**, 1735–1738. doi:10.1126/science.1136188

2020 Le Quéré, C., Raupach, M. R., Canadell, J. G., Marland, G., Bopp, L., Ciais, P., Conway, T. J.,
2021   Doney, S. C., Feely, R. A., Foster, P., Friedlingstein, P., Gurney, K., Houghton, R. A.,
2022   House, J. I., Huntingford, C., Levy, P. E., Lomas, M. R., Majkut, J., Metzl, N., Ometto, J.
2023   P., Peters, G. P., Prentice, I. C., Randerson, J. T., Running, S. W., Sarmiento, J. L.,
2024   Schuster, U., Sitch, S., Takahashi, T., Viovy, N., van der Werf, G. R. and Woodward, F.
2025   I. (2009). Trends in the sources and sinks of carbon dioxide. *Nature Geosciences,* **2**, 831–
2026   836. doi:10.1038/ngeo689

2027 Le Quéré, C., Takahashi, T., Buitenhuis, E. T., Rödenbeck, C. and Sutherland, S. C. (2010).
2028   Impact of climate change and variability on the global oceanic sink of CO_2. *Global
2029   Biogeochemical Cycles,* **24**(4), GB4007. doi:10.1029/2009GB003599

2030 Le Quéré, C., Andres, R. J., Boden, T., Conway, T., Houghton, R. A., House, J. I., Marland, G.,
2031   Peters, G. P., van der Werf, G. R., Ahlström, A., Andrew, R. M., Bopp, L., Canadell, J.
2032   G., Ciais, P., Doney, S. C., Enright, C., Friedlingstein, P., Huntingford, C., Jain, A. K.,
2033   Jourdain, C., Kato, E., Keeling, R. F., Klein Goldewijk, K., Levis, S., Levy, P., Lomas,
2034   M., Poulter, B., Raupach, M. R., Schwinger, J., Sitch, S., Stocker, B. D., Viovy, N.,
2035   Zaehle and S. and Zeng, N. (2013). The global carbon budget 1959–2011. *Earth Syst. Sci.
2036   Data,* **5**, 165–185. doi:10.5194/essd-5-165-2013

2037 Le Quéré, C., Peters, G. P., Andres, R. J., Andrew, R. M., Boden, T. A., Ciais, P., Friedlingstein,
2038   P., Houghton, R. A., Marland, G., Moriarty, R., Sitch, S., Tans, P., Arneth, A., Arvanitis,
2039   A., Bakker, D. C. E., Bopp, L., Canadell, J. G., Chini, L. P., Doney, S. C., Harper, A.,
2040   Harris, I., House, J. I., Jain, A. K., Jones, S. D., Kato, E., Keeling, R. F., Klein
2041   Goldewijk, K., Körtzinger, A., Koven, C., Lefèvre, N., Maignan, F., Omar, A., Ono, T.,
2042   Park, G.-H., Pfeil, B., Poulter, B., Raupach, M.R., Regnier, P., Rödenbeck, C., Saito, S.,
2043   Schwinger, J., Segschneider, J., Stocker, B.D., Takahashi, T., Tilbrook, B., van Heuven,

2044   S., Viovy, N., Wanninkhof, R., Wiltshire, A. and Zaehle, S. (2014). Global carbon budget
2045   2013. *Earth Syst. Sci. Data,* **6**, 235–263. doi:10.5194/essd-6-235-2014

2046 Le Quéré, C., Moriarty, R., Andrew, R. M., Peters, G. P., Ciais, P., Friedlingstein, P., Jones, S.
2047   D., Sitch, S., Tans, P., Arneth, A., Boden, T. A., Bopp, L., Bozec, Y., Canadell, J. G.,
2048   Chini, L. P., Chevallier, F., Cosca, C. E., Harris, I., Hoppema, M., Houghton, R. A.,
2049   House, J. I., Jain, A. K., Johannessen, T., Kato, E., Keeling, R. F., Kitidis, V., Klein
2050   Goldewijk, K., Koven, C., Landa, C. S., Landschützer, P., Lenton, A., Lima, I. D.,
2051   Marland, G., Mathis, J. T., Metzl, N., Nojiri, Y., Olsen, A., Ono, T., Peng, S., Peters, W.,
2052   Pfeil, B., Poulter, B., Raupach, M. R., Regnier, P., Rödenbeck, C., Saito, S., Salisbury, J.
2053   E., Schuster, U., Schwinger, J., Séférian, R., Segschneider, J., Steinhoff, T., Stocker, B.
2054   D., Sutton, A. J., Takahashi, T., Tilbrook, B., van der Werf, G. R., Viovy, N., Wang, Y.-
2055   P., Wanninkhof, R., Wiltshire, A. and Zeng, N. (2015). Global carbon budget 2014. *Earth*
2056   *Syst. Sci. Data,* **7**, 47–85. doi:10.5194/essd-7-47-2015

2057 Le Quéré, C., Moriarty, R., Andrew, R. M., Canadell, J. G., Sitch, S., Korsbakken, J. I.,
2058   Friedlingstein, P., Peters, G. P., Andres, R.J., Boden, T. A., Houghton, R. A., House, J. I.,
2059   Keeling, R. F., Tans, P., Arneth, A., Bakker, D. C .E., Barbero, L., Bopp, L., Chang, J.,
2060   Chevallier, F., Chini, L. P., Ciais, P., Fader, M., Feely, R. A., Gkritzalis, T., Harris, I.,
2061   Hauck, J., Ilyina, T., Jain, A. K., Kato, E., Kitidis, V., Klein Goldewijk, K., Koven, C.,
2062   Landschützer, P., Lauvset, S. K., Lefèvre, N., Lenton, A., Lima, I. D., Metzl, N., Millero,
2063   F., Munro, D. R., Murata, A., Nabel, J. E. M. S., Nakaoka, S., Nojiri, Y., O'Brien, K.,
2064   Olsen, A., Ono, T., Pérez, F. F., Pfeil, B., Pierrot, D., Poulter, B., Rehder, G., Rödenbeck,
2065   C., Saito, S., Schuster, U., Schwinger, J., Séférian, R., Steinhoff, T., Stocker, B. D.,
2066   Sutton, A. J., Takahashi, T., Tilbrook, B., van der Laan-Luijkx, I. T., van der Werf, G. R.,
2067   van Heuven, S., Vandemark, D., Viovy, N., Wiltshire, A., Zaehle, S. and Zeng, N.
2068   (2015). Global Carbon Budget 2015. *Earth Syst. Sci. Data,* **7**, 349–396. doi:10.5194/essd-
2069   7-349-2015

2070 Le Quéré, C., Andrew, R. M., Canadell, J. G., Sitch, S., Korsbakken, J. I., Peters, G. P.,
2071   Manning, A. C., Boden, T. A., Tans, P. P., Houghton, R. A., Keeling, R. F., Alin, S.,
2072   Andrews, O. D., Anthoni, P., Barbero, L., Bopp, L., Chevallier, F., Chini, L. P., Ciais, P.,
2073   Currie, K., Delire, C., Doney, S. C., Friedlingstein, P., Gkritzalis, T., Harris, I., Hauck, J.,
2074   Haverd, V., Hoppema, M., Klein Goldewijk, K., Jain, A. K., Kato, E., Körtzinger, A.,
2075   Landschützer, P., Lefèvre, N., Lenton, A., Lienert, S., Lombardozzi, D., Melton, J. R.,
2076   Metzl, N., Millero, F., Monteiro, P. M. S., Munro, D. R., Nabel, J. E. M. S., Nakaoka, S.,
2077   O'Brien, K., Olsen, A., Omar, A. M., Ono, T., Pierrot, D., Poulter, B., Rödenbeck, C.,
2078   Salisbury, J., Schuster, U., Schwinger, J., Séférian, R., Skjelvan, I., Stocker, B. D.,
2079   Sutton, A. J., Takahashi, T., Tian, H., Tilbrook, B., van der Laan-Luijkx, I. T., van der
2080   Werf, G. R., Viovy, N., Walker, A. P., Wiltshire, A. J. and Zaehle, S. (2016). Global
2081   Carbon Budget 2016. *Earth Syst. Sci. Data,* **8**, 605–649. doi:10.5194/essd-8-605-2016

2082 Le Quéré, C., Andrew, R. M., Friedlingstein, P., Sitch, S., Hauck, J., Pongratz, J., Pickers, P. A.,
2083   Korsbakken, J .I., Peters, G. P., Canadell, J. G., Arneth, A., Arora, V. K., Barbero, L.,
2084   Bastos, A., Bopp, L., Chevallier, F., Chini, L.P., Ciais, P., Doney, S. C., Gkritzalis, T.,
2085   Goll, D. S., Harris, I., Haverd, V., Hoffman, F. M., Hoppema, M., Houghton, R. A.,
2086   Hurtt, G., Ilyina, T., Jain, A.K., Johannessen, T., Jones, C. D., Kato, E., Keeling, R. F.,
2087   Goldewijk, K. K., Landschützer, P., Lefèvre, N., Lienert, S., Liu, Z., Lombardozzi, D.,
2088   Metzl, N., Munro, D. R., Nabel, J. E. M. S., Nakaoka, S., Neill, C., Olsen, A., Ono, T.,

Patra, P., Peregon, A., Peters, W., Peylin, P., Pfeil, B., Pierrot, D., Poulter, B., Rehder, G., Resplandy, L., Robertson, E., Rocher, M., Rödenbeck, C., Schuster, U., Schwinger, J., Séférian, R., Skjelvan, I., Steinhoff, T., Sutton, A., Tans, P. P., Tian, H., Tilbrook, B., Tubiello, F. N., van der Laan-Luijkx, I. T., van der Werf, G. R., Viovy, N., Walker, A. P., Wiltshire, A. J., Wright, R., Zaehle, S. and Zheng, B. (2018a). Global Carbon Budget 2018. *Earth Syst. Sci. Data,* **10**, 2141–2194. doi:10.5194/essd-10-2141-2018

Le Quéré, C., Andrew, R. M., Friedlingstein, P., Sitch, S., Pongratz, J., Manning, A. C., Korsbakken, J. I., Peters, G. P., Canadell, J. G., Jackson, R. B., Boden, T. A., Tans, P. P., Andrews, O. D., Arora, V. K., Bakker, D. C. E., Barbero, L., Becker, M., Betts, R. A., Bopp, L., Chevallier, F., Chini, L. P., Ciais, P., Cosca, C .E., Cross, J., Currie, K., Gasser, T., Harris, I., Hauck, J., Haverd, V., Houghton, R. A., Hunt, C. W., Hurtt, G., Ilyina, T., Jain, A. K., Kato, E., Kautz, M., Keeling, R. F., Klein Goldewijk, K., Körtzinger, A., Landschützer, P., Lefèvre, N., Lenton, A., Lienert, S., Lima, I, Lombardozzi, D., Metzl, N., Millero, F., Monteiro, P. M. S., Munro, D. R., Nabel, J. E. M. S., Nakaoka, S., Nojiri, Y., Padin, X. A., Peregon, A., Pfeil, B., Pierrot, D., Poulter, B., Rehder, G., Reimer, J., Rödenbeck, C., Schwinger, J., Séférian, R., Skjelvan, I., Stocker, B. D., Tian, H., Tilbrook, B., Tubiello, F. N., van der Laan-Luijkx, I. T., van der Werf, G. R., van Heuven, S., Viovy, N., Vuichard, N., Walker, A. P., Watson, A. J., Wiltshire, A. J., Zaehle, S. and Zhu, D. (2018b). Global Carbon Budget 2017. *Earth Syst. Sci. Data,* **10**, 405–448. doi:10.5194/essd-10-405-2018

Liu, J., Bowman, K., Schimel, D., Parazoo, N., Jiang, Z., Lee, M., Bloom, A., Wunch, D., Gurney, K., Menemenlis, D., Girerach, M., Crisp, D. and Eldering A. (2017). Contrasting carbon cycle responses of the tropical continents to the 2015–2016 El Niño. *Science,* **358**, eaam5690. doi: 10.1126/science.aam5690

Liu, J., Wennberg, P. O., Parazoo, N. C., Yin, Y. and Frankenberg, C. (2020). Observational constraints on the response of high-latitude northern forests to warming. *AGU Advances*, **2**, e2020AV000228. doi:10.1029/2020AV000228

Liu, Z., Dreybrodt, W. and Wang, H. (2010). A new direction in effective accounting for the atmospheric CO_2 budget: Considering the combined action of carbonate dissolution, the global water cycle and photosynthetic uptake of DIC by aquatic organisms. *Earth Science Reviews,* **99**, 169-172. doi:10.1016/j.earscirev.2010.03.001

Long, M. C., Lindsay, K., Peacock, S., Moore, J. K., and Doney, S. C. (2013). Twentieth-century oceanic carbon uptake and storage in CESM1(BGC). *Journal of Climate*, **26**, 6775–6800. doi:10.1175/JCLI-D-12-00184.1

Lovenduski, N. S., Gruber, N. and Doney, S.C. (2008). Toward a mechanistic understanding of the decadal trends in the Southern Ocean carbon sink: Southern Ocean CO_2 flux trends. *Global Biogeochemical Cycles,* **22**(3), GB3016. doi:10.1029/2007GB003139

Lovenduski, N. S., Gruber, N., Doney, S. C. and Lima, I. D. (2007). Enhanced CO_2 outgassing in the Southern Ocean from a positive phase of the Southern Annular Mode. *Global Biogeochemical Cycles,* **21**(2), GB2026. doi:10.1029/2006GB002900

Lucht, W., Prentice, C., Myneni, R. B., Sitch, S., Friedlingstein, P., Cramer, W., Bousquet, P., Buermann, W. and Smith, B. (2002). Climatic control of the high-latitude vegetation

2131   greening trend and Pinatubo effect. *Science*, **296**(5573), 1687–1689.
2132   doi:10.1126/science.1071828

2133 MacDougall, A. H., Frölicher, T. L., Jones, C. D., Rogelj, J., Matthews, H. D., Zickfeld, K.,
2134   Arora, V. K., Barrett, N. J., Brovkin, V., Burger, F. A., Eby, M., Eliseev, A. V., Hajima,
2135   T., Holden, P. B., Jeltsch-Thömmes, A., Koven, C., Mengis, N., Menviel, L., Michou,
2136   M., Mokhov, I. I., Oka, A., Schwinger, J., Séférian, R., Shaffer, G., Sokolov, A., Tachiiri,
2137   K., Tjiputra , J., Wiltshire, A. and Ziehn, T. (2020). Is there warming in the pipeline? A
2138   multi-model analysis of the zero emissions commitment from CO_2. *Biogeosciences,* **17**,
2139   2987–3016. doi:10.5194/bg-17-2987-2020

2140 Maier-Reimer, E. (1993). Geochemical cycles in an ocean general circulation model.
2141   Preindustrial tracer distributions. *Global Biogeochemical Cycles,* **7**, 645–677, 1993.
2142   doi:10.1029/93GB01355

2143 Marsay, C.M., Sanders, R. J., Henson, S. A., Pabortsava, K., Achterberg, E. P. and Lampitt, R. S.
2144   (2015). Attenuation of sinking particulate organic carbon flux through the mesopelagic
2145   ocean. *Proceedings of the National Academy of Sciences,* **112**, 1089.
2146   doi:10.1073/pnas.1415311112

2147 Mau, A. C., Reed, S. C., Wood, T. E. and Cavaleri, M. A. (2018). Temperate and tropical forest
2148   canopies are already functioning beyond their thermal thresholds for photosynthesis.
2149   *Forests*, **9**, 47. doi:10.3390/f9010047

2150 McKinley, G., Follows, M., and Marshall, J. (2004). Mechanisms of air-sea CO_2 flux variability
2151   in the equatorial Pacific and the North Atlantic. *Global Biogeochemical Cycles*, **18**(2),
2152   GB2011. doi:10.1029/2003GB002179

2153 McKinley, G. A., Fay, A. R., Takahashi, T. and Metzl, N. (2011). Convergence of atmospheric
2154   and North Atlantic carbon dioxide trends on multidecadal timescales. *Nature Geosci,* **4**,
2155   606–610. doi:10.1038/ngeo1193

2156 McKinley, G. A., Pilcher, D. J., Fay, A. R., Lindsay, K., Long, M. C. and Lovenduski, N. S.
2157   (2016). Timescales for detection of trends in the ocean carbon sink. *Nature*, **530**(7591),
2158   469–472. doi:10.1038/nature16958

2159 McKinley, G. A., Fay, A. R., Lovenduski ,N. S. and Pilcher, D. J. (2017). Natural variability and
2160   anthropogenic trends in the ocean carbon sink. *Annual Review of Marine Science*, **9**(1),
2161   125–150, doi:10.1146/annurev-marine-010816-060529

2162 McKinley, G. A., Fay, A. R., Eddebbar, Y. A., Gloege L. and Lovenduski, N. S. (2020). External
2163   forcing explains recent decadal variability of the ocean carbon sink. *AGU Advances*, **1**(2),
2164   1, e2019AV000149. doi:10.1029/2019AV000149

2165 Mikaloff Fletcher, S. E., Gruber, N., Jabobson, A. R., Doney, S., C., Sutkiewicz, S., Gerber, M.,
2166   Follows, M., Joos, F., Lindsay, K., Menemenlis, D., Mouchet, A., Müller, S., A. and
2167   Sarmiento, J. L. (2006). Inverse estimates of anthropogenic CO_2 uptake, transport, and
2168   storage by the ocean, *Global Biogeochemical Cycles*, **20**, GB2002.
2169   doi:10.1029/2005GB002530

2170 Miller, J. B., Lehman, S. J., Montzka, S. A., Sweeney, C., Miller, B. R., Karion, A., Wolak, C.,
2171   Dlugokencky, E. J., Southon, J., Turnbull, J. C. and Tans, P. P. (2012). Linking emissions

2172   of fossil fuel CO_2 and other anthropogenic trace gases using atmospheric $^{14}CO_2$. *Journal*
2173   *of Geophysical Research: Atmospheres,* **117**, D08302. doi:10.1029/2011JD017048

2174   Miller, J. B., Lehman, S. J., Verhulst, K. R., Miler, C., E., Duren, R. M., Yadav, V., Newman, S.
2175   and Sloop, C. D. (2020). Large and seasonally varying biospheric CO_2 fluxes in the Los
2176   Angeles megacity revealed by atmospheric radiocarbon. *Proceedings of the National*
2177   *Academy of Sciences*, **117**, 26681-26687. doi:10.1073/pnas.2005253117

2178   Mongwe, N. P., Vichi, M. and Monteiro, P. M. S. (2018). The seasonal cycle of pCO_2 and CO_2
2179   fluxes in the Southern Ocean: diagnosing anomalies in CMIP5 Earth system models.
2180   *Biogeosciences*, **15**, 2851–2872. doi:10.5194/bg-15-2851-2018

2181   Moore, J. K., Fu, W., Primeau, F., Britten, G. L., Lindsay, K., Long, M., Doney, S. C.,
2182   Mahowald, N., Hoffman, F. and Randerson, J. T. (2018). Sustained climate warming
2183   drives declining marine biological productivity. *Science,* 359, 1139–1143.
2184   doi:10.1126/science.aao6379

2185   Nassar, R., Hill, T. G., McLinden, C. A., Wunch, D., Jones, D. B.A. and Crisp D. (2017).
2186   Quantifying CO_2 emissions from individual power plants from space. *Geophysical*
2187   *Research Letters*, **44**(19), 10045-10053. doi:10.1002/2017GL074702

2188   Oda, T., Maksyutov, S. and Andres, S. J. (2018). The Open-source Data Inventory for
2189   Anthropogenic Carbon dioxide (CO_2), version 2016 (ODIAC2016): A global, monthly
2190   fossil-fuel CO_2 gridded emission data product for tracer transport simulations and surface
2191   flux inversions. *Earth Syst. Sci. Data,* **10**, 87-107. doi:10.5194/essd-10-87-2018

2192   O'Dell, C. W., Eldering, A., Wennberg, P. O., Crisp, D., Gunson, M. R., Fisher, B., Frankenberg,
2193   C., Kiel, M., Lindqvist, H., Mandrake, L., Merrelli, A., Natraj, V., Nelson, R. R., Osterman,
2194   G. B., Payne, V. H., Taylor, T. E., Wunch, D., Drouin, B. J., Oyafuso, F., Chang, A.,
2195   McDuffie, J., Smyth, M., Baker, D. F., Basu, S., Chevallier, F., Crowell, S. M. R., Feng, L.,
2196   Palmer, P. I., Dubey, M., García, O. E., Griffith, D. W. T., Hase, F., Iraci, L. T., Kivi, R.,
2197   Morino, I., Notholt, J., Ohyama, H., Petri, C., Roehl, C. M., Sha, M. K., Strong, K.,
2198   Sussmann, R., Te, Y., Uchino, O. and Velazco, V. A. (2018). Improved retrievals of carbon
2199   dioxide from Orbiting Carbon Observatory-2 with the version 8 ACOS algorithm,
2200   *Atmospheric Measurement Techniques*, **11**(12): 6539–6576. doi:10.5194/amt-11-6539-2018

2201   Olsen, A., Lange, N., Key, R. M., Tanhua, T., Bittig, H. C., Kozyr, A., Àlvarez, M., Azetsu-
2202   Scott, K., Becker, S., Brown, P. J., Carter, B. R., Cotrim da Cunha, L., Feely, R. A., van
2203   Heuven, S., Hoppema, M., Ishii, M., Jeansson, E., Jutterström, S., Landa, C. S., Lauvset,
2204   S. K., Michaelis, P., Murata, A., Pérez, F. F., Pfeil, B., Schirnick, C., Steinfeldt, R.,
2205   Suzuki, T., Tilbrook, B., Velo, A., Wanninkhof, R., and Woosley, R. J. (2021).
2206   GLODAPv2.2020 – the second update of GLODAPv2. *Earth Syst. Sci. Data Discuss.*
2207   doi:10.5194/essd-2020-165, in review, 2020.

2208   Palmer, P. I., Feng, L., Baker, D., Chevallier, F., Bösch, H. and Somkuti, P. (2019). Net carbon
2209   emissions from African biosphere dominate pan-tropical atmospheric CO_2 signal, *Nature*
2210   *Communications*, **10**, 3344. doi:10.1038/s41467-019-11097-w

2211   Pan, Y., Birdsey, R. A., Fang, J., Houghton, R., Kauppi, P. E., Kurz, W. A., Phillips, O. L.,
2212   Shvidenko, A., Lewis, S. L., Canadell, J. G., Ciais, P., Jackson, R. B., Pacala, S. W.,
2213   McGuire, A. S., Piao, S., Rautiainen, A., Sitch, S. and Hayes, D. (2011). A large and

2214   persistent carbon sink in the world's forests. Science, 333, 988-993.
2215   doi:10.1126/science.1201609

2216 Panassa, E., Santana-Casiano, J. M., González-Dávila, M., Hoppema, M., van Heuven, S. M. A.
2217   C., Völker, C., Wolf-Gladrow, D. and Hauck, J. (2018). Variability of nutrients and
2218   carbon dioxide in the Antarctic Intermediate Water between 1990 and 2014. *Ocean
2219   Dynamics,* **68**, 295–308. doi:10.1007/s10236-018-1131-2

2220 Parazoo, N. C., Magney, T., Norton, A., Raczka, B., Bacour, C., Maignan, F., Baker, I., Zhang,
2221   Y., Qiu, B., Shi, M., MacBean, N., Bowling, D. R., Burns, S., Blanken, P. D., Stutz, J.,
2222   Grossmann, K. and Frankenberg, C. (2020). Wide discrepancies in the magnitude and
2223   direction of modeled solar-induced chlorophyll fluorescence in response to light
2224   conditions. *Biogeosciences*, **17**, 3733–3755. doi:10.5194/bg-17-3733-2020

2225 Pardo, P. C., Tilbrook, B., Langlais, C., Trull, T.W. and Rintoul, S. R. (2017). Carbon uptake
2226   and biogeochemical change in the Southern Ocean, south of Tasmania. *Biogeosciences,
2227   14*, 5217–5237. doi:10.5194/bg-14-5217-2017

2228 Pearson, T. R. H., Brown, S., Murray, L. and Sidman, G. (2017). Greenhouse gas emissions from
2229   tropical forest degradation: an underestimated source. *Carbon Balance and Management*,
2230   **12**, 3. doi:10.1186/s13021-017-0072-2

2231 Peng, B., Guan, K. Y., Zhou, W. , Jiang, C. Y., Frankenberg, C., Sun, Y., He, L. Y. and Kohler,
2232   P. (2020). Assessing the benefit of satellite-based Solar-Induced Chlorophyll
2233   Fluorescence in crop yield prediction. *International Journal of Applied Earth
2234   Observation and Geoinformation*, **90**, 102126. doi:10.1016/j.jag.2020.102126

2235 Petrescu, A. M. R., Peters, G. P., Janssens-Maenhout, G., Ciais, P., Tubiello, F. N., Grassi, G.,
2236   Nabuurs, G.-J., Leip, A., Carmona-Garcia, G., Winiwarter, W., Höglund-Isaksson, L.,
2237   Günther, D., Solazzo, E., Kiesow, A., Bastos, A., Pongratz, J., Nabel, J. E. M. S.,
2238   Conchedda, G., Pilli, R., Andrew, R. M., Schelhaas, M.-J. and Dolman, A. J. (2020).
2239   European anthropogenic AFOLU greenhouse gas emissions: a review and benchmark
2240   data. *Earth Syst. Sci. Data*, **12**, 961–1001, doi:10.5194/essd-12-961-2020

2241 Pfeil, B., Olsen, A., Bakker, D. C. E., Hankin, S., Koyuk, H., Kozyr, A., Malczyk, J., Manke, A.,
2242   Metzl, N., Sabine, C. L., Akl, J., Alin, S. R., Bates, N., Bellerby, R. G. J., Borges, A.,
2243   Boutin, J., Brown, P. J., Cai, W.-J., Chavez, F. P., Chen, A., Cosca, C., Fassbender, A. J.,
2244   Feely, R. A., González-Dávila, M., Goyet, C., Hales, B., Hardman-Mountford, N.,
2245   Heinze, C., Hood, M., Hoppema, M., Hunt, C. W., Hydes, D., Ishii, M., Johannessen, T.,
2246   Jones, S. D., Key, R. M., Körtzinger, A., Landschützer, P., Lauvset, S. K., Lefèvre, N.,
2247   Lenton, A., Lourantou, A., Merlivat, L., Midorikawa, T., Mintrop, L., Miyazaki, C.,
2248   Murata, A., Nakadate, A., Nakano, Y., Nakaoka, S., Nojiri, Y., Omar, A. M., Padin, X.
2249   A., Park, G.-H., Paterson, K., Perez, F. F., Pierrot, D., Poisson, A., Ríos, A. F., Santana-
2250   Casiano, J. M., Salisbury, J., Sarma, V. V. S. S., Schlitzer, R., Schneider, B., Schuster,
2251   U., Sieger, R., Skjelvan, I., Steinhoff, T., Suzuki, T., Takahashi, T., Tedesco, K.,
2252   Telszewski, M., Thomas, H., Tilbrook, B., Tjiputra, J., Vandemark, D., Veness, T.,
2253   Wanninkhof, R., Watson, A. J., Weiss, R., Wong, C. S. and Yoshikawa-Inoue, H. (2013).
2254   A uniform, quality controlled Surface Ocean CO_2 Atlas (SOCAT). *Earth Syst. Sci. Data,
2255   5*, 125–143. doi:10.5194/essd-5-125-2013

Piao, S., Wang, X., Park, T., Chen, C., Lian, X., He, Y. Bjerke, J. W., Chen, A., Ciais, P., Tommervik, H., Nemani, R. R. and Myneni, R. B. (2020). Characteristics, drivers and feedbacks of global greening. *Nat. Rev. Earth Environ.,* **1**, 14–27. doi:10.1038/s43017-019-0001-x

Quegan, S., Toan, L. T., Chave, J., Dall, J., Exbrayat, J. F., Minh, D. H. T., Lomas, M., D'Alessandro, M. M., Paillou, P., Papathanassiou, K., Rocca, F., Saatchi, S., Scipal, K., Shugart, H., Smallman, T. L., Soja, M. J., Tebaldini, S., Ulander, L., Villard, L. and Williams, M. (2019). The European Space Agency BIOMASS mission: measuring forest above-ground biomass from space. *Remote Sens. Environ.,* **227**, 44–60. doi:10.1016/j.rse.2019.03.032

Qiu, B., Ge, J., Guo, W. D., Pittman, A. J. and Mu, M. Y. (2020). Responses of Australian dryland vegetation to the 2019 heat wave at a sub daily scale. *Geophysical Research Letters,* **47**, e2019GL086569. doi:10.1029/2019GL086569

Ramankutty N., Gibbs, H. K., Achard, F., Defries, R., Foley, J. A. and Houghton, R. A. (2007). Challenges to estimating carbon emissions from tropical deforestation. *Global Change Biology,* **13**, 51–66. doi: 10.1111/j.1365-2486.2006.01272.x

Randerson, J. T., Hoffman, F. M., Thornton, P. E., Mahowald, N. M., Lindsay, K., Lee, Y. H., Nevison, C. D. Doney, S. C., Bonan, G., Stöckli, R., Covey, C., Running, S. W. and Fung, I. Y. (2009). Systematic assessment of terrestrial biogeochemistry in coupled climate–carbon models. *Global Change Biology*, **15**(10), 2462-2484. doi: 10.1111/j.1365-2486.2009.01912.x

Randerson, J. T., Lindsay, K., Munoz, E., Fu, W., Moore, J. K., Hoffman, F. M., Mahowald, N. M. and Doney, S. C. (2015). Multi-century changes in ocean and land contributions to the climate-carbon feedback. *Global Biogeochemical Cycles*, **29**, 744-759. doi:10.1002/2014GB005079

Raupach, M. R., Canadell, J. G. and Le Quéré, C. (2008). Anthropogenic and biophysical contributions to increasing atmospheric CO_2 growth rate and airborne fraction. *Biogeosciences*, **5**, 1601–1613. doi:10.5194/bg-5-1601-2008

Raupach, M. R., Gloor, M., Sarmiento, J. L., Canadell, J. G., Frölicher, T. L., Gasser, T., Houghton, R. A., Le Quéré, C. and Trudinger, C. M. (2014). The declining uptake rate of atmospheric CO_2 by land and ocean sinks. *Biogeosciences*, **11**(13), 3453–3475. doi:10.1007/s10584-009-9596-0

Regnier, P., Friedlingstein, P., Ciais, P., Mackenzie, F. T., Gruber, N., Janssens, I. A., Laruelle, G. G., Lauerwald, R., Luyssaert, S., Andersson, A. J., Arndt, S., Arnosti, C., Borges, A. V., Dale, A. W., Gallego-Sala, A., Goddéris, Y., Goossens, N., Hartmann, J., Heinze, C., Ilyina, T., Joos, F., LaRowe, D. E., Leifeld, J., Meysman, F. J. R., Munhoven, G., Raymond, P. A., Spahni, R., Suntharalingam, P. and Thullner, M. (2013). Anthropogenic perturbation of the carbon fluxes from land to ocean. *Nature Geosciences,* **6**, 597–607. doi:10.1038/ngeo1830

Resplandy, L., Keeling, R. F., Rodenbeck, C.,. Stephens, B. B, Khatiwala, S., Rodgers, K. B., Long, M. C., Bopp, L. and. Tans, P. P. (2018). Revision of global carbon fluxes based on a reassessment of oceanic and riverine carbon transport. *Nature Geoscience*, **11**, 504–509. doi:10.1038/s41561-018-0151-3

2299   Reuter, M., Buchwitz, M., Schneising, O., Noël, S., Bovensmann, H. and Burrows, J. P. (2017).
2300   A fast atmospheric trace gas retrieval for hyperspectral instruments approximating
2301   multiple scattering—Part 2: Application to XCO_2 retrievals from OCO-2. *Remote*
2302   *Sensing*, **9**, 1102. doi: 10.3390/rs9111102

2303   Reuter, M., Buchwitz., M., Schneising, O., Krautwurst, S., O'Dell, C. W., Richter, A.,
2304   Bovensmann, H. and Burrows, J. P. (2019). Towards monitoring localized CO_2 emissions
2305   from space: Co-located regional CO_2 and NO_2 enhancements observed by the OCO-2 and
2306   S5P satellites. *Atmospheric Chemistry and Physics*, **19**, 9371–9383. doi:10.5194/acp-19-
2307   9371-2019

2308   Ridge, S. M. and McKinley, G. A. (2020a). Advective controls on the North Atlantic
2309   anthropogenic carbon sink. *Global Biogeochemical Cycles*, **34**(7), 1138.
2310   doi:10.1029/2019GB006457

2311   Ridge, S. M. and G. A. McKinley (2020b). Ocean carbon uptake under aggressive emission
2312   mitigation. *Biogeosciences Discussions* doi:10.5194/bg-2020-254, in review, 2020.

2313   Rödenbeck, C., Bakker, D. C. E., Metzl, N., Olsen, A., Sabine, C., Cassar N., Reum, F., Keeling,
2314   R. F and Heimann, M. (2014). Interannual sea-air CO_2 flux variability from an
2315   observation-driven ocean mixed-layer scheme. *Biogeosciences*, **11**(1), 4599–4613.
2316   doi:10.5194/bg-11-4599-2014

2317   Rödenbeck, C., Bakker, D. C. E., Gruber, N., Iida, Y., Jacobson, A. R., Jones, S., Landschützer,
2318   P., Metzl, N., Nakaoka, S., Olsen, A., Park, G.-H., Peylin, P., Rodgers, K. B., Sasse, T.
2319   P., Schuster, U., Shutler, J. D., Valsala, V., Wanninkhof, R. and Zeng, J. (2015). Data-
2320   based estimates of the ocean carbon sink variability – first results of the Surface Ocean
2321 pCO_2 Mapping intercomparison (SOCOM). *Biogeosciences*, **12**, 7251–7278.
2322   doi:10.5194/bg-12-7251-2015

2323   Rodgers, K. B., Schlunegger, S., Slater, R. D., Ishii, M., Frolicher, T. L., Toyama, K.,
2324   Plancherel, Y., Aumont, O. and Fassbender, A. J. (2020). Reemergence of anthropogenic
2325   carbon into the ocean's mixed layer strongly amplifies transient climate sensitivity.
2326   *Geophysics Research Letters*, **47**(18), 130. doi:10.1002/2017GL073758

2327   Rosen, P., Hensley, S., Shaffer, S., Edelstein, W., Kim, Y., Kumar, R., Misra, T., Bhan, R.,
2328   Satish, R. and Sagi, R. (2016). An update on the NASA-ISRO dual-frequency dbf SAR
2329   (NISAR) mission. *2016 IEEE International Geoscience and Remote Sensing Symposium*.
2330   IEEE, New York, pp. 2106–2108. doi:10.1109/IGARSS.2016.7729543

2331   Rudnick, D. L. (2016). Ocean Research Enabled by Underwater Gliders. *Annual Review of*
2332   *Marine Science*, **8**, 519-541. doi:10.1146/annurev-marine-122414-033913

2333   Saatchi, S. S., Harris, N. L., Brown, S., Lefsky, M., Mitchard, E. T. A., Salas, W., Zutta, B. R.,
2334   Buermann, W., Lewis, S. L., Hagen, S., Petrova, S., White, L., Silman, M. and Morel, A.
2335   (2011). Benchmark map of forest carbon stocks in tropical regions across three
2336   continents. *Proceedings of the National Academy of Sciences*, **108**, 9899-9904. doi:
2337   10.1073/pnas.1019576108

2338   Sabine, C. L., Feely, R. A., Gruber, N., Key, R. M., Lee, K., Bullister, K. L., Wanninkhof, R.
2339   Wong, C. S., Wallace, D. W. R. Wallace, Tilbrook, B., Millero, F. J., Peng, T.-H., Kozyr,

A., Ono, T. and Rois, A. F. (2004). The oceanic sink for anthropogenic CO_2. *Science, 305*, 367–371. doi:10.1126/science.1097403

Sabine, C. L. and Tanhua, T. (2010). Estimation of anthropogenic CO_2 inventories in the ocean. *Annual Reviews of Marine Sciences, 2*, 175-198. doi:10.1146/annurev-marine-120308-080947

Sabine, C., Sutton, A., McCabe, K., Lawrence-Slavas, N., Alin, S., Feely, R., Jenkins, R., Maenner, S., Meinig, C., Thomas, J., van Ooijen, E., Passmore, A. and Tilbrook, B. (2020). Evaluation of a new carbon dioxide system for autonomous surface vehicles. *J. Atmos. Ocean. Technol.*, **37**, 1305-1317. doi:10.1175/JTECH-D-20-0010.1

Sarmiento, J. L., and Sundquist E. T. (1992). Revised budget for the oceanic uptake of anthropogenic carbon dioxide, *Nature*, **356**, 589–593. doi:10.1038/356589a0

Sarmiento, J. L. and Gruber, N. (2006). Ocean Biogeochemical Dynamics. Princeton University Press. ISBN: 0-691-01707-7. doi:10.1017/S0016756807003755

Scharlemann, J. P. W., Tanner, E. V. J., Hiederer, R. and Kapos, V. (2014). Global soil carbon: understanding and managing the largest terrestrial carbon pool. *Carbon Management*, **5**, 81-91. doi:10.4155/cmt.13.77

Schepaschenko, D., Moltchanova, E., Shvidenko, A., Blyshchyk, V., Dmitriev, E., Martynenko, O., See, L. and Kraxner F. (2018). Improved estimates of biomass expansion factors for russian forests. *Forests*, **9**, 312. doi:10.3390/f9060 312

Schourup-Kristensen, V., Sidorenko, D., Wolf-Gladrow, D. A. and Völker, C. (2014). A skill assessment of the biogeochemical model REcoM2 coupled to the Finite Element Sea Ice–Ocean Model (FESOM 1.3). *Geosci. Model Dev.*, **7**, 2769–2802. doi:10.5194/gmd-7-2769-2014

Schuur, E. A. G., McGuire, A. D., Schädel, C., Grosse, G., Harden, J. W., Hayes, D. J., Hugelius, G., Koven, C. D., Kuhry, P., Lawrence, D. M., Natali, S. M., Olefeldt, D., Romonovsky, V. E. Schaefer, K., Truetsky, M. R., Treat, C. C. and Vonk, J. E. (2015). Climate change and the permafrost carbon feedback. *Nature*, **520**, 171-179. doi:10.1038/nature14338

Schwinger, J., Tjiputra, J. F., Heinze, C., Bopp, L., Christian, J. R., Gehlen, M., Ilyina, T., Jones, C. D., Salas-Mélia, D., Segschneider, J., Séférian, R. and Totterdell, I. (2014). Nonlinearity of ocean carbon cycle feedbacks in CMIP5 Earth system models. *Journal of Climate, 27*, 3869–3888. doi:10.1175/JCLI-D-13-00452.1

Schwinger, J., Goris, N., Tjiputra, J. F., Kriest, I., Bentsen, M., Bethke, I., Ilicak, M., Assmann, K. M. and Heinze, C. (2016). Evaluation of NorESM-OC (versions 1 and 1.2), the ocean carbon-cycle stand-alone configuration of the Norwegian Earth System Model (NorESM1). *Geosci. Model Dev.*, **9**, 2589–2622. doi:10.5194/gmd-9-2589-2016

Schwinger, J. and Tjiputra, J. (2018). Ocean carbon cycle feedbacks under negative emissions. *Geophysical Research Letters*, **26**(3), 5289. doi:10.1088/1748-9326/11/5/055006

Seelmann, K., Aßmann, S. and Körtzinger, A. (2019). Characterization of a novel autonomous analyzer for seawater total alkalinity: Results from laboratory and field tests. *Limnology and Oceanography: Methods*, **17**, 515-532. doi:10.1002/lom3.10329

2381 Sellers, P. J., Schimel, D. S., Moore III, B., Liu, J. and Eldering, A. (2018). Observing Carbon
2382 Cycle-Climate Feedbacks from Space, *Proceedings of the National Academy of Sciences*,
2383 **115**(31), 7860-7868. doi:10.1073/pnas.1716613115

2384 Sigman, D. M., Hain, M. P. and Haug, G. H. (2010). The polar ocean and glacial cycles in
2385 atmospheric CO_2 concentration. *Nature,* **466**, 47–55. doi:10.1038/nature09149

2386 Sitch, S., Friedlingstein, P., Gruber, N., Jones, S. D., Murray-Tortarolo, G., Ahlström, A.,
2387 Doney, S. C., Graven, H., Heinze, C., Huntingford, C., Levis, S., Levy, P. E., Lomas, M.,
2388 Poulter, B., Viovy, N., Zaehle, S., Zeng, N., Arneth, A., Bonan, G., Bopp, L., Canadell, J.
2389 G., Chevallier, F., Ciais, P., Ellis, R., Gloor, M., Peylin, P., Piao, S. L., Le Quéré, C.,
2390 Smith, B., Zhu, Z. and Myneni, R. (2015). Recent trends and drivers of regional sources
2391 and sinks of carbon dioxide. *Biogeosciences*, **12**, 653–679. doi:10.5194/bg-12-653-2015

2392 Smith P., Bustamante, M., Ahammad, H., Clark, H., Dong, H., Elsiddig, E. A., Haberl, H.,
2393 Harper, R., House, J., Jafari M., Masera, O., Mbow, C., Ravindranath N. H., Rice C. W.,
2394 Robledo Abad, C., Romanovskaya, A., Sperling, F. and Tubiello F. (2014) Agriculture,
2395 Forestry and Other Land Use (AFOLU). In: Climate Change 2014: Mitigation of Climate
2396 Change. Contribution of Working Group III to the Fifth Assessment Report of the
2397 Intergovernmental Panel on Climate Change [Edenhofer, O., R. Pichs-Madruga, Y.
2398 Sokona, E. Farahani, S. Kadner, K. Seyboth, A. Adler, I. Baum, S. Brunner, P.
2399 Eickemeier, B. Kriemann, J. Savolainen, S. Schlömer, C. von Stechow, T. Zwickel and
2400 J.C. Minx (eds.)]. Cambridge University Press, Cambridge, United Kingdom and New
2401 York, NY, USA.

2402 Song, X.-P., Hansen, M. C., Stehman, S. V., Potapov, P. V., Tyukavina, A., Vermote, E. F. and
2403 Townshend, J. R. (2018). Global land change from 1982 to 2016. *Nature*, **560**., 639-343.
2404 doi:10.1038/s41586-018-0411-9

2405 Soong, J. L., Fuchslueger, L., Marañon-Jimenez, S., Torn, M. S., Janssens, I. A., Penuelas, J.,
2406 and Richter, A. (2019). Microbial carbon limitation, 2021. The need for integrating
2407 microorganisms into our understanding of ecosystem carbon cycling. *Global Change
2408 Biology,* **26**, 1953–1961. doi:10.1111/gcb.14962

2409 Spawn, S. A., Sullivan, C. C., Lark, T. J. and Gibbs, H. K. (2020). Harmonized global maps of
2410 above and belowground biomass carbon density in the year 2010. *Scientific Data,* **7,** 112.
2411 doi:10.1038/s41597-020-0444-4

2412 Stamell, J., Rustagi, R. R., Gloege, L. and McKinley, G. A. (2021). Strengths and weaknesses of
2413 three Machine Learning methods for pCO_2 interpolation. *Geosci. Model Dev. Discuss.*
2414 [preprint], https://doi.org/10.5194/gmd-2020-311, in review, 2020.

2415 Stock, C. A., Dunne, J. P., Fan, S., Ginoux, P., John, J., Krasting, J. P., Laufkötter, C., Paulot, F.
2416 and Zadeh, N. (2020). Ocean biogeochemistry in GFDL's Earth System Model 4.1 and its
2417 response to increasing atmospheric CO_2. *J. Adv. Model. Earth Syst.*, **12**,
2418 e2019MS002043. doi:10.1029/2019MS002043

2419 Sun, Y., Frankenberg, C., Jung, J., Joiner, J., Guanter, L., Köhler, P. and Magney, T. (2018).
2420 Overview of solar-Induced chlorophyll fluorescence (SIF) from the Orbiting Carbon
2421 Observatory-2: Retrieval, cross-mission comparison, and global monitoring for GPP.
2422 *Remote Sensing of Environment*, **209**, 808-823. doi:10.1016/j.rse.2018.02.016

2423 Sundquist, E.T., (1993). The global carbon dioxide budget. *Science,* **259**, 934–941.
2424   doi:10.1126/science.259.5097.934

2425 Sutton, A. J., Sabine, C. L., Maenner-Jones, S., Lawrence-Slavas, N., Meinig, C., Feely, R. A.,
2426   Mathis, J. T., Musielewicz, S., Bott, R., McLain, P. D., Fought, H. J. and Kozyr, A.
2427   (2014). A high-frequency atmospheric and seawater pCO_2 data set from 14 open-ocean
2428   sites using a moored autonomous system. *Earth Syst. Sci. Data,* **6**, 353-366.
2429   doi:10.5194/essd-6-353-2014

2430 Takahashi, T., Sutherland, S. C., Sweeney, C., Poisson, A., Metzl, N., Tilbrook, B., Bates, N.,
2431   Wanninkhof, R., Feely, R. A., Sabine, C., Olafsson, J., Nojiri, Y. (2002). Global sea–air
2432 CO_2 flux based on climatological surface ocean pCO_2, and seasonal biological and
2433   temperature effects. *Deep Sea Research Part II: Topical Studies in Oceanography*, **49**, 9–
2434   10, 1601-1622. doi:10.1016/S0967-0645(02)00003-6

2435 Takahashi, T., Sutherland, S. C., Wanninkhof, R., Sweeney, C., Feely, R. A., Chipman, D. W.,
2436   Hales, B., Friederich, G., Chavez, F., Sabine, C., Watson, A., Bakker, D. C. E., Schuster,
2437   U., Metzl, N., Yoshikawa-Inoue, H., Ishii, M., Midorikawa, T., Nojiri, Y., Körtzinger, A.,
2438   Steinhoff, T., Hoppema, M., Olafsson, J., Arnarson, T.S., Tilbrook, B., Johannessen, T.,
2439   Olsen, A., Bellerby, R., Wong, C. S., Delille, B., Bates, N. R. and de Baar, H. J. W.
2440   (2009). Climatological mean and decadal change in surface ocean pCO_2, and net sea–air
2441 CO_2 flux over the global oceans. *Deep Sea Research Part II: Topical Studies in
2442   Oceanography,* **56**, 554–577. doi:10.1016/j.dsr2.2008.12.009

2443 Takeshita, Y., Johnson, K. S., Coletti, L. J., Jannasch, H. W., Walz, P. M. and Warren, J. K.
2444   (2020). Assessment of pH dependent errors in spectrophotometric pH measurements of
2445   seawater. *Marine Chemistry*, **223**, 103801. doi:10.1016/j.marchem.2020.103801

2446 Takeshita, Y., Johnson, K. S., Martz, T. R., Plant, J. N. and Sarmiento, J. L. (2018). Assessment
2447   of autonomous pH measurements for determining surface seawater partial pressure of
2448 CO_2. *Journal of Geophysical Research: Oceans,* **123**, 4003-4013.
2449   doi:10.1029/2017jc013387

2450 Tanhua, T., van Heuven, S., Key, R. M., Velo, A., Olsen, A. and Schirnick, C. (2010). Quality
2451   control procedures and methods of the CARINA database. *Earth Syst. Sci. Data* **2**, 35–49.
2452   doi:10.5194/essd-2-35-2010

2453 Tanhua, T. and Keeling, R. F. (2012). Changes in column inventories of carbon and oxygen in
2454   the Atlantic Ocean. *Biogeosciences,* **9**, 4819-4833. doi:10.5194/bg-9-4819-2012

2455 van der Werf, G. R., Randerson, J. T., Giglio, L., van Leeuwen, T. T., Chen, Y., Rogers, B. M.,
2456   Mu, M., van Marle, M. J. E., Morton, D. C., Collatz, G. J., Yokelson, R. J. and
2457   Kasibhatla, P. S. (2017). Global fire emissions estimates during 1997–2016. *Earth Syst.
2458   Sci. Data*, **9**, 697–720. doi:10.5194/essd-9-697-2017

2459 Verdy, A. Mazloff, M. R. (2017). A data assimilating model for estimating Southern Ocean
2460   biogeochemistry. *Journal of Geophysical Research: Oceans,* **122**, 6968–6988.
2461   doi:10.1002/2016JC012650

2462 Wang, S., Zhang, Y., Hakkarainen, J., Ju, W., Liu, Y., Jiang, F. and He, W. (2018).
2463   Distinguishing anthropogenic CO_2 emissions from different energy intensive industrial

2464   sources using OCO-2 observations: A case study in northern China. *Journal of*
2465   *Geophysical Research: Atmospheres*, **123**, 9462–9473. doi:10.1029/2018JD029005

2466   Wang, S., Zhang, Y., Ju, W., Chen, J. M., Ciais, P., Cescatti, A., Sardans, J., Janssens, I. A., Wu,
2467   M., Berry, J. A., Campbell, E., Fernandez-Martinez, M., Alkama, R., Sitch, S.,
2468   Friedlingstein, P., Smith, W. K., Yuan, W., He, W., Lombardozzi, D., Kautz, M., Zhu,
2469   D., Lienert, S., Kato, E., Poulter, B., Sanders, T. G. M., Kruger, I., Wang, R., Zeng, N.,
2470   Tian, H., Vulchard, N., Jian, A., K., Wiltshire, A., Haverd, V., Goll, D. S. and Penuelas,
2471   J. (2020). Recent global decline of CO_2 fertilization effects on vegetation photosynthesis.
2472   *Science*, **370**, 1295–1300. doi: 10.1126/science.abb7772

2473   Watson, A. J., Schuster, U., Shutler, J. D., Holding, T., Ashton, I. G. C.,Landschützer, P. ,
2474   Woolf, D. K. and Goddijn-Murphy, L. (2020). Revised estimates of ocean-atmosphere
2475 CO_2 flux are consistent with ocean carbon inventory. *Nature Communications*, **11**, 4422.
2476   doi:10.1038/s41467-020-18203-3

2477   Waugh, D. W., Hall, T. M., McNeil, B. I., Key, R. and Matear, R. J. (2006). Anthropogenic CO_2
2478   in the oceans estimated using transit-time distributions. *Tellus,* **58B**, 376-389.
2479   doi:10.1111/j.1600-0889.2006.00222.x

2480   Welp, L., Keeling, R. and Meijer, H. A. J. (2011). Interannual variability in the oxygen isotopes
2481   of atmospheric CO_2 driven by El Niño. *Nature*, **477**, 579–582. doi:10.1038/nature10421

2482   Wigneron, J.-P., Fan, L., Ciais, P., Bastos, A., Brandt, M., Chave, J., Saatchi, S., Baccini, A. and
2483   Fensholt, R. (2020). Tropical forests did not recover from the strong 2015–2016 El Niño
2484   event. *Science Advances*, **6**, eaay4603. doi:10.1126/sciadv.aay4603

2485   Williams, N. L., Juranek, L. W., Feely, R. A., Johnson, K. S., Sarmiento, J. L., Talley, L. D.,
2486   Dickson, A. G., Gray, A. R., Wanninkhof, R., Russell, J. L., Riser, S. C. and Takeshita,
2487   Y. (2017). Calculating surface ocean pCO_2 from biogeochemical Argo floats equipped
2488   with pH: An uncertainty analysis. *Global Biogeochemical Cycles*, **31**, 591-604.
2489   doi:10.1002/2016GB005541

2490   Willey, J. D., Kieber, R. J., Eyman, M. S. and Avery Jr., G. B. (2000). Rainwater dissolved
2491   organic carbon: Concentrations and global flux. *Global Biogeochemical Cycles*, **14**, 139-
2492   148. doi: 10.1007/s11270-008-9774-0

2493   Woolf, D. K., Shutler, J. D., Goddijn-Murphy, L., Watson, A. J., Chapron, B., Nightingale, P. D.,
2494   Donlon, C. J., Piskozub, J., Yelland, M. J., Ashton, I., Holding, T., Schuster, U., Girard-
2495   Ardhuin, F., Grouazel, A., Piolle, J.-F., Warren, M., Wrobel-Niedzwiecka, I., Land, P. E.,
2496   Torres, R., Prytherch, J., Moat, B., Hanafin, J., Ardhuin, F. and Paul, F. (2019). Key
2497   uncertainties in the recent air-sea flux of CO_2. *Global Biogeochemical Cycles*, **33**, 1548-
2498   1563. doi:10.1029/2018GB006041

2499   Wu, D., Lin, J. C., Fasoli, B., Oda, T., Ye, X., Lauvaux, T., Yang, E. G. and Kort, E. A. (2018). A
2500   Lagrangian approach towards extracting signals of urban CO_2 emissions from satellite
2501   observations of atmospheric column CO_2 (XCO_2): X-Stochastic Time-Inverted Lagrangian
2502   Transport model ("X-STILT v1"). *Geoscientific Model Development*, **11**(12): 4843–4871.
2503   doi:10.5194/gmd-11-4843-2018

2504   Wu, D. E., Lin, J. C., Oda, T. and Kort, E. A. (2020). Space-based quantification of per capita
2505   CO2 emissions from cities, *Environmental Research Letters*, **15**, 035004. doi:10.1088/1748-
2506   9326/ab68eb

2507 Wunch, D., Wennberg, P. O., Osterman, G., Fisher, B., Naylor, B., Roehl, C. M., O'Dell, C.,
2508   Mandrake, L., Viatte, C., Griffith, D. W., Deutscher, N. M., Velazco, V. A., Notholt, J.,
2509   Warneke, T., Petri, C., De Maziere, M., Sha, M. K., Sussmann, R., Rettinger, M., Pollard,
2510   D., Robinson, J., Morino, I., Uchino, O., Hase, F., Blumenstock, T., Kiel, M., Feist, D.
2511   G., Arnold, S. G., Strong, K., Mendonca, J., Kivi, R., Heikkinen, P., Iraci, L., Podolske,
2512   J., Hillyard, P. W., Kawakami, S., Dubey, M. K., Parker, H. A., Sepulveda, E.,
2513   Rodriguez, O. E. G., Te, Y., Jeseck, P., Gunson, M. R., Crisp, D. and Eldering, A. (2017).
2514   Comparisons of the Orbiting Carbon Observatory-2 (OCO-2) XCO_2 measurements with
2515   TCCON, *Atmospheric Measurement Tech*niques, **10**, 2209–2238. doi:10.5194/amt-10-
2516   2209-2017

2517 Xiao, J., J. Chen, Davis, K. J. and Reichstein, M. (2012). Advances in upscaling of eddy
2518   covariance measurements of carbon and water fluxes. *Journal Geophysical Research:*
2519   *Biogeosciences*, **117**, G00J01. doi:10.1029/2011JG001889

2520 Xiao, J., Chevallier, F., Gomez, C., Guanter, L., Hicke, J. A., Huete, A. R., Ichii, K., Ni, W.,
2521   Pang, Y., Rahman, A. F. Sun, G., Yuan, W., Zhang, L. and Zhang, X. (2019). Remote
2522   sensing of the terrestrial carbon cycle: A review of advances over 50 years. Remote
2523   Sensing of Environment, 233, 111383. doi:10.1016/j.rse.2019.111383

2524 Yin, Y., Byrne, B., Liu, J., Wennberg, P., Davis, K. J., Magney, T., Koehler, P., He, L., Jeyaram,
2525   R., Humphrey, V., Gerken, T., Feng, S., Digangi, J. P. and Frankenberg, C. (2020).
2526   Cropland carbon uptake delayed and reduced by 2019 Midwest floods. *AGU Advances*, **1**,
2527   e2019AV000140. doi:10.1029/2019AV000140

2528 Zavarsky, A. and Marandino, C. A. (2019). The influence of transformed Reynolds number
2529   suppression on gas transfer parameterizations and global DMS and CO_2 fluxes.
2530   *Atmospheric Chemistry and Physics*, **19**, 1819-1834. doi:10.5194/acp-19-1819-2019

2531 Zeebe, R. and Wolf-Gladrow, D. (2001). CO_2 in seawater: Equilibrium, kinetics, isotopes.
2532   *Elsevier Oceanogr. Ser.*, **65**, Elsevier, Amsterdam.

2533 Zeng, N., Zhao, F., Collatz, G. J., Kalnay, E., Salawitch, R., West, T. O. and Guanter, L. (2014).
2534   Agricultural Green Revolution as a driver of increasing atmospheric CO_2 seasonal
2535   amplitude. *Nature,* **515**, 394–397. doi: 10.1038/nature13893

2536 Zickfeld, K., MacDougall, A. H., and Matthews, H. D. (2016). On the proportionality between
2537   global temperature change and cumulative CO_2 emissions during periods of net negative
2538 CO_2 emissions. *Environmental Research Letters*, **11**(5), 055006, doi:10.1088/1748-
2539   9326/11/5/055006